OFFICE OF CIVILIAN RADIOACTIVE WASTE MANAGEMENT
ANALYSIS/MODEL COVER SHEET
Complete Only Applicable Items

1. QA: QA

2. ☒ Analysis — Check all that apply

Type of Analysis:
- ☐ Engineering
- ☒ Performance Assessment
- ☐ Scientific

Intended Use of Analysis:
- ☐ Input to Calculation
- ☐ Input to another Analysis or Model
- ☒ Input to Technical Document
- ☐ Input to other Technical Products

Describe use:

Abstracts CSNF rod failure for TSPA

Abstracts CSNF rod unzipping for TSPA

3. ☐ Model — Check all that apply

Type of Model:
- ☐ Conceptual Model
- ☐ Abstraction Model
- ☐ Mathematical Model
- ☐ System Model
- ☐ Process Model

Intended Use of Model:
- ☐ Input to Calculation
- ☐ Input to another Model or Analysis
- ☐ Input to Technical Document
- ☐ Input to other Technical Products

Describe use:

4. Title:

Clad Degradation – Summary and Abstraction

5. Document Identifier (including Rev. No. and Change No., if applicable):

ANL-WIS-MD-000007 REV 00 ICN 01

6. Total Attachments:

2

7. Attachment Numbers - No. of Pages in Each:

I-2, II-25

		Printed Name	Signature	Date
8.	Originator	E. Siegmann	Eric R. Siegmann	12/8/00
9.	Checker	T. Thornton	Ramya Mr for T. Thornton	12/8/00
		Kevin McCoy	Kevin McCoy	DEC 8, 2000
10.	Lead/Supervisor	R. Rechard	R. Rechard	12/8/00
11.	Responsible Manager	R. MacKinnon	Robert MacKinnon	12/8/00

12. Remarks:

This is associated with AMR F0155.

Enclosure 5

OFFICE OF CIVILIAN RADIOACTIVE WASTE MANAGEMENT
ANALYSIS/MODEL REVISION RECORD
Complete Only Applicable Items

2. Model or Analysis Title:

Clad Degradation – Summary and Abstraction

3. Document Identifier (including Rev. No. and Change No., if applicable):

ANL-WIS-MD-000007 REV 00 ICN 01

4. Revision/Change No.	5. Description of Revision/Change
REV 00	Initial Issue
REV 00 ICN 01	Revised cladding creep calculation. Rod failure from rockfall included. Expanded discussions of assumptions about commercial cladding design. Made some editorial corrections and updated procedure references. Addressed concerns cited in the self-assessment documented in SA-PA-2000-005 (MOL.20000719.0414). Vertical change bars in the right margin indicate changes.

CONTENTS

FIGURES

Page

TABLES

Page

LIST OF ACRONYMS

AMR	Analysis and Model Report
ASTM	American Society for Testing and Materials
BWR	Boiling Water Reactor
CCDF	Complementary Cumulative Distribution Function
CDF	Cumulative Distribution Function
CFR	Code of Federal Register
CPU	Central Processing Unit
CRC	Chemical Rubber Company
CRWMS	Civilian Radioactive Waste Management System
CSNF	Commercial Spent Nuclear Fuel
DCCG	Diffusion Controlled Cavity Growth
DHC	Delayed Hydride Cracking
DIRS	Document Input Reference System
DOE	U.S. Department of Energy
DTN	Data Tracking Number
EPRI	Electric Power Research Institute
EBS	Engineered Barrier System
FEPs	Features, Events & Processes
IRSR	Issue Resolution Status Report
KTI	Key Technical Issues
ISG	Interim Staff Guidance
LWR	Light Water Reactor
M&O	Management and Operating Contractor
MGR	Monitored Geologic Repository
NRC	U.S. Nuclear Regulatory Commission
PA	Performance Assessment
PAO	Performance Assessment Operations Department
PCI	Pellet-Clad Interaction
PWR	Pressurized Water Reactor
QA	Quality Assurance
QARD	Quality Assurance Requirements and Description
SCC	Stress Corrosion Cracking
SS	Stainless Steel
TSPA	Total System Performance Assessment
TSPAI	Total System Performance Assessment and Integration
US	United States
WP	Waste Package
YMP	Yucca Mountain Project

1. PURPOSE

The purpose of this analysis is to develop the summary cladding degradation abstraction that is consistent with and used in the Total System Performance Assessment - Site Recommendation (TSPA-SR). This analysis is to describe the postulated condition of commercial Zircaloy clad fuel after it is placed in the Yucca Mountain Project (YMP) site (post-closure) as a function of time. Most commercial nuclear fuel is encased in Zircaloy cladding. This analysis is developed to describe cladding degradation from the expected failure modes. These include failure before receipt at YMP (reactor operation impacts including incipient failures; during spent fuel storage in pool and dry storage; and impacts due to transportation) and degradation in the repository (cladding creep, seismic failures, localized corrosion and cladding unzipping). This Interim Change Notice (ICN01) contains a revision of the creep calculations and includes cladding failure from rockfalls. This AMR does not address potential damage to assemblies that might occur at the YMP surface facilities. In accordance with AP-2.13Q (since superceded by ICN 04), *Technical Product Development Planning*, a work plan (CRWMS M&O 1999a) was developed, issued, and utilized in the preparation of this document. Though AP-2.13Q has been superseded by AP-2.21Q, *Quality Determinations and Planning for Scientific, Engineering, and Regulatory Compliance Activities*, it has been determined that this work plan remains in effect for this analysis.

There are constraints, caveats and limitations to this analysis. This cladding degradation analysis is based on commercial Pressurized Water Reactor (PWR) fuel with Zircaloy cladding but is applicable to Boiling Water Reactor (BWR) fuel. Fuel reliability from reactor operation is determined for both PWRs and BWRs. This analysis is also limited to fuel exposed to normal operation and anticipated operational occurrences (i.e. events which are anticipated to occur within a reactor lifetime), and is not applicable to fuel that has been exposed to severe accidents. Fuel burnup projections have been limited to the current commercial reactor licensing environment with restrictions on fuel enrichment, oxide coating thickness, and rod plenum pressures. Ranges and uncertainties have been defined. The information provided in this analysis will be used in evaluating the post-closure performance of the Monitored Geologic Repository (MGR) in relation to waste form degradation.

2. QUALITY ASSURANCE

The Quality Assurance program applies to the development of this analysis documentation. The Performance Assessment Operations responsible manager has evaluated the technical document development activity in accordance with QAP-2-0, *Conduct of Activities*. The QAP-2-0 activity evaluation, *Conduct of Performance Assessment* (CRWMS M&O 1999b), has determined that the preparation and review of this technical document is subject to *Quality Assurance Requirements and Description* DOE/RW-0333P (DOE 2000) requirements. Note that the activity evaluation (CRWMS M&O 1999b) remains in effect even though QAP-2-0 has been superseded by AP-2.21Q, *Quality Determinations and Planning for Scientific, Engineering, and Regulatory Compliance Activities*. Preparation of this analysis did not require the classification of items in accordance with QAP-2-3, *Classification of Permanent Items*. This activity is not a field activity. Therefore, an evaluation in accordance with NLP-2-0, *Determination of*

Importance Evaluations was not required. The methods used to control the electronic management of data as required by AP-SV.1Q, *Control of the Electronic Management of Information*, were not specified in the Development Plan, *Clad Degradation – Abstraction and Summary Analysis Results for Input to TSPA Analysis* (CRWMS M&O 1999a). With regard to the development of this AMR, the control of electronic management of data was evaluated in accordance with YAP-SV.1Q, *Control of the Electronic Management of Data*. The evaluation (CRWMS M&O 2000n) determined that current work processes and procedures are adequate for the control of electronic management of data for this activity. Though YAP-SV.1Q has been replaced by AP-SV.1Q, this evaluation remains in effect.

This AMR has been developed in accordance with procedure AP-3.10Q, *Analyses and Models*.

3. COMPUTER SOFTWARE AND MODEL USAGE

Microsoft Excel for Windows Version 4.0 was used in the analysis to develop a software routine. Excel is commercially available software, and one macro was used. The software routine was run on a Dell personal computer (CPU number 113068 located in the M&O Summerlin offices, Las Vegas, NV) with a Windows NT Workstation 4.0 operating system. The software routine, including the one macro, is documented in Attachments I and II of this AMR in accordance with AP-SI.1Q, *Software Management*, Section 5.1.1. The software routine is contained in file "AMR-F0155-V2.xls" and the version number is two (2) as implied in the file name. This file is contained in Data Tracking Number (DTN: MO0011SPACMU07.049).

There were no models used in support of this analysis activity.

This AMR was documented using only commercially available software (Microsoft Word 97-SR2) for word processing, which is exempt from qualification requirements in accordance with AP-SI.1Q, *Software Management*. There were no additional applications (routines or macros) developed for documentation using this commercial software.

SigmaPlot, Scientific Graphic Software, Version 2.0, Jandel Corporation is used to plot data from the analysis. No calculations are performed with this software.

4. INPUTS

4.1 DATA AND PARAMETERS

This AMR summarizes several other AMRs and generates the cladding degradation abstraction that is to be used in the TSPA-SR. Much of the design information used in this AMR and the cited AMRs is from published literature for Pressurized Water Reactor (PWR) fuel performance and the respective reference is cited where the information is used. The data cited below are appropriate for describing commercial nuclear fuel since they are published descriptions of

commercial fuels. The following AMRs or calculations supply input (with Data Tracking Numbers (DTNs) noted) to this AMR:

a) *Initial Cladding Condition* (CRWMS M&O 2000a).
Contains discussion and analysis of cladding condition as received at YMP.

Data supplied in DTN: MO0001SPAICC48.037.

1) Complementary Cumulative Distribution Function (CCDF) for rods perforated before receipt at Yucca Mountain Project (YMP) (Table 14), used in Section 6.1.
2) Rod pressure and wall thickness distributions is from file = Rod-Initial-C.xls, Sheet = "Crack", Cells = H15 through I2015. The free volume distribution is from file = Rod-Initial-C.xls, Sheet = "Free Volume", Cells = C27 through C2027. These distributions are used to calculate an improved stress in Section 6.2.2. Rod dimensions, given in Table 2 are used for a creep volume correction calculation used in Section 6.2.2.
3) Dry storage history: file = Rod-Initial-C.xls, Sheet = "Creep", Cells B25 through C36, used in Section 6.2.1.
4) Assembly handling damage statistics are taken from Table 8. The conversion of 2.2 rods damaged per damaged assembly is taken from Section 6.8.1. These are used in Section 6.4.1.

b) *CSNF Waste Form Degradation: Summary Abstraction* (CRWMS M&O 2000d).
Intrinsic dissolution rate equation for basic and acidic conditions (Equation 16, 18, page 82) and Figure 12 of this AMR showing the intrinsic dissolution equation. Gap inventories for cesium and iodine as a function of fission gas release fraction. Roughness factors are taken from this reference.

c) *Thermal History of Cladding in a 21-PWR SNF WP Loaded with Average Fuel,* (CRWMS M&O 2000f).

Design information ACC: MOL.20000216.0105.
Radial temperature distribution across the waste package (WP) and change in temperature in WP as a function of time. Peak internal WP temperatures from Table 6-2 are used in Section 6.2.1 for establishing uncertainties. Difference in temperature between rod gas plenum and peak cladding temperature are taken from Table 6-4 and used in Section 6.2.2.

Thermal Evaluation of Breached 21-PWR Waste Packages (CRWMS M&O 1999e).

Design information ACC: MOL.20000120.0447.
Peak internal WP temperature profile from Table 6-7 used for establishing uncertainties. Used in Section 6.2.1.

In-Drift Thermodynamic Environment and Percolation Flux (CRWMS M&O 2000h).

Data used for this AMR: DTN: SN0001T0872799.006.
Bin 4 average temperatures used in Section 6.2.1.

Bin 4 peak temperatures used to define waste package surface temperature uncertainties in Section 6.2.1.

Stainless Steel in Waste Packages for TSPA-SR.(CRWMS M&O 2000k).

Data used from this AMR: DTN: SN0001T0810599.008.
WP fraction with stainless steel cladding and fraction of stainless steel in them. Used in Section 6.7.

Breakage of Commercial Spent Nuclear Fuel Cladding by Mechanical Loading, (CRWMS M&O 1999d).

Design information used from ACC: MOL.19991213.0237.
Frequency of seismic event that damages all cladding determined to be 1.1×10^{-6} events/year. This frequency is used in Section 6.4.1. Static loading from rockfalls fails the cladding (from Section 6.2 of the reference, and used in Section 6.4.1. of this report)

Data Qualification Report: Composition of J-13 Well Water for Use on the Yucca Mountain Project, Revision 0. (CRWMS M&O 2000g, p. 10).

Data used in DTN: MO0006J13WTRCM.000.
Content of fluorides in J-13 water used to calculate fluoride corrosion rate from flow through geometry in Section 6.3. Alkalinity is used to calculate UO_2 dissolution rate in Section 6.5.2.

Outside sources of data include:

CRC Handbook of Chemistry and Physics (Lide 1995).

Accepted data from handbook in TIC: 216194.
The molar masses of H (1.00794 g/mol), C (12.011 g/mol), O (15.9994 g/mol), F (19.0 g/mol), Zr (91.2 g/mol), and U (238.0289 g/mol) taken from the inside cover are used in Sections 6.5.2 and 6.6.1. Density of UO_2 and zirconium, taken from page 4-94 through 4-98, are used in 6.3, 6.5.2, and 6.6.1.

4.2 CRITERIA

The criteria that were specified in the Development Plan for this AMR (CRWMS M&O 1999a, Section 3) were used. In addition, the U.S. Nuclear Regulatory Commission's (NRC's) Total System Performance Assessment and Integration (TSPAI) Issue Resolution Status Report (IRSR) (NRC 1999) establishes generic technical acceptance criteria considered by the NRC staff to be essential to a defensible, transparent, and comprehensive assessment methodology for the repository system. These regulatory acceptance criteria address four fundamental elements of the DOE TSPA analysis for the Yucca Mountain site, namely:

Data and analysis shall address their justification (The AMR shall focus on sufficiency of data to support the conceptual basis of the process analysis and abstractions)

1. The AMR shall address the data uncertainty and verification (focusing on technical basis for bounding assumptions and statistical representations of uncertainties and parameter variabilities)

2. Analysis uncertainty shall be addressed (focusing on alternative conceptual analysis consistent with available site data)

3. Analysis verification shall be addressed (focusing on testing of analysis abstractions using detailed process-level analysis and empirical observations)

4. Integration shall be addressed (focusing on appropriate and consistent coupling of analysis abstractions).

Relevant to the topic of this AMR, elements (1) through (4) of the acceptance criteria are addressed herein. Element (5) of the acceptance criteria, which strictly applies to the completed synthesis of process-level analysis and abstractions, will be addressed separately in the Total System Performance Assessment-Site Recommendation (TSPA-SR).

In addition, a second NRC IRSR Key Technical Issue: Container Life and Source Term (NRC 1999) establishes generic technical acceptance criteria used by the NRC staff for the waste form, with the cladding degradation abstraction being part of this Key Technical Issue (KTI). Section 7 describes how this AMR addresses the IRSR issues.

4.3 CODES AND STANDARDS

American Society for Testing and Materials (ASTM) Standard C1174-97–*Standard Practice for the Long-Term Behavior of Materials, Including Waste Forms, Used in Engineered Barrier Systems (EBS) for Geologic Disposal of High-Level Radioactive Waste* (ASTM 1998) is used to support the degradation analysis development methodology, categorize the analysis developed with respect to its usage for long-term TSPA, and relate the information/data used to develop the analysis to the requirements of the standard.

This AMR was prepared to conform with the above NRC TSPAI acceptance criteria, as well as the DOE interim guidance (Dyer 1999) which requires the use of specified Subparts/Sections of the proposed NRC high-level waste rule, 10 Code of Federal Register (CFR) Part 63 (64 FR 8640). Subparts of this proposed rule that are particularly applicable to data include Subpart B, Section 15 (Site Characterization) and Subpart E, Section 114 (*Requirements for Performance Assessment*). Subparts applicable to analysis are outlined in Subpart E, Sections 114 (*Requirements for Performance Assessment*) and 115 (*Characteristics of the Reference Biosphere and Critical Group*).

5.0 ASSUMPTIONS

5.1 CLADDING CONDITION AS RECEIVED

5.1.0 It is assumed that the spent fuel (CSNF) that is accepted for disposal in the repository will have characteristics similar to those described in the sources listed in Table 1. The basis for this assumption is: 1) the information in Table 1 was collected for a broad range of fuels, 2) it is compared with other sources in Section 6, 3) the information was measured on actual spent nuclear fuel of the various types currently in use or in storage at nuclear facilities, 4) this technical information was generally produced under NRC-accepted or foreign-nuclear-agency-accepted nuclear quality assurance programs, and 5) much of this information was produced to support the licensing process for the fuel. Column 1 of Table 1 gives the technical information, Column 2 provides the source, and Column 3 gives the section where the specific assumption is used. These assumptions are used to develop statistical distributions (ranges) for the properties of the fuel to be received (Sections noted in Table 1).

5.1.1 It is assumed that the Waste Packages (WP) will be loaded with spent fuel in the order of discharge of the fuel from the various reactors as a function of calendar years. This generates some variability in the fraction of rods failed within a WP. This loading sequence tends to place fuel with higher cladding failure rates into the same WP or consecutively loaded WPs and produces larger variations in rod failure fractions than would be expected if thermal blending were employed. This is a credible and reasonable assumption based on the fuel that current owners would be expected to ship first (Section 6.1).

5.1.2 Each failed Pressurized Water Reactor (PWR) fuel assembly has an average of 221 rods and has an average of 2.2 failed fuel rods. The basis for the average of 2.2 failed fuel rods per failed assembly is described in the Initial Cladding Condition AMR (CRWMS M&O 2000a). This failure value applies for the early years of nuclear reactor power operations in the US (the 1960s and 1970s) and the number of failed rods per failed assembly has decreased to be closer to one (1) today. It is reasonably bounding to apply this failure rate for all time since it increases the fuel available for unzipping (Section 6.1).

5.1.3 It is assumed that all rods are exposed to the conditions of dry storage with the center rod in the cask operating at the design temperature history of the Castor Mark V (CRWMS M&O 2000a) cask after being vacuum dried using a temperature history defined by Spilker and Fleish (1986, Figure 14). The maximum cladding temperature during vacuum drying is assumed to be 430°C (Nuclear Assurance Corporation 1999, p.8.1-50. This assumption also includes the vacuum drying time of 24 hours. This is reported by both Spilker and Fleish and Hopf 1999, Table 2-1. The vacuum drying times are restricted to maintain a maximum cladding temperature during drying. Comparisons of reported peak cladding temperatures given in Section 6.2.1 also justifies the use of 430°C as a peak cladding temperature. The bases for the assumption The design temperature of the Castor Mark V cask with 55 MWd/kgU burnup fuel was selected to be reasonably bounding for the dry storage period since actual temperatures

are lower than design temperatures. Sensitivity studies presented in Section 6.2.4 show that these temperature assumptions are not critical and do not need verification (Section 6.2.1).

Table 1. Technical Information on Fuel Characteristics

Technical Information	Source	Section cited in AMR
Vacuum drying temperature axial profile and history	Spilker and Fleisch 1986. Figure 14	6.2.1
Maximum vacuum drying temperature	Nuclear Assurance Corporation 1999. P. 8.1-50	6.2.1
Dry storage history and maximum temperature	Peehs 1998, Figure 13a	6.2.1, Figure 2
Creep strain measurements, Irradiated Cladding	Kaspar et al. 1985. pp. 56, 57.	6.2.2
Creep strain measurements, Irradiated Cladding	Einziger and Kohli 1984. Table III.	6.2.2
Creep strain measurements, Irradiated Cladding	Chung et al. 1987. Tables 1, 2	6.2.2
Creep strain measurements, Irradiated Cladding	Bredel et al. 2000, p.14	6.2.2
Creep strain measurements, Irradiated Cladding	Goll et al. et al. (Macheret 2000, Att. 2,Tables 6, 7)	6.2.2
Strain failure measurements, Irradiated Cladding	Chung et al. 1987. Tables 1, 2	6.2.3, Table 6
Strain failure measurements, Irradiated Cladding	Garde 1986. Tables 17,18,19	6.2.3, Table 6
Strain failure measurements, Irradiated Cladding	Garde et al. 1996. Tables 1, 2	6.2.3, Table 6
Strain failure measurements, Irradiated Cladding	Goll et al. et al. (Macheret 2000 Att. 2, Figure 8)	6.2.3, Table 6
Release fractions of Np through failed cladding	Wilson 1985. Tables 3, 12	6.5.2
Release fractions of Np through failed cladding	Wilson 1987. Tables 13, A.3, A.4, A.7, and A.8	6.5.2
Release fractions of Np through failed cladding	Wilson 1990. Tables 13.8, A.5, and A.6	6.5.2
Stress failure threshold for SCC	Tasooji et al. 1984. Figure 3	6.2.5
Crack Dimensions for cladding unzipping	Wilson 1990, p. 2.7, Figure 2.3	6.5.2

(DTN: MO0011SPACMU07.049)

5.1.4 It is assumed that no further creep damage occurs during shipment. Most rods will actually be exposed to lower temperatures for a shorter time frame during shipment because of the age of the fuel and the assumption that it is exposed to dry storage for 20 years. Since CRWMS M&O 2000a, Figure 25 shows little additional creep occurs from shipping after dry storage no further verification is necessary. Fuel stored in spent fuel pools will undergo no creep and assuming dry storage is conservative (Section 6.2.1).

5.1.5 It is assumed that the uncertainty value for the rod failure data is four (4). This is based on a square pitch array of fuel rods in the fuel assembly. The rods more likely to have damage are these rods near the damaged rod. There are four rods near the damaged rod in a square pitch. This is bounding when compared to operating experience which shows reliability improves with time in reactor (little incipient failures)and no further confirmation is needed (Section 6.1).

5.1.6 It is assumed that BWR cladding degrades in a similar manner as the base case PWR fuel. This is reasonably bounding since, in comparison to PWR fuel, the BWR cladding is thicker, the BWR fuel typically is discharged with lower burnups and stresses, and each BWR fuel assembly is enclosed in a flow channel for additional protection. BWR fuel also operates at a lower pressure and has lower flow rates (less erosion). No further conformation is needed (Section 6.1).

5.1.7 It is assumed that no further cladding degradation occurs at the YMP surface facilities. This is accomplished by appropriate operating and administrative procedures. Sufficient care will be exercised in these facilities such that damaging the cladding which would lead to radionuclide contamination, higher operating expenses, and greater radiation risk to employees, does not occur. Analysis of handling errors in Section 6.4.1 supports this assumption and no further conformation is needed (Section 7).

5.2 CREEP AND SCC FAILURE

5.2.1 It is assumed that creep is analyzed using a Modified Murty correlation. *Comparison of Creep Correlations* (CRWMS M&O, 2000j) compares the various creep correlation. Both Murty's correlation and Matsuo's correlation (Matsuo 1987, p. 23) fit the available data almost equally well. Murty's correlation was selected because it explicitly considers Coble Creep, a type of creep that could be important at lower stresses and temperatures. This assumption also considers that the creep measurements of irradiated cladding performed by Kaspar et al. 1985 (pp. 56, 57), Einziger and Kohli 1984 (Table III), Chung et al. 1987 (Tables 1,2), Bredel et al. (2000, page 14), Goll et al. (Macheret 2000, Attachment 2, Tables 6, 7) represent typical commercial fuel and these measurements can be used to modify the Murty correlation to better predict creep of irradiated cladding. *Creep Strain Values and Correlation for Irradiated Spent Nuclear Fuel,* Input Transmittal PA-WP-00383.Ta, (CRWMS M&O, 2000m) gives a Modification of Murty creep correlation (page 1) and the average relative error factor of 1.79 is given on Item Line 224. Since the Modified Murty correlation is compared to over 200 experimental measurements, no further confirmation of this creep correlation is needed. The uncertainty in the creep correlation is 0.80, the maximum error range for the Modified Murty correlation. The uncertainty is assumed to be uniformly distributed with the calculation of creep for all the rods and varies in the range of ±80% (Section 6.2.2).

5.2.2 It is assumed that the creep failure distribution is determined by a series of tests by Chung et al. 1987 (Tables 1 and 2), Garde 1986 (Tables 17, 18, 19), Garde et al. 1996 (Tables 1 and 2), Goll et al. (Macheret 2000, Att. 2, Figure 8), and that these series of

tests on commercial fuel is representative of the fuel that is received at the repository. The use of this failure criterion accounts for crack damage, spalled oxide, and possibly weaker cladding types (i.e. BWR fuel) as described in Section 6.2.3. Since test results of 52 experiments are used in this failure distribution, no further confirmation is needed (Section 6.2.3).

5.2.3 It is assumed that any rod with a stress greater than 180 MPa is assumed to fail from Stress Corrosion Cracking (SCC). This is based on both experiments and analysis presented by Tasooji et al. (1984, p. 600, Figure 3). This assumption also considers that these experiments on Zircaloy cladding is representative of the behavior of the cladding that is received at the repository. In this AMR, sufficient iodine is assumed to exist such that SCC occurs at the stress threshold of 180 MPa. Pescatore et al. 1990 (p. 108) reviewed the information on SCC and concluded that the threshold of 200 MPa was applicable. A threshold of 180 MPa is a reasonable bounding assumption and needs no further conformation (Section 6.2.5).

5.3 LOCALIZED CORROSION

5.3.1 It is assumed that localized corrosion by aggressive species can be analyzed by idealized corrosion of fluorides. It is assumed that corrosion of the cladding is limited by the supply of fluoride. Fluoride is known to form salts and not act as a catalyst when corroding zirconium. The rationale for this assumption is that little information is available on the rate of consumption of fluoride in a waste package. In the absence of information, a bounding approach is needed. Since the assumption is an upper limit, no confirmation is necessary (Section 6.3).

5.3.2 It is assumed that fluoride attack is assumed to completely degrade the cladding on a 10 mm length of one fuel rod before degradation begins on another rod. This length represents a reasonable drip width. The corrosion of one rod at a time is not an important assumption. If the fluoride attacks 10 rods at a time, the corrosion rate would be one tenth and the results would be the same. If the fluoride attacks all the zirconium in the WP (a fully mixed bath tub scenario) the cladding would not fail in a million years because of the large amount of zirconium in the WP and the small amount of fluorides in the J13 well water. This corrosion mechanism requires the fluoride to travel in a flow path and discretely attack only limited sections of a rod. The rationale for this assumption is that little information is available on how corrosion is distributed within a waste package. This assumption is reasonably bounding because each rod breaches as soon as enough fluoride is available; there is no delay in breaching one rod because fluoride is being diverted to start the degradation of another. Since the assumption is a reasonable bound, no confirmation is necessary (Section 6.3).

5.3.3 It is assumed that all fuel rods are subject to fluoride corrosion. The rationale for this assumption is that little information is available on how water flows within a waste package. This assumption is a reasonable bound because each rod is exposed to water and therefore subject to fluoride corrosion. Under many exposure conditions, some of

the fuel rods would be out of the flow path. In those cases, only the fuel rods in the flow path would be subject to fluoride corrosion. Since the assumption is an upper limit, no confirmation is necessary (Section 6.3).

5.3.4 In determining the amount of fluoride that is necessary to breach a fuel rod, it is assumed that fluoride removes all the cladding from a 10-mm length of the fuel rod. The rationale for this assumption is that this width is comparable to the width of typical water drop splat sizes and water flow paths. However, the actual wetted width would be wider because the rough, porous products of corrosion on the surface of fuel rods would tend to wick water and promote wider flow paths. Since this assumption is a reasonable bound, it does not require verification (Section 6.3).

5.4 OTHER FAILURE MECHANISMS

5.4.1 It is assumed that a severe seismic event fails all of the cladding. Seismic analysis showed that rods would fail from a very severe earthquake (a once per million year event) and that most of the rods would fail. Therefore, in the TSPA-SR, the seismic event is assumed to have a frequency of 1.1×10^{-6} /yr and it is assumed that all the cladding is failed at the rod center and available for clad unzipping when a seismic event occurs. Failing all the rods is an upper limit and failing the rods in the center minimizes the release time for unzipping. Since this assumption is a reasonable bound, it does not require verification (Section 6.4.1).

5.4.2 It is assumed that a static loading from rockfalls onto the fuel assemblies fails the cladding. The rocks fall onto the WP well before the WP fails and cladding failure starts when 50% of the WP patches are open permitting sufficient rock pressure to start static loading on the assemblies. Cladding failure increases linearly to 100% failure when all the patches on the WP are open. Since this assumption is a reasonable bound, it does not require verification (Section 6.4.1).

5.5 FAST RELEASE OF RADIONUCLIDES

5.5.1 It is assumed that the absolute rate of fast release of radionuclides from a breached fuel rod is proportional to the length of the rod. Results for short rod segments are used to predict the performance of full-length rods, and the same fractional release rate is used for both. The rationale for this assumption is that, over the time necessary to plug the cracks in a fuel rod, the characteristic distance for aqueous diffusion is comparable to the active length of a fuel rod (Section 6.5.2). The assumption could be inaccurate if transport limitations result in smaller release rates, and in that case the assumption would be reasonably bounding. Since this assumption is both realistic and a reasonable bound, it does not require verification (Section 6.5).

5.5.2 It is assumed that, during the fast release phase, the fuel reacts with water to form metaschoepite. This assumption is consistent with a similar assumption for the unzipping phase. Reaction products with a large volume increase would tend to produce small fast release fractions (because cracks would plug quickly) and fast

unzipping, whereas reaction products with a small volume increase would tend to produce larger fast release fractions and slower unzipping. However, the fast release fraction is small, so it is reasonably bounding to favor fast unzipping. Since the assumption is reasonably bounding, no confirmation is necessary (Section 6.5).

5.5.3 It is assumed that the measured releases of technetium (Tc) in three sets of experiments represents the expected behavior of the commercial spent fuel received at YMP. Wilson performed a series of three (Wilson, C.N. 1985, Tables 3 and 12; Wilson, C.N. 1987, Tables 13, A.3, A.4, A.7, and A.8; Wilson, C.N. 1990, Tables 3.8, A.5, and A.6). In these tests commercial spent fuel, which was intentionally perforated, was perforated was placed in J13 water and Tc releases were measured. Technetium release is a measure of the fuel dissolution because of its high solubility (Section 6.5.2).

5.6 CLADDING UNZIPPING AND FUEL DISSOLUTION

5.6.1 It is assumed that, during the unzipping phase, the fuel reacts with water to form metaschoepite. Oxidation and hydration of uranium dioxide can result in a variety of mineral species. Of these, metaschoepite is the one that entails the largest change in volume, and larger volume increases correspond to faster degradation. Other uranium minerals (such as sodium boltwoodite) can also be formed from uranium dioxide, but these require a supply of a solute (such as sodium), so the rate of formation will be limited by the supply of solute. Therefore, the rationale for this assumption is that conversion to metaschoepite provides the largest plausible volume increase. Since the assumption is reasonably bounding, no confirmation is necessary (Section 6.6).

5.6.2 It is assumed that the rate of reaction of the uranium dioxide with water is controlled by the intrinsic dissolution rate of UO_2. The rationale for this assumption is that this is the fastest rate at which reaction can advance into a uranium dioxide pellet surface. If the products of reaction of UO_2 limit the transport of water to the uranium dioxide surface, the reaction will necessarily be slower. Since this assumption is reasonably bounding, no confirmation is necessary (Section 6.6).

5.6.3 It is assumed that all cladding breaches occur at the center of the active fuel length. The rationale for this assumption is that this location provides the fastest unzipping of a fuel rod. If the breach is at the center of the active fuel length, propagation of the breach by a distance of half the active fuel length (toward each end) will result in complete unzipping of the active fuel length of the rod. If the breach is at some other location, the required propagation distance will be larger for one end. Since this assumption is reasonably bounding, no confirmation is necessary (Section 6.6).

5.6.4 It is assumed that reported crystallographic results on uranium compounds are applicable to fuel that will be disposed in the repository. The rationale for this assumption is as follows. Nuclear fuel starts as uranium dioxide, and weathering in a repository is expected to produce minerals that are seen in nature. Because of the strength of the rationale, this assumption does not require confirmation.

Crystallographic results reported by Finch et al. (1992, Table 2, column labeled "β-$UO_3 \cdot 2H_2O$") yield a molar volume of 64.5 cm^3/g for metaschoepite. For a discussion of how the molar volumes are calculated, see Cunnane (2000, pp. 140-142). The mineralogical terminology of Cunnane is used here (Section 6.6).

5.6.5 It is assumed that, during the unzipping phase, the fuel acts as a monolithic cylinder, that is, cracks in pellets and joints between pellets fill with alteration products and are sealed by them. The rationale for this assumption is that alteration products filling a gap will block transport of water. Without water as an oxygen source, oxidative conversion of spent fuel to metaschoepite cannot proceed. Since this assumption is based on standard chemical principles, it does not require confirmation (Section 6.6).

5.6.6 It is assumed that, during the unzipping phase, the linear molar density of uranium (moles of U per meter of fuel rod) is the same after oxidation as before oxidation. This is equivalent to assuming that no fuel falls out of the rod. The rationale is that this is a bounding assumption: any loss of fuel will reduce the severity of splitting. Since the assumption is bounding, it does not require confirmation (Section 6.6).

5.6.7 It is assumed that, during the unzipping phase, enlargement of the fuel is accommodated by splitting rather than stretching of the cladding. The rationale is that this is a bounding assumption: any stretching will reduce the severity of splitting. Since the assumption is bounding, it does not require confirmation (Section 6.6).

5.6.8 Three alternative assumptions are made concerning contact of water with the fuel during the unzipping phase: (a) Once a given length of cladding is split, water has free access to the surface of the fuel that is surrounded by that length of cladding. In other words, oxidation proceeds inward from the circumference of the fuel, not just from the split. (b) Once the cladding is split, water has access to the surface of the fuel only where the fuel is exposed by the split. In other words, oxidation proceeds outward from the split. (c) In spite of splitting, water has access only to the circular end of the fuel stack. The rationale is that these water contact areas correspond to reasonable geometries. The assumptions provide an upper bound, a reasonable mode, and a lower bound on the extent of exposure to water. Since the assumptions cover the range of possibilities, they do not require confirmation (Section 6.6).

5.6.9 It is assumed that the apex angle of a split in a fuel rod is proportional to the ductility or fracture toughness of the cladding. The rationale is that split propagation involves deformation and fracture of the material near the tip of the split. Since this assumption is based on standard principles of mechanical metallurgy, it does not require confirmation (Section 6.6.1).

5.6.10 It is assumed that the cracks in the fuel pellet have the dimensions as shown by Wilson 1990, p. 2.7, Figure 2.3. This figure is of commercial nuclear fuel (Turkey Point PWR fuel) is typical of the commercial fuel received at the repository. The crack selected for analysis is the largest in the figure and the analysis is not sensitive to this dimension since uncertainties are assigned to the fast release fraction. Since this assumption is reasonably bounding, no confirmation is necessary (Section 6.6).

5.7 STAINLESS STEEL CLADDING

5.7.1 It is assumed that the stainless steel (SS) clad fuel is loaded into WPs as it is received at the YMP facilities. This is used to define the number of WPs containing SS cladding and the fraction of SS cladding in these WPs. The basis of this assumption is that it simplifies surface facility operations. This assumption is not critical since the product of WPs containing SS cladding and fraction of SS in each WP is constant (i.e. there is a fixed amount of SS cladding) (Section 6.7).

6. ANALYSIS

Earlier studies (Ahn et al. 1999, Henningson 1998, Rothman 1984, Pescatore et al. 1990, Manaktala, 1993) have evaluated cladding degradation under repository conditions. Others (Cunningham et al. 1987, Peehs 1998, Einziger and Kohli 1984) evaluated fuel performance under dry storage conditions, which are similar to early repository conditions. As part of the Environmental Protection Agency's development of environmental standards, S. Cohen & Associates (1999) did a detailed study of cladding degradation, both before reception at a repository and in the repository. Sanders et al. (1992) reviewed the condition of cladding after reactor operation and reviewed the potential of damage from external mechanical loading. Experiments (Wilson 1985, 1987, 1990) also measured the releases from damaged cladding. The Yucca Mountain Project (YMP) 1998 Total System Performance Assessment Viability Assessment (TSPA-VA, CRWMS M&O 1998b) included cladding degradation as part of the fuel degradation analysis. TSPA-1995 (CRWMS M&O 1995), a previous analysis of repository performance, neglected the presence of cladding, as did most earlier performance assessments (PAs). In doing so, all the fuel in the Waste Package (WP) was considered available for dissolution at the speed of the intrinsic fuel dissolution rate. For some radionuclides, solubility limits were reached which controlled the rate of those radionuclides leaving the WP.

In the Total System Performance Assessment Site Recommendation (TSPA-SR), the cladding is considered an integral part of the waste form. Screening criteria for principal factors or potentially disruptive events are discussed in *Managing Technical Product Inputs*, AP-3.15Q. This analysis is classified as "Level 2" since it does support "Commercial Spent Nuclear Fuel Waste Form Performance" which is not classified as a principal factor.

The cladding degradation abstraction summarizes numerous studies of cladding degradation and is incorporated into the TSPA-SR computer analysis as an abstraction. The abstraction consists of two phases, cladding perforation and cladding unzipping. Cladding perforation is the formation of small cracks or holes in the cladding from various sources ranging from failures during reactor operation to cladding creep rupture during repository storage. Perforation permits the fuel inside the cladding to begin to react with moisture or air and potentially leads to the cladding unzipping phase. In the unzipping phase, the cladding is torn open by the formation of secondary mineral phases on the UO_2 fuel, and the radionuclides are available for release. The various components of the abstraction are discussed below.

The numbers reported in this section are given to three (3) figures to assist in making the numbers more traceable. This analysis is considered accurate to only the first significant figure, that is, accurate to approximately 80% to 90%. The remaining figures are only reported for traceability.

6.1 CLADDING CONDITION AS RECEIVED

The Initial Cladding Condition AMR (CRWMS M&O 2000a) describes the condition of the commercial nuclear fuel as it is expected to be received at the YMP site. This analysis generates the initial boundary condition for the subsequent analysis of degradation of the cladding in the repository. It also evaluates the fraction of fuel rods that are perforated before emplacement in the repository and are immediately available for cladding unzipping when the WP fails.

A distribution for the fraction of cladding within a WP that failed as a result of reactor operation was developed from the fraction of rods failed as a function of calendar years by presuming that the fuel assemblies are loaded into WPs in their order of discharge from the reactors. This is the Complementary Cumulative Distribution Function (CCDF) shown in Table 2. This loading sequence tends to place fuel with high failure rates (BWR fuel in 1970 and also in 1973-1976, and PWR fuel in 1972, 1983, and 1989) into the same or consecutive WPs and produces larger variations in rod failure fractions than would be expected if thermal blending were employed. A factor of four uncertainty was applied to represent the uncertainty in rod failure data. Rod failure from dry storage (0.045% of rods failed per WP) and transportation (vibration and impact, at 0.01% of rods failed per WP) were also included (CRWMS M&O 2000a, Section 7). Failure from creep during dry storage and transportation is included with the creep analysis presented in Section 6.2 of this AMR. Table 2 gives the distribution of rods that have failed cladding at emplacement in the repository. This table is the same as Table 14 of CRWMS M&O 2000a and is given in the Excel file: fuel-rel.xls, cells G112 through J134 of DTN: MO0001SPAICC48.037. In the TSPA-SR, the WPs are grouped into 5 bins, each representing approximately 1500 CSNF WPs. Table 2 represents the distribution of individual WPs and cannot be applied to the individual bins because of the limited number of WPs represented by the distribution tail. For example, the very far point of the distribution is represented by the BWR fuel discharged in 1970 with 4.5% of the rods failed. That year, only 29 assemblies were discharged, about 70% of a single BWR WP containing 44 assemblies. In sampling for a bin or group of 1500 WPs, it would be incorrect to represent the whole group by an individual WP that exists in such small numbers. For the TSPA-SR abstraction of bins or groups, the bins are represented by the 98% to 5% range of the CCDF in Table 2 with the median representing the mode. A triangular distribution was assigned. In summary, the initial failure percentage for the rods in a WP in the TSPA-SR for the five bins or groups of WPs is represented by:

Minimum = 0.0155%
Mode = 0.0948%
Maximum = 1.285%

and the probabilistic distribution is triangular. These percentages of fuel rods undergo cladding unzipping and fuel dissolution when the WP fails.

As received at YMP, the cladding of rods that are not perforated also has an internal pressure resulting from reactor operation and therefore will be stressed. The creep strain calculations in

this AMR use the rod characteristics developed in the Initial Cladding Condition AMR. This includes the internal pressure distribution, (CRWMS M&O 2000a, file = Rod-Initial-C.xls, Sheet = "Crack", Cells = K15 through M2014). The cladding analysis is based on the Westinghouse 17 x 17 fuel design. This design represents over 30% of the PWR fuel discharged to date and is also the thinnest Zircaloy cladding design. The BWR cladding degrades in a similar manner. This is reasonably bounding since BWR cladding is thicker, is discharged with lower burnups and stresses, and is enclosed in flow channels for additional protection. Starting with a distribution of PWR fuel burnups that are anticipated for storage at YMP, distributions for various cladding properties were developed, culminating with the room temperature stress distribution represented by Figure 1.

Table 2. CCDF of Rod Perforation for As-Received Fuel

CCDF	Lower Uncertainty,%.	Mode % Failure	Upper Uncertainty, %
1.000	0.0138	0.0550	0.220
0.999	0.0146	0.0585	0.234
0.985	**0.0155**	0.0622	0.249
0.856	0.0179	0.0717	0.287
0.655	0.0212	0.0849	0.340
0.582	0.0224	0.0895	0.358
0.506	0.0237	**0.0948**	0.379
0.271	0.0284	0.1136	0.454
0.1966	0.0361	0.1445	0.578
0.1084	0.0507	0.2028	0.811
0.0970	0.0522	0.2089	0.836
0.0766	0.0741	0.2965	1.186
0.0640	0.0746	0.2983	1.193
0.0503	0.0803	0.3213	**1.285**
0.0373	0.1248	0.4990	1.996
0.0323	0.247	0.9875	3.95
0.0221	0.289	1.1568	4.63
0.0196	0.450	1.7985	7.19
0.0190	0.509	2.035	8.14
0.0115	0.694	2.776	11.10
0.0036	0.763	3.051	12.20
0.0002	1.321	5.286	21.14
0.0000	1.321	5.286	21.14
DTN: MO0001SPAICC48.037			

6.2 CREEP STRAIN AND SCC FAILURE

The current repository design does not utilizes backfill but future design options might affect the waste package (WP) and therefore cladding temperatures. In this analysis, the WP surface temperature is treated as an independent variable. A statistical distribution of rod properties has been developed so that creep failure is included in the analysis. All the rods are exposed to a temperature history that includes a vacuum drying period followed by 20 years of dry storage. Transportation effects are neglected since they follow 20 years of dry storage cooler

temperatures are expected. Rods at six zones across the WP are evaluated, and modified version of Murty's creep strain correlation is used. The failure strain criterion is a distribution based on fifty two (52) tests of irradiated cladding. The peak surface temperature of the WP is varied and the fraction of rods failed is calculated. The following sections discuss the analysis in more detail.

6.2.1 Temperature History

The rods are first exposed to 24 hours of vacuum drying that is shown in the left hand side of Figure 2. The shape of this temperature history was taken from Spilker and Fleisch (1986, Figure 14). In addition, the difference in temperature between the maximum cladding temperature and the cladding plenum temperature is taken from location 14 and 15 in their Figure 14. This is used to more accurately calculate the rod pressure as a function of time. The peak cladding temperature during drying is design sensitive. Spilker and Fleisch (1986, Figures 13 through 16) report peak temperatures of 425°C (Castor Ic), 500°C (Castor Ib, shown in Figure 2), 400°C (Castor Ia), and 340°C (TN-1300). The Nuholms-24P design has a maximum cladding temperature during vacuum drying of 410°C (Nutech 1989, p. 8.1-50). During 10 hours of drying, in the NAC-MPC design, the fuel could heat up to a maximum of 217°C (Nuclear Assurance Corporation 1999, p. 4.4-42) and a maximum allowable temperature of 430°C is reported. For the Westflex W21 storage canister (Hopf 1999, Figures 2-1 and 2-2), the maximum cladding temperature during the vacuum drying is restricted to be less than 400°C. These figures also show that the average cladding temperature across the peak rod is 350°C, 50°C less than the maximum cladding temperature. The plenum temperature is used to calculate the stress as a function of time.

In studying the potential for cladding damage during the drying period, a sensitivity study was performed by increasing the drying temperature profile (left side of Figure 2) and calculating the fraction of rods that fail from creep after drying and 20 years of dry storage. The storage period will start at a maximum temperature of 350°C). For other studies, the maximum cladding temperature of 430°C during drying was used. This is maximum allowable temperature for the NAC-MPC design cited above. Having a maximum cladding temperature of 430°C and using the same temperature uncertainties as the WP design (+/- 13.5% uniformly distributed, discussed in later paragraphs of this section), the peak temperature of both the mean and median rod in the center of the canister will be 372°C, 58°C less than the maximum.

After vacuum drying, the rods are exposed to a temperature history that includes 20 years of dry storage starting at a maximum of 350°C and then decreasing during time (CRWMS M&O 2000a, Section 6.10.1, cladding initial condition data, file = Rod-Initial-C.xls, Sheet = "Creep", Cells B25 through C39). Best estimate dry storage temperatures were not available at the time of this analysis and the peak (center rod) temperature history for the Castor V package with 55 MWd/kgU fuel (Peehs 1998, his Figure 13a) was used in this analysis. These temperatures were given for the first ten years and have been extrapolated to 20 years. This temperature history is shown on the right hand side of Figure 2. The Nuholms-24P design has a maximum cladding temperature during storage of 349°C (Nutech 1989, p. 4-7). In the NAC-STC-TSAR, (NAC 1993, p. 4.4-1 and 4.4-29) a maximum allowable temperature of 360°C and the predicted temperature is 346°C is cited. For the Westflex W21 storage canister (Hopf 1999, Figures 2-1 and 2-2), the peak cladding temperature during the dry storage is 380°C for the maximum and

340°C for the average cladding across peak rod. Plenum temperatures during the dry storage period were not available. The difference in temperature between the plenum and rod peak cladding was interpolated from vacuum drying temperature differences and early repository temperature differences. The estimate of plenum temperature is used to estimate the plenum pressure and therefore, the stress.

In studying the potential of cladding damage during the dry storage period, a sensitivity study will be performed by increasing or decreasing the dry storage temperature profile (right side of Figure 2) and calculating the fraction of rods that fail from creep after drying and 20 years of dry storage. For this study, the maximum cladding temperature of 430°C during vacuum drying will be used. Having a maximum cladding temperature of 350°C during dry storage and using the same temperature uncertainties (+/- 13.5% uniformly distributed, discussed in later paragraphs of this section), the temperature of both the mean and median rod in the center of the canister will peak at 303°C, 47°C less than the maximum rod. For the vacuum drying sensitivity studies and the YMP WP surface temperature studies, the maximum cladding temperature during dry storage will start at 350°C.

After vacuum drying and 20 years of dry storage, the fuel is shipped to the YMP facility. Any creep damage during shipping has been neglected. After 20 years of dry storage, the temperatures would be low and earlier studies (CRWMS M&O 2000a, Figure 25) shows that even at maximum shipping temperatures, little damage occurs.

For storage in the WP, the temperature distribution across the WP was obtained from CRWMS M&O 2000f. These temperatures are reproduced in AMR-F0155-V2.xls, Sheet "TempC2", Cells = D5 through U44. This temperature distribution varies both radially across the WP and with time. Figure 3 shows the location of the different temperature nodes. The WP internals were divided into 6 zones, which are also shown in Figure 3. An estimate of the fraction of each assembly in each zone is made by visual inspection of Figure 3. Table 3 gives the fraction of rods in each zone and the temperature nodes used to calculate the zone temperature. The temperature of the WP surface was obtained from CRWMS M&O 2000h. Temperatures for 5 bins, grouped by water ingression, were supplied in CRWMS M&O 2000h and are shown here as Figure 4. The bin numbers are assigned by increasing water ingression rate with Bin 4 representing 20 to 60 mm/year water ingression. This AMR uses Bin 4 with water ingression in the range of 20 to 60 mm/yr. Bin 4 has one of the widest temperature peaks and therefore could produce the most creep but, more importantly, it also represents over 53% of the WPs. Figure 5 shows the WP surface temperature, temperature increase across the WP, and center rod temperature. Figure 6 shows the total center rod temperature profile used for the creep analysis. This profile (reading from left to right) shows dry storage for 20 years starting at 350°C, three (3) weeks of shipping at 350°C, preclosure with forced ventilation for 50 years, and then the postclosure temperature profile. This profile extends for 1000 years although only 200 years are shown on the figure. All rods undergo identical dry storage and shipping conditions. The creep analysis of the different phases of the life cycle of the rods must be integrated so that the creep components from the various stages (dry storage, shipping) are added. Creep failures during dry storage are combined with the creep failures during shipping because the damage is cumulative.

Table 3. Fuel Rod Zones in a WP

Zone	Assemblies	Fraction of Rods	Temperature Nodes	Temperature (°C) Scaling Factor
1	0.4	0.019	1	1.000
2	0.6	0.029	Avg, 1 & 2	0.933
3	2.4	0.114	Avg, 5 & 6	0.888
4	4.4	0.210	Avg, 6 & 7	0.820
5	7.0	0.333	Avg, 9 & 10	0.661
6	6.2	0.295	Avg,10 & 11	0.446
Sum	21	1.0	N/A	N/A

DTN: MO0011SPACMU07.049

Temperature uncertainties are also included in the creep strain analysis. The difference between the maximum WP surface temperature for Bin 4 and the average WP surface temperature is 22.1°C (CRWMS M&O 2000h) (see Figure 8 of this AMR). The uncertainty in WP internal temperature was 19.5°C (at peak times), which is the difference in peak temperature between a helium filled WP (CRWMS M&O 2000f, p. 29) and an air/water vapor filled WP (CRWMS M&O 1999e, p. 38). These differences sum to 41.6°C and represent an uncertainty of 13.5% above the peak temperature for the average WP of 308°C. The uncertainty is uniformly distributed with a range of ± 13.5%. The uncertainty in the WP internal power was neglected because of the small predicted uncertainty (CRWMS M&O 1999c, Item 1, p.1/1). This uncertainty is also applied during vacuum drying and dry storage. For plenum pressure calculations, the time dependent difference between the plenum temperature and peak cladding temperature is taken from CRWMS M&O 2000f, Table 6-4. These are interpolated for the appropriate time steps in Attachment II, sheet = "TempC2", Cells J46 through K91.

The creep analysis is performed for 12,000 fuel rods. The initial room temperature stress as received at YMP for each of 2000 rods is determined from the CCDF in Figure 1. A rod with each of these 2000 initial stresses is then placed into each of the six WP zones (totaling 2000 rods/zone x 6 zones = 12,000 rods) and is exposed during repository storage to the temperature profile predicted for that particular zone (with uncertainty included). The temperature scaling factors to calculate the temperature of a rod in each zone are given in Column 5 of Table 2. The temperature of the center rod is multiplied by this factor to calculate the rod temperature for each zone. The uncertainty is then applied for each rod in each zone. The temperature uncertainty is uniformly distributed over a range of ± 13.5%. These shaping factors are also applied to the vacuum drying and dry storage periods.

The center rod in an average WP peaks at 308°C at 53 years, three years after closure. At this time, the outer rods peak at 291°C and the WP surface temperature is 277°C. After an additional 50 years, the center rod has cooled to 226°C and the outer rod is 215°C. The hottest center rod will peak at 350°C (13.5% above 308°C) while the hottest outer rod will peak at 314°C (see Attachment II, Table II-10a).

In generating the failure probability distribution for stress and SCC, the WP peak surface temperature is treated in this analysis as an independent variable and failures are predicted for various WP peak surface temperatures. In the TSPA-SR for each realization, the WP peak

temperature will be established and then creep and SCC rod failure fractions will be looked up on a table.

6.2.2 Creep Strain Correlation

CRWMS M&O 2000j compares the creep predictions using six (6) different creep correlations to the results from five (5) different experiments (Tables 4 and 5). The tables give the relative error, that is the absolute value of the difference between the calculated and measured values divided by the measured values [Abs((Calculated-Measured)/Measured)]. Using relative error as a measurement, the smaller numbers represent the better fit. The five (5) different experiments were for unirradiated material, with the temperature range: 250°C < T°C < 385°C, and the stress range: 55 MPa < Stress < 275 MPa. There were a total of 503 reported strain measurements, many of which were obtained at intermediate times in the analysis and 95 of which were at end points (last measured strain). Table 4 compares the equations for all the data points, including the intermediate and end points. Both Murty's correlation and Matsuo's correlation fit the data approximately equally well. Murty's correlation was selected because it explicitly considers Coble creep, a type of creep that could be important at lower stresses and temperatures and that might not have been observed in the ranges of these experiments. Table 5 compares the fit at the end points (last measured strain) for each of the 95 analyses. This prediction is more important for this AMR because failure is predicted for the larger creep strains, for which the end points of the analyses should be more representative. It is important to note that the experimental ranges, 250°C < T°C < 385°C and 55 MPa < Stress (MPa) < 275 MPa are close to the upper end of repository conditions shortly after closure. Some of these tests also ran for 10,000 hours (1.1 years) (CRWMS M&O 2000j, p.II-1). Again, Murty's correlation gives one of the better fits and will be used for creep failure calculations. For Murty's correlation, the uncertainty in the creep correlation for all 503 data points ranges from 0.283 to 0.727 and with a weighted average of 0.557 (Table 4).

Table 4. Comparison of Relative Error of Creep Correlations for All Data Points

		Creep Correlations*					
Ref.[2]	Total Data Points[1]	Matsuo	Murty	Mayuzumi	Limback	Spilker	Peehs
Spilker, T2	192	0.758	0.739	0.648	0.560	0.344	0.726
Spilker, T3	240	0.340	0.440	0.901	1.779	2.256	0.546
Matsuo	21	0.135	0.379	0.640	0.557	1.994	0.521
Mayuzumi	31	0.282	0.301	0.121	0.477	1.291	0.579
Limback	19	0.334	0.445	0.142	0.145	1.354	0.596
Weighted Average	N/A	0.487	0.543	0.717	1.121	1.431	0.606

NOTE: *Values are: Absolute Value [(Calculated-Measured)/Measured]

[1]Total number of points : 503

[2]Tests: unirradiated material, over the range 250≤T (°C) ≤385 and 55≤ Stress (MPa) ≤ 275

(Source: CRWMS M&O 2000j)

Table 5. Comparison of Relative Error of Creep Correlations for Experimental End Points

		Creep Correlations*					
Ref.[2]	Total Data Points[1]	Matsuo	Murty	Mayuzumi	Limback	Spilker	Peehs
Spilker, T2	32	0.780	0.684	0.603	0.581	0.166	0.762
Spilker, T3	40	0.294	0.317	0.834	2.533	1.871	0.653
Matsuo	15	0.092	0.746	2.886	0.931	3.042	0.271
Mayuzumi	4	0.338	0.135	0.148	0.993	1.099	0.612
Limback	4	0.411	0.368	0.134	0.147	0.980	0.680
Weighted Average	N/A	0.432	0.503	1.022	1.457	1.232	0.638

NOTE: *Values are: Absolute Value [(Calculated-Measured)/Measured]
[1]Total number of points : 95
[2]Tests: unirradiated material, over the range 250≤T (°C) ≤385 and 55≤ Stress (MPa) ≤ 275
(Source: CRWMS M&O 2000j)

The Murty correlation is described in Henningson (1998, Section 4, pp. 51 to 61) and the recommended equations (Henningson 1998, p. 57) are reproduced below. Hoop creep characteristics of Zircaloy tubing were collected at temperatures between 316°C and 427°C and at stress levels in the range of 55 MPa to 235 MPa. Three different sets of experimental data were used by Murty in generating the equations. The equations combine a high-stress creep mechanism of glide creep with a low-stress creep mechanism of Coble creep:

$$\dot{\varepsilon}_{Glide} = 4.97x10^{6}\, e^{-31200/T}\, \frac{E}{T}[\sinh(807\frac{\sigma}{E})]^{3} \qquad \text{(Eq. 6.2-1)}$$

$$\dot{\varepsilon}_{Coble} = 8.83e^{-21000/T}\, \frac{\sigma}{T} \qquad \text{(Eq. 6.2-2)}$$

Glide creep strain:

$$\varepsilon_{glide} = \dot{\varepsilon}_{glide}t + \frac{K\varepsilon_{T}\dot{\varepsilon}_{glide}t}{\varepsilon_{T} + K\dot{\varepsilon}_{glide}t} \qquad \text{(Eq. 6.2-3)}$$

Coble creep strain:

$$\varepsilon_{Coble} = \dot{\varepsilon}_{Coble}t \qquad \text{(Eq. 6.2-4)}$$

Total creep:

$$\varepsilon = \varepsilon_{glide} + \varepsilon_{Coble} \qquad \text{(Eq. 6.2-5)}$$

Various parameters and constants include:

$\varepsilon_T = 0.008$,

$\kappa = 10$

$E = (1.148 \times 10^5 - 59.9T) \times 10^6$, Young's Module, Pa (T in K) (Eq. 6.2-6)

T = temperature (K)

σ = stress (Pa)

t = time (hours)

The above equations calculate the creep for a specific time at a constant temperature. To calculate creep strain for a rod exposed to the temperature history shown in Figure 6, the temperature history is divided into finite intervals and a time hardened technique recommended by Murty (Henningson 1998, p. 57, equation 15) and given below is used:

$$\varepsilon(t_i) = \varepsilon(T_{i-1}, t_{i-1}) + [\varepsilon(T_i, t_i) - \varepsilon(T_i, t_{i-1})] \quad \text{(Eq. 6.2-7)}$$

Where the subscript i-1 represents the previous time step and the subscript i represents the current time step. This is necessary because the creep rate for a constant temperature starts out very fast (primary creep) and then decreases to a slower secondary creep rate. If Equations 6.2-2 through 6.2-6 were applied separately to each time step, the primary creep would never saturate and the total creep would be over-predicted and also would be dependent on the number of time steps (number of times that the primary creep calculation was started). The actual analytical method and the software routine are discussed in Attachment II.

The Murty creep correlation is for unirradiated cladding. Peehs (1998, Figure 10) compares the creep for irradiated and unirradiated cladding and shows that the creep for irradiated cladding is significantly less than that of unirradiated cladding. Creep strain measurements were taken on commercial nuclear fuel by Kaspar et al. 1985 (pp. 56, 57), Einziger and Kohli 1984 (Table III), Chung et al. 1987 (Tables 1,2), Bredel et al. (2000, page 14), and Goll et al. (Macheret 2000, Att.2, Figures 6, 7). Irradiated cladding creep data was collected and the Murty correlation was used to predict the creep in 223 creep measurements reported by five different experimenters (CRWMS M&O 2000m). Figure 9 shows the comparison of the measured creep to the calculated creep. The diagonal line represents a perfect fit (calculated = measured) and the two parallel lines represent an over prediction and under prediction of one order of magnitude. The figure shows that the Murty equation consistently and systematically over predicts the data and in many cases, by over an order of magnitude. CRWMS M&O 2000m analyzed the error in Murty's predictions and developed the correction:

$$MM(\%) = 0.233 * M(\%)^{0.488} \quad \text{(Eq. 6.2-8)}$$

Where: M = % creep strain from Eq. 6.2-5, and

MM = Modified Murty Creep Correlation

Figure 10 shows the comparison of the experimental data and the Modified Murty correlation. This correction was first fitted by a least square fit so that approximately 50% of the creep measurements were over predicted by the correlation and then modified so that 75% of the measured creep strains are over predicted by the equation. This can be seen in the figure with 75% of the points being below the diagonal. The uncertainty used in the creep correlation is 0.80 uniformly distributed with the calculated creep for each of the 12,000 rods and varies in the range of +/- 80% of the calculated value. This is the average relative error of the Modified Murty creep correlation in predicting the experimental data for irradiated cladding.

The Modified Murty correlation is to be applied to cladding that has undergone irradiation hardening. If the cladding is heated to a sufficiently high temperature, the irradiation damage is annealed out and higher creep rates would be expected. The current vacuum drying temperatures (example: Hopf 1999, Figure 2-1) are selected so that annealing does not occur. If annealing occurs, both the creep rate and the creep failure criteria will increase. This is further discussed in Section 6.2.3.

The analysis presented in this section is based on an empirical creep equation developed by Murty and modified above. Many of the alternative equations are discussed by Pescatore and Cowgill (1994, pp. 47-86). One equation discussed is the Diffusion Controlled Cavity Growth (DCCG). Pescatore and Cowgill (1994, p. 83-85) concludes that the DCCG has not been validated against cavity data and voids or cavities are very infrequently seen in irradiated Zircaloy. He recommends (p. 85) a methodology similar to the approach used here. Commercial power plant dry storage license applicants were once required by the NRC to use the DCCG method to evaluate dry storage designs. The current NRC Interim Staff Guidance (ISG) - 11 (NRC 2000a) recognizes the controversy with this conceptual method and permits commercial power plant license applicants to use other creep equations and methods in their license application. The use of Murty's correlation is consistent with this ISG.

In a feedback effect, the creeping of the cladding increases the free volume and reduces the pressure and stress. Einziger et al. (1982, p. 78) concludes that this feedback is important to extending the fuel lifetime. For each rod analyzed, the existing free volume (obtained from CRWMS M&O 2000a, Section 6.3.5) is increased at each time step by the equation (derived here from elementary geometry):

$$Vn = L\,(2*\pi*Ri) * Ri * (0.01* \epsilon) \qquad \text{(Eq. 6.2-9)}$$

$$Vn = 4.227 * \epsilon$$

Where
- Vn = new free volume, cm^3
- L = Rod Length, 385 cm
- Ri = Rod inner radius, 0.418 cm
- ϵ = cladding strain, %

The dimensions are presented in CRWMS M&O 2000a, Table 2. As an example of this feedback effect, if the initial free volume of the rod is 17.7 cm^3 and the rod undergoes 1% creep, the new free volume is 21.9 cm^3 (4.2 * 1 + 17.7) and the stress would be decreased by about 20% (1-17.7/21.9).

6.2.3 Creep Failure Criterion

To estimate what percent of the rods will fail from creep, creep failure criteria must be established. For this, data from various burst tests or other type tests with irradiated cladding has been collected and a CCDF has been generated. Figure 7 gives the resulting CCDF. Table 6 summarizes the 52 data points used to create the CCDF. It should be noted that over 70% of this data are for cladding that was irradiated in excess of 40 MWd/kgU. The specific experiments are discussed below.

The CCDF was approximated by three linear equations that are also shown in Figure 7. This was used to simplify the statistical sampling the equations are:

$$Fs = 14.4 - 135 * P, \qquad 0.0 < P \leq 0.06 \qquad \text{(Eq. 6.2-10a)}$$

$$Fs = 6.77 - 7.81 * P, \qquad 0.06 < P \leq 0.5 \qquad \text{(Eq. 6.2-10b)}$$

$$Fs = 5.33 - 4.93 * P, \qquad 0.5 < P < 1.0 \qquad \text{(Eq. 6.2-10c)}$$

Where Fs = Strain Failure limit, %

P = random probability between 0 and 1.

The above equations were selected to be conservative with respect to the data and therefore are below the data in Figure 7. The mean and median values of the creep failure data are 3.54% and 2.86% respectively. The mean and median values of the linear fit are 3.40% and 2.80% respectively. The details of developing these equations and incorporating them into the cladding creep analysis are described in Attachment II.

Table 6. Experimental Data Used to Develop Strain Failure CCDF

Source	Alloy, BU (MWd/kgU), Reactor	Temperature, °C	Stress, MPa	Ultimate Strain, %
Chung et al. 1987, Table 1	Zirc-2, 22.4, Big Rock Pt.	325	337 - 514	1.1, 0.8, 0.4, 1.0
Chung et al. 1987, Table 1	Zirc-4, 27.7, H.B. Robinson	292 - 325	469 - 552	11.7, 2.5, 1.4, 2.4
Chung et al. 1987, Table 2	Zirc-4, 27.7, H.B. Robinson	292 - 325	Mandrel	3.3, 4.7, 6.0, 4.7, 6.0, 3.6, 4.7
Garde 1986, Table 17	Zirc-4, 54 – 62, Ft. Calhoun	315	793 - 862	2.73, 1.24, 4.19, 1.53, 2.15, 4.03
Garde 1986, Table 18	Zirc-4, 42 – 53, Ft. Calhoun	315	793 - 820	6.9, 5.6, 4.5, 4.7
Garde 1986, Table 19	Zirc-4, 58 – 63, Ft. Calhoun	27, 200, 300, 400	793 - 820	1.07, 5.23, 9.06, 6.19
Garde et al. 1996, Table 1	Zirc-4, 60, Calvert Cliff 1	315	480[a], 860-1010	2.69, 6.47, 3.30, 5.04, 2.41, 2.22, 3.16, 0.58[a]
Garde et al. 1996, Table 2	Zirc-4, 60, ANO2	315	860-1010	2.28, 2.08, 2.28, 1.64, 2.58, 2.06, 1.73, 1.47, 2.45
Goll et al. (Macheret 2000, Figure 8)	Zirc-4, 54 - 64,	300, 370	397 - 622	2.5, 3.0, 4.5, 5.0, 5.0, 6.0

a: Failure stress and strain in sample with spalled oxide.

Chung et al. (1987, pp. 780-781)

Chung et al. (1987) conducted a series of 20 slow burst tests and mandrel tests with irradiated cladding. Approximately half of these tests extended for over 200 hours. Four tests were on BWR Zircaloy 2 cladding with a burnup of 22 MWd/kgU and the remaining tests were on PWR Zircaloy 4 cladding with a burnup of 28 MWd/kgU. For the samples that were tested to failure, they measured an average strain at failure was 3.6% with a range of 0.4% to 11.7%. They also conducted scanning electron microscope inspection of the failures and found evidence that, in 11

of the tests, the failures occurred at cracks formed in the cladding. The use of these results as a component in the failure criteria CCDF addresses the potential for lower failure strains from pre-existing internal cracks and the situation that failure might not be from pure material creep. These failure criteria do not address potential changes in the strain failure criteria with strain rate. The strain rates in Chung's gas pressurization experiment varied from 3 10^{-6} s^{-1} to 5.4 10^{-9} s^{-1} with an average of 5.8 10^{-7} s^{-1}. The mandrel tests were in the range of 5 10^{-5} to 7 10^{-8} s^{-1}. While these strain rates are faster than expected in repository conditions, they are not rapid burst tests.

Garde 1986

Garde studied the characteristics of Fort Calhoun PWR fuel after achieving rod average burnups of 56 MWd/kgU. The fuel experienced fission gas release of less than 2%, oxide thichnesses of 35 to 52 μm, and hydrogen concentrations of 240 to 490 ppm. Garde's Table 17 (row 5 of the above table) shows a decrease in ultimate creep strain with burnup when compared with his Table 18 (Row 6 above). Row 7 shows a strong increase in ultimate strain with temperatures. As the test temperature increased from 27°C to 400°C, the ultimate strain increased from 1.07% to 6.19%. This shows that during the time of maximum temperatures, when the maximum stresses occur, the strain limit should also be highest. The failure criteria used in this analysis is not temperature dependent but most of the measured data used in the generation of the CCDF is in the temmperature range where the maximum creep is expected (292°C to 325°C). The tests averaged 4.2% for total strain.

Garde et al. 1996

Tube burst tests were performed on Zircaloy-4 cladding with fast fluence range between 9 and 12.3 x 10^{25} n/m^2, (E>1MeV). This corresponds to a burnup of approximately 47 to 64 MWd/kgU (conversion from Edsinger et al. 2000, p. 328). The cladding came from two different PWR reactors. The test temperature was 315°C and stresses were up to 1010 MPa. One of the samples contained spalled oxide and the cladding had a hydrogen content of 731 ppm. This sample failed at a total strain of 0.58% at 480 MPa. The inclusion of this data in the CCDF of 52 data points is comparable to having 2% of the CCDF determined by cladding with spalled oxides. These tests had a total strain averaging 2.6%. The creep rate in these tests was 6.7 x 10^{-5} sec^{-1}.

Goll et al. (Macheret 2000, Att. 2)

Goll et al. reported creep tests with Zircaloy-4 cladding after a burnup of 54 to 64 MWd/kgU. The tests were done at two temperatures, about 300 and 370°C and two stresses, 400 and 622 MPa. The test duration was 3 to 4 days. The high stresses were selected to obtain strains in excess of 2% during the tests. Six tests led to cladding failure and the average ultimate strain at failure was 4.3%. Six other tests did not fail and all the samples reached strains in excess of 2%, the value recommended in this paper as failure criteria.

Lower Limit

In the German (Peehs) analysis (Pescatore et al. 1990, p. 39), a conservative value for a strain at which cladding failure occurs, 1% strain, was selected. The NRC (Brach 2000, P. 1) concluded that "the staff believes that Zircaloy cladding can withstand uniform creep strains (i.e., creep prior to tertiary or accelerated creep strain rates) of about 1% before the cladding can become perforated ···." For the analysis presented here, a 1% failure criteria is used as the lower limit failure criteria.

Upper Limit

Sanders et al. (1992, p. III-53) recommend a median value of 6 percent for rupture strain. This will be used as an upper limit for failure criteria.

Corroborating data

Sanders et al. (1992, p. III-53) recommend a median value of 6 percent for rupture strain and also report a series of experiments with irradiated cladding that had a median failure strain of 4% (Sanders et al. 1992, p. III-51). Van Swam et al. (1997, p. 430) report 10 ring tensile tests on irradiated cladding with the resulting total elongation being 7.6% (1.5% to 15% range) at 27°C and 15.8% (5% to 21% range) at 350°C. These results suggest that the creep failure criteria being used are very conservative because of the effect of the elevated temperatures. The Technical Basis Document (CRWMS M&O 1998a, Table 6-19, p. 6-14) showed 54 tensile tests or high temperature rod creep tests. The average uniform elongation strain for these tests is 4%. A failure criteria of with a mean value of 3.4% is used in this AMR to predict creep failure and is more conservative (lower) than most other reported values, especially since no correction has been made for the elevated temperatures.

Einziger and Strain (1986 p. 90) performed dry unzipping experiments on irradiated fuel rod samples. In these experiments, the UO_2 is converted to U_3O_8 and the increase in volume stresses the cladding to failure. They report strain to breach values of 5.3% and 6.5% to 7.5%. The CCDF used in this work predicts an approximate 6% chance of having creep failure in excess of 6.5% strain. This suggests that the failure criteria are conservative.

Annealing and End Plug Weld

The cladding creep failure criteria are developed for irradiated cladding that has not been annealed. This is consistent with the creep correlation, which is also for irradiated cladding. If the cladding is annealed, both the creep rate would be greater (see Section 6.2.2) and the failure criteria would be higher. Einziger et al. (1982, Figure 3) performed creep tests with irradiated cladding at 571°C. This temperature is high enough for annealing. They measured strains close to 12% without any rod failures. From Figure 6 or Equation 6.2-10a, the CCDF used in this work would predict failure before 12% or greater stress in only 3% or the samples.

Bouffioux and Legras (2000, Figure 7) show the times to start and complete recovery as a function of temperature. Their results are summarized in Table 7. With peak drying

temperatures less than 425°C, and peak dry storage temperatures starting at 350°C, little or no recovery should occur.

Table 7. Irradiation Hardening Recovery Times

Temperature, °C	Recovery Starts	Recovery Complete
250	30,000 yrs	400,000 yrs
300	200 yrs	30,000 yrs
350	1+ yrs	200 yrs
400	300 hrs	3 yrs
450	10 hrs	2000 hrs
500	< 1 hr.	90 hrs.

(from Bouffioux and Legras 2000, Figure 7)

Analyzing the cladding directly over the fuel rather than the end-plug welds represents a more conservative case for repository failures than a separate set of failure criteria at the welds. This is based on the fact that there are more cladding restraint (and less creep-out), lower storage temperatures, less irradiation damage, less total hydrogen, and no PCI in this region. Whereas high residual stresses occur in these weld areas, and there is a potential for larger incipient cracks, rods with faulty welds with large incipient cracks were either removed during rod fabrication leak testing, discovered during non-destructive evaluation, or failed in reactor. Therefore failures in end plug welds are included in the overall database and are not treated as a separate, more-restrictive failure mode.

6.2.4 Creep Failure Results

Figure 1 gives the CCDF for the hoop stress (at room temperature of 27°C) in the rods expected to be received at YMP. A sampling of 2000 rods with stresses that are defined by this distribution was used for the stress variation. A rod (total of 12,000 rods analyzed, 6 x 2000) with each of these 2000 stresses was placed in each of the six (6) zones shown in Figure 3 and described in Table 3. This rod represents the fraction of the total WP inventory in the zones as given in Table 2, Column 3. Each rod is exposed first to a temperature profile represented by Figure 2 (vacuum drying and dry storage) and then to the repository temperature history (Figure 6). During all of these periods the rods are normalized by the WP radial scaling factor corresponding to the particular zone as given in Table 3, Column 5. A uniform temperature uncertainty of ± 13.5% is included. The creep strain is then calculated for the rod using the equations in Section 6.2.2 (including a uniform uncertainty of ± 80%). This strain is compared

to a random sampling of the creep failure strain criteria CCDF in Figure 7. If the rod creep strain exceeds the creep failure strain criterion, the fraction of the rods in that radial zone of the WP has become perforated and that fraction of a rod is available for cladding unzipping. This procedure is repeated for 12,000 rods in a software routine and the fraction of the WP inventory perforated is calculated. The details of this analysis are described in Attachment II and the software routine AMR-F0155-V2.xls has been submitted as DTN: MO0011SPACMU07.049.

Three specific sensitivity studies are presented. In the first, the vacuum drying temperatures is varied while the dry storage temperatures were held constant. In the second study, the dry storage temperatures were varied while the vacuum drying temperatures were held constant. In the third study, the WP surface temperatures were varied while the vacuum drying and storage temperatures were held constant.

Vacuum Drying

The various designers of dry storage canisters have different projected maximum vacuum drying temperatures. A sensitivity study was performed to see the effect of peak drying temperature on the creep failures. The analysis shifts the vacuum drying temperatures upwards or downwards (left side of Figure 2) while maintaining the maximum peak dry storage cladding temperature history starting at 350°C. Creep failure is predicted after 20 years of dry storage and any creep during repository emplacement is neglected by setting low repository temperatures. Figure 11 gives the results of this sensitivity study. No rod failures are predicted for maximum rod temperatures currently being considered as summarized in Section 6.2.1. If the rod temperatures exceed 525°C, rod failures start to increase, and at 570°C to 600°C the failures start to exceed 0.5%, a very low probability guideline (NRC 1997, p. 4-2). At these high temperatures, annealing of irradiation hardening would be expected and both the creep rate and creep failure would increase. Dry storage tests at 571°C did not cause rod failure (Einziger et al. 1982, p.65). Rod failure fraction predicted from creep during vacuum drying are failures in addition to the 0.045% predicted to be failed in normal dry storage and included as part of the "as received" rod failures (CRWMS M&O 2000a, Section 6.10).

Dry Storage

A second sensitivity study varied the initial dry storage temperature (right hand side of Figure 2) while holding the peak vacuum drying temperature at 430°C. The results of this study are presented in Figure 12. No rod failures are predicted for maximum rod temperatures that are currently being considered in dry storage designs as summarized in Section 6.2.1. If the maximum rod temperatures in dry storage exceed 400°C, rod failures start to increase. At 430°C the failures start to approach 0.5%, a very low probability guideline for dry storage facilities (NRC 1997, p. 4-2). Rod failure fraction predicted from creep during dry storage are failures in addition to the 0.045% predicted to be failed in normal dry storage and included as part of the "as received" rod failures (CRWMS M&O 2000a, Section 6.10).

Repository Emplacement

The last sensitivity study starts with the maximum vacuum drying temperature of 430°C and the maximum dry storage temperature of 350°C for the center rod in the WP. The WP surface

temperature (right side of Figure 6) is shifted upward or downward and the fraction of rods that fail from creep is calculated. The results of this study are presented in Figure 13. No rod failures are predicted for maximum rod temperatures that are currently being considered in the repository. If the peak WP temperatures during repository emplacement exceed 325°C, rod failures start to increase. At 350°C, the failures start to exceed become significant.

Figure 14 gives the fraction of rods failed as a function of maximum cladding temperature. Below 350°C, little or no cladding failures is predicted but after 350°C, the cladding failures starts to increase. A design limit of 350°C for the maximum cladding temperature in a WP can be justified based on the creep analysis described in this AMR.

The above analysis has not been directly incorporated into the TSPA-SR but an abstraction has been included. For this abstraction, the independent variable is the peak WP surface temperature. The above analysis was performed for peak WP surface temperatures that vary from 177°C to 527°C. The WP temperature history as shown in Figure 6 is linearly shifted upward or downward by the difference between the base case and new peak WP surface temperature. Figure 8 shows the WP temperature for the peak, average and minimum WP in group 4 (CRWMS M&O 2000h). The peak temperatures are approximately a constant shift above the average temperatures. The minimum temperature falls off more quickly than the average. Analyzing the minimum temperature WPs as a constant temperature difference below the average WP temperature is reasonably bounding because it increases the amount of time at an elevated temperature. The change in temperature radially across the WP is then added to the scaled WP surface temperature. The temperature uncertainty is established to cover the maximum temperatures.

Table 8 gives the fraction of rods failed in a WP (failed from creep) as a function of peak WP surface temperature. This table is imported into the TSPA-SR and the TSPA-SR interpolates the fraction of rods failed in a realization after establishing the peak WP surface temperature for that realization. Figure 13 is a graphical representation of this table. Rods have undergone some creep during dry storage and shipping and start to accumulate additional creep from that point. Figure 13 shows that above a peak WP surface temperature of about 350°C, the estimated fraction of rods perforated from creep increases dramatically. This is because the creep correlation has an Arrhenius temperature dependency and the activation energy is reached at that point. The upper limit curve represents the fraction of rods failed from creep if the failure criterion were 1.0% creep, the minimum value in the creep failure strain criterion CCDF. The lower limit curve represents the fraction of rods failed from creep if the maximum creep failure strain criterion of 6.0% were applied. The mode value represents a random sampling of the creep failure strain criterion CCDF. In the TSPA-SR, a triangular distribution is used between the upper limit, mode and lower limit to incorporate uncertainties. At the WP wall temperature of 227°C, the mode (0.01%) is larger than the upper limit value (0.0%). This can occur when a rod is predicted to fail from sampling the full CCDF at a value below the upper limit of 1% strain. This only occurs when sampling at the very tail of the statistical distribution. For the TSPA, the maximum value is put equal to the mode at this temperature so the probabilistic distribution is possible (Attachment I, line 42)

Table 8. Fraction of Rods Perforated From Creep as a Function of Peak WP Surface Temperature

WP Peak Temperature, C	Upper Limit	Mode	Lower limit
≤177	0.0000	0.0000	0.0000
227	0.0000	0.0001	0.0000
277	0.0001	0.0001	0.0000
302	0.0005	0.0002	0.0000
327	0.0039	0.0019	0.0000
352	0.0325	0.0127	0.0001
377	0.1495	0.0540	0.0009
427	0.5638	0.2802	0.0617
477	0.8991	0.6113	0.3418
502	0.9683	0.7499	0.5067
527	0.9921	0.8516	0.6727
≥547	0.9980	0.9050	0.7841

(DTN: MO0011SPACMU07.049)

6.2.5 Stress Corrosion Cracking

Stress corrosion cracking (SCC) occurs when cracks propagate in materials subjected to a combination of local stress concentrations and aggressive chemicals concentrating at crack tips. The combination of stress levels and chemicals required for SCC vary form material to material. One example of SCC is the cracking of certain stainless steels under tension and in a chlorine environment. In the case of nuclear fuel there has been evidence that iodine and cesium fission products may cause SCC of the cladding ID during high stress conditions such as accelerated reactor start-up (Cox 1990a, p.249).

Stress Corrosion Cracking on Cladding Internal Surface

Under irradiation, SCC can occur in locations where the cladding is being pressed against the pellet producing pellet-clad interaction (PCI). For nuclear fuel, these terms (PCI and SCC) are sometimes used interchangeably (Cox 1990a p. 250). In early fuel designs, the pins were not pressurized and the cladding crept against the pellets (due to the reactor operating pressure on the order of 15 MPa (2,200 psi)). The cladding tended to fail at the pellet ridges where, during rapid power changes, the fuel expanded faster than the cladding, causing high local stresses and PCI or SCC. Limiting reactor maneuvering during start-up and operation, pressurizing the pins during manufacturing, and eliminating sharp edges on the pellets minimized the local stresses in the cladding and solved the PCI problem.

SCC or PCI is not predicted to be a spent fuel problem under any normal storage or shipping conditions. As discussed above the conditions required in reactor for SCC to occur are well understood and procedures have been instituted to solve the problem (Armijo et. al. 1994, p.3, Mardon et.al 1994, p. 329). The solution has focused on eliminating excessive clad stresses. In the case of spent fuel, the cladding stresses are much lower than those encountered in reactor. After reactor operation, the fuel pellet, which is hotter than the cladding, contracts away from the cladding, thus eliminating any localized pressure on cladding. During dry storage, if there is any cladding movement, it will be away from the fuel pellets reducing further the possibility of localized pellet/clad contact (outward cladding creep is the predicted dry storage failure mode although it has not been observed in dry storage to date). Therefore, no PCI/SCC failures will occur during dry storage since all of the required SCC conditions cannot exist.

The above argument is considered sufficient to demonstrate that internal SCC/PCI is not a viable failure mechanism for spent fuel. However, to provide further support a number of other investigators have evaluated the situation and reached the same conclusion. Einziger et al. (1982, p. 35, 1984, p. 107) conducted two series of tests on rods in dry storage under conditions identical to repository conditions. The time period was, of course, much shorter but the greatest probability for internal cladding damage to occur is during the early years, perhaps 20 years, when the temperature is highest. Thus the Einziger tests provide a good measure of repository conditions. Subsequent examination of the cladding showed no internal attack supporting the earlier arguments. Pescatore et al. (1990, p. 108), EPA (S. Cohen & Associates 1999, p. 7-3), Cunningham et al. (1987, p. iii), Tasooji et al. (1984, p. 621) have all reviewed the possibility of fuel side SCC under dry storage conditions and concluded that it is not a failure mechanism. Similarly the U.S. Nuclear Regulatory Commission (NRC) concluded that SCC was not a major failure mechanism and is focused only on cladding creep as a possible failure mechanism during dry storage (NRC 1997, NUREG-1536, p. 4-3).

Despite the above conclusions that SCC will not occur during dry storage, an assessment was made of the minimum conditions required to initiate SCC. With such information, a determination can be made of whether there are any scenarios for concern. Iodine induced SCC requires an iodine concentration in the cladding inner surface greater than 5×10^{-6} g/cm^2 (Cunningham et al. 1987, p. A.5). Below this free iodine concentration threshold, SCC has not been observed in Zircaloy. However, for this analysis the amount of free iodine was considered to be present in sufficient quantities for SCC to occur although this is most unlikely in actual fuel rods. The time at high stress and elevated temperature is considered sufficiently long such that once cracking initiates there is sufficient time for crack propagation through the cladding (crack velocities are not considered). A stress threshold of 180 MPa was reported by Tasooji et al. (1984, p.600, Figure 3) for failure by SCC. This threshold is consistent with the 200 MPa stress needed for SCC quoted by Pescatore et al. (1990, p.108). In practice few rods have such high stresses. Note that the reactor operating pressure limits the end-of-life fuel rod pressures so that high repository rod pressures can only be achieved with high rod temperatures. Reasoning however that SCC could occur, the resultant failure rates have been calculated separately. Table 9 gives the fraction of rods that reach the SCC threshold and therefore are presumed to fail. These failures are almost independent of waste package temperature because any failures would most likely occur during vacuum drying for dry storage. For the TSPA the fraction of rods

perforated by SCC is 0.00473 since low waste package cladding surface temperatures are predicted.

Table 9. Fraction of Rods that undergo SCC Failure or Hydride Reorientation

Peak WP surface Temperature, °C	SCC	Reorientation Possibility [a]
177	0.00458	0.0466
277	0.00473	0.0575
327	0.00525	0.0765

a: Reorientation is not expected to lead to rod failure
(DTN: MO0011SPACMU07.049)

Stress Corrosion Cracking on Cladding External Surface.

Many of the SCC experiments reported in the literature have used electrochemical procedures performed on fresh zirconium or zirconium alloy surfaces or on slightly oxidized surfaces. Experiments on the fresh metal surfaces have often investigated the effects of surface finish. Those on oxidized surfaces have been restricted to coatings that are fractions of a micron thick. No electrochemical studies are known to have been performed on zirconium alloys with oxide coatings in the range 10 to 100 micron, which is typical of spent nuclear fuel. Such oxides have very high electrical resistivity and electrochemical experiments are probably impractical. Any conclusions drawn from electrochemical experiments might therefore be considered as "worst-case" scenarios and not representative of actual conditions.

A review paper by Cox (1990b Table 1 page 3) identified environments that are of potential concern for SCC. Of the environments listed that could be anticipated in the YM program, aqueous chloride solutions were identified as having the greatest potential for causing SCC. Although organic liquids, halogen vapors and hot or fused halides were also listed as causing SCC, these environments are not predicted to be present in the repository and are not discussed further.

In an earlier study, Cox (1973) determined that SCC could be obtained in unnotched specimens of Zircaloy2 in neutral aqueous chloride solutions provided the specimen was polarized anodically. The required breakdown potential for the film was found to be +100 mV (SCE) in 5% NaCl solution. It was concluded that this degree of anodic polarization might be achieved on preoxidized specimens by galvanic coupling. The experiment used cladding pickled in HNO_3/HF solution to provide clean surfaces. To determine the effects of zirconium oxide films, some samples were oxidized at 400°C (3 days) and 500°C (7days) in moist air. (It is estimated that 400°C (3 days) oxidation would produce a pre-transition oxide film of about 1 micron; a 500°C (7days) oxidation should produce a post-transition film with an estimated 4 to 8 micron of oxide).

The rings were slit and stressed on preoxidized Zircaloy2 blocks to give a maximum stress at the yield point. Electrical connecting wires of Zircaloy2 were spot welded to the specimens adjacent

to the stressing block where the applied stress was lowest. Relevant results are shown in Table 10a (Table 4 of the Cox 1973, p. 160). These demonstrate that the presence of the thicker post-transition oxide films significantly increase the failure time and may in fact prevent SCC. Similar beneficial effects provided by a protective oxide in preventing iodine SCC are discussed by Mattas et. al. (1982 p.166). In summary, no crack propagation was observed in 5% NaCl solution, even with precracked double cantilever beam (DCB) specimens under open circuit or cathodic potentials.

Table 10a Effect of pH and Preoxidation on Times to Failure in 5% Sodium Chloride Solution of Specimens Galvanically Coupled to Pt.

Specimen	Pre-oxidation	pH	Final Potential mV (SCE)	Time to Failure (Mins)
ML 240	As Pickled	1	+ 78	<1000
ML 121	As Pickled	1	+ 76	362
ML 243	As Pickled	2	+ 85	835
ML 207	As Pickled	3	+ 98	3450
ML 306	As Pickled	4	+ 106	No Failure
ML 306	As Pickled	7	+ 215	No Failure
ML 208	3 days/400C	7	+ 97	2778
ML 220	7 days/500C	7	+ 97	~10,000 hrs
ML 223	7 days/500C	7	+ 420	No Failure (10^3 hrs)
ML 224	7 days/500C	7	+ 162	No Failure (10^3 hrs)
Ref: Cox 1973, Table 4				

In the later review article on SCC, Cox (1990b, p.11) concluded that *"the necessity to polarize anodically to obtain cracking in aqueous halide solutions is clearly associated with the primary oxide breakdown step in the crack initiation process, since the condition is not relaxed even when pre-cracked fracture toughness specimens are used."* The oxide film in question relates to the protective film grown in air. No details were given of thickness but from general zirconium alloy corrosion rates, the air oxide thickness will be orders of magnitude thinner than that present on spent fuel cladding. It might therefore be concluded that the presence of the much thicker oxide with very high electrical resistivity would essentially eliminate chloride attack and prevent SCC. Again, the statement by Mattas (1982 p.159) would tend to support this theory: *"Unirradiated cladding is usually coated with an air-formed oxide only 10.0 to 15.0 nm thick. This is not likely to supply much protection, since there is some evidence that iodine can directly penetrate thin oxides. The oxide layer on the inside-diameter surface of irradiated cladding may reach several micrometers (microns) in thickness, however, and would be expected to provide a greater degree of protection to the cladding. Wood has found that specimens irradiated in an environment of flowing dry air are resistant to iodine SCC."*

In addition to the various reviews by Cox 1990b, Yau and Webster (1987, p.718) investigated the SCC resistance of zirconium in many environments such as NaCl, HCl, $MgCl_2$, NaOH and H_2S. They reported that the high SCC resistance of zirconium can probably be attributed to its high repassivation rate. Although they noted that SCC is possible in certain environments ($FeCl_3$, $CuCl_2$, CH_3OH and HCl mixture and some others), these conditions are not expected to occur

under repository conditions. Yau (1984, p. 140/1 – 140/8) published results of SCC tests with zirconium in concentrated acids to simulate concentrated geothermal salts. Both welded and non-welded samples were exposed to U-bend SCC tests. Tests were conducted at room temperature and under high temperature/pressure autoclave conditions. The pH was between 2.3 and 3 (room temperature). The most aggressive condition was that in which Zr 702 and Zircaloy-2 samples were subjected to the U-bend test with steel coupling. No cracking was observed in the zirconium alloys although the steel bolts and nuts corroded badly during the test. The tests showed that Zircaloy is susceptible to SCC under extreme chemical conditions of hydrochloric acids and ferric ions which are the same conditions for which Zircaloy pitting is possible. Such extreme chemical conditions are unlikely but are included in the localized corrosion analysis. In summary, SCC is not expected to play a role in cladding degradation in the repository. Further details of the tests and results are given in CRWMS M&O 2000c.

Although the evidence reported by various investigators suggests that SCC will not occur under repository conditions even under aggressive environmental conditions particularly with a thick adherent oxide coating, an estimate has been made of the stresses required for initiation of SCC. Relevant values of the threshold stress intensity factor for Iodine induced SCC (K_{ISCC}) taken from the literature are shown in Table 10b.

Table 10b. Threshold Stress Intensity Factors for Zirconium Alloys from the Open Literature

Reference	Solution	K_{ISCC}
Cox 1990b, Fig 14, p.12	3 M Potassium Iodide (KI)	12 (100°C) to 22 (22°C) MPa-$m^{0.5}$
Cox 1990b, Fig 15, p.12	1 M KBr + 0.25 M Br_2	12 MPa-$m^{0.5}$ (22°C)
Cox 1990b, Fig 20, p.15	Chlorine (Moist)	28 MPa-$m^{0.5}$ (70°C)
Cox 1990b, Fig 20, p.15	Iodine + air	13 MPa-$m^{0.5}$ (22°C)
Cox 1990b, Fig 20, p.15	Nitrate/Iodide Melt	5 MPa-$m^{0.5}$
Cox 1990b, Fig 7a, p.7	Hydrogen Gas (6.7-86 kPa)	20 - 28 MPa-$m^{0.5}$ (Zirc4)
Cox 1990b, Fig 7b, p.7	Hydrogen Gas (1-100 kPa)	13 - 22 MPa-$m^{0.5}$ (Zirc2)
Tasooji et al. 1984, Fig.12, p.612	Iodine, 0.001 kg./m^2	4.0 - 15 MPa-$m^{0.5}$ (Zirc2 varies with texture, 300°C)

(DTN: MO0011SPACMU07.049)

If chlorine is considered the most aggressive environment for the cladding OD then a value of 28 MPa-$m^{0.5}$ at 70°C (Cox 1990b, Fig 20) may be considered for a moist chlorine condition. This value compares with a maximum calculated stress intensity for the expected CSNF stress of 1.27 MPa-$m^{0.5}$ (using Attachment II, Sheet "Creep-WP," Column AH) at room temperature. The lower mean and median stress intensity values are as follows:

Min	0.0009 MPa-$m^{0.5}$
Median	0.219 MPa-$m^{0.5}$
Mean	0.249 MPa-$m^{0.5}$
95%	0.546 MPa-$m^{0.5}$

98% 0.680 MPa-$m^{0.5}$
Max 1.27 MPa-$m^{0.5}$

It is seen that the above values are an order of magnitude lower than that required for SCC in a chlorine environment, thus it is concluded that neither of the conditions required for external SCC are present.

6.2.6 Reorientation Potential

Hydride reorientation is discussed in Section 6.2.12.5 of CRWMS M&O 2000b. Zirconium hydride is formed from the surface corrosion of zirconium and the hydrides tend to form in flat platelets that are orientated inside the cladding with their normal in the radial direction. As discussed in CRWMS M&O 2000b, reorientation requires most if not all of the hydrides to go into solution before precipitating out of solution and does not significantly weaken the material. The analysis presented below only addresses what fraction of rods might see sufficient stresses at high temperatures to undergo reorientation. This analysis does not address whether sufficient hydride sights still exist to prevent reorientation or the strength of the material if reorientation should occur.

Figure 1 of CRWMS M&O 2000b shows a region of stress and temperature where hydride reorientation has been observed. The division between these two regions can be defined by a straight line going through the points (T=225°C, σ_r = 200 MPa) and (T=350°C, σ_r = 125 MPa). This line can be defined:

$$\sigma_r = 335 - 0.6 * T°C \qquad \text{(Eq. 6.2-11)}$$

Where σ_r = stress, MPa, required for reorientation
T = Temperature, °C, required for reorientation.

This equation is evaluated for the maximum temperature of each rod exposed to the temperature profile represented in Figure 6. The same method of analysis is used to calculate reorientation potential as is used to calculate cladding creep damage except Eq. 6.2-11 is used instead of the creep correlation. The details of the analysis are given in Attachment II. The results are summarized in Table 9. For WPs with peak temperatures less than 277°C, about 6% of the rods could have stresses and temperatures where reorientation is possible. As discussed earlier, reorientation would probably not occur because existing hydride sites would be the prefered sites for hydride formation. In addition, failure is not expected because the material has sufficient strength (CRWMS M&O 2000b, Section 6.2.12.5).

6.3 LOCALIZED CORROSION

CRWMS M&O 2000c reviewed the corrosion potential of zirconium and concluded that the material is only corroded by a few very aggressive species such as ferric chloride in a pH below 2.5 or fluoride ions at a pH below 3.2. Such chemical conditions are not predicted in the WPs (CRWMS M&O 2000i). It still might be possible that aggressive species could exist for a short time period or in a localized area by combinations of things such as microbial activities suppressing the pH or radiolysis suppressing the pH and ferric chloride existing in that region. While these combination of events were not explicitly analyzed, idealized localized corrosion by fluorides is analyzed as representative localized corrosion mechanism.

Corrosion of zirconium has been observed in fluoride-containing environments. Since fluoride is present in Yucca Mountain groundwater, fluoride corrosion may occur in waste packages. Two scenarios for fluoride corrosion may be considered. In the first (water filled WP scenario), the waste package is full of water, and fluoride ions are transported to the cladding by aqueous diffusion. In the second (flow-through scenario), water enters the waste package through one or more breaches on the upper surface of the waste package and drips out through a breach on the bottom. These two scenarios represent extremes of the rate of drainage.

The flow-through scenario is the more severe of the two. In this scenario, fluoride can be rapidly transported through the waste package by advection, whereas in the water filled WP scenario it is transported by diffusion, which is a comparatively slow mechanism. In the flow-through scenario, advective flow is directed downward by gravity, so fluoride attack can be localized on a relatively small area of cladding (and even on a small area of an individual fuel rod). In contrast, diffusion does not have a preferred direction, so in the water filled WP scenario the fluoride can be transported to a large volume of the waste package. Spreading the fluoride over a larger area of cladding (i.e. a larger area on an individual rod or area on more than one fuel rod) means that more fluoride will be consumed in breaching each fuel rod. Since the flow-through scenario is more severe, the water filled WP scenario will not be considered further.

A bounding approach has been used to describe the flow-through scenario. At least three sources of conservatism have been identified. First, it might be expected that the corrosion of zirconium is sufficiently slow, and the flow of groundwater through the waste package is sufficiently fast, that some fluoride will simply flow through the waste package without reacting. Credit has not been taken for this loss of fluoride. Instead, corrosion of the cladding is limited by the supply of fluoride.

A second source of conservatism is that fluoride attack degrades one fuel rod before degradation begins on another rod. This is reasonably bounding because each rod breaches as soon as enough fluoride is available to corrode a 10-mm length of cladding; there is no delay in breaching one rod because fluoride is being diverted to start degrading another. Credit has not been taken for simultaneous attack of more than one fuel rod. Instead, all the available fluoride goes to and reacts with a single fuel rod. When that patch on a fuel rod is completely degraded (corroded through), the fluoride starts to attack another fuel rod.

Finally, there is conservatism in that all fuel rods are subject to fluoride corrosion. Such an exposure might result if the water entered through numerous breaches or through a cracked

circumferential weld over the top half of the waste package. In that case, drips could be distributed over all of the fuel rods. Under many other exposure conditions, however, some of the fuel rods would be out of the flow path. In those cases, only the fuel rods in the flow path would be subject to fluoride corrosion.

In determining the amount of fluoride that is necessary to breach a fuel rod, fluoride removes all the cladding from a 10-mm length of the fuel rod by reacting to form ZrF_4. The as-manufactured thickness of the cladding may be used because, although some of the zirconium may be oxidized, the zirconium atoms remain in the products of corrosion.

The volume of zirconium V_{Zr} that must react to breach all of the fuel rods may be calculated with the formula

$$V_{Zr} = mL\frac{\pi}{4}(d^2 - (d-2w)^2) = mL\pi w(d-w) \qquad \text{(Eq. 6.3-1)}$$

where m is the number of fuel rods, L is the length that is subject to corrosion, d is the outside diameter of the cladding, and w is the wall thickness of the cladding. For this calculation, the most common waste package type (21 PWR) and the most common fuel assembly type (W1717WL) are used. Since W1717WL is a 17 × 17 assembly and the waste package contains 21 assemblies, the number of positions is $m = 17^2 \times 21 = 6069$. Since the control rod guide tubes and instrument tubes are similar in geometry to fuel rod cladding, all rod positions are counted, rather than just the number of fuel rods.

In a volume of water V_w with a fluoride concentration of c_F, the number of moles of fluoride is $V_w c_F / m_F$, where m_F is the molar mass of fluorine. In forming ZrF_4, $n = 4$ moles of fluoride are required for each mole of zirconium. Therefore, the volume of zirconium V_{Zr} that can be reacted with this volume of water is

$$V_{Zr} = \frac{V_w c_F v_{Zr}}{m_F n} \qquad \text{(Eq. 6.3-2)}$$

where v_{Zr} is the molar volume of zirconium. By combining Equations 6.3-1 and 6.3-2 , one finds that

$$V_w = \frac{m_F n}{c_F v_{Zr}} mL\pi w(d-w) \qquad \text{(Eq. 6.3-3)}$$

In Equation 6.3-3, m_F = 19.0 g/mol (Lide 1995, inside front cover), c_F = 2.18 mg/L = 2.18 g/m^3 (CRWMS M&O 2000g, Table 1.1), $n = 4$, $m = 6069$, L = 10 mm, w = 0.5715 mm, and d = 9.50 mm (CRWMS M&O 2000a, Table 2). The molar volume of zirconium is $v_{Zr} = m_{Zr} / \rho_{Zr}$, where m_{Zr} = 91.2 g/mol (Lide 1995, inside front cover) is the molar mass of zirconium and ρ_{Zr} = 6520 kg/m^3 (Lide 1995, p. 4-98) is the density of zirconium. Evaluation of Equation 6.3-3 yields V_w = 2424 m^3. The result is that the fraction of fuel rods failed by fluoride corrosion starts at zero when the waste package is breached. After breach, the fraction failed is proportional to the volume of water that has entered the package, reaching one when 2424 m^3 of water has entered

the waste package. An alternative description is that the fraction of fuel rods that fail in a given year is the volume of water that enters the waste package during that year divided by 2424 m^3. This volume (2424 m^3) is equivalent to filling and emptying the waste package hundreds of times. Upper and lower limits are 10 times and 1/10 the best estimate rate to represent the uncertainties in this analysis and a log uniform distribution is selected between the maximum and minimum values. This analysis makes the rod failure fraction linearly dependent on the water ingression rate (% failed = 0.0413 * m^3 water in WP) or approximately 2.3 rods (W1717 design) failures /m^3 of water. The water ingression into the WP increases with time as additional patches on the WP fail or open. Rod failure rate also depends on the location of the WP group because of different drip rates in different repository regions. Figure 15 is an example; with 50 liters/year of J13 water (2.2 ppm fluorides) entering the WP, 20% of the rods would fail by fluoride corrosion in 10,000 years.

6.4 OTHER FAILURE MECHANISMS

6.4.1 Mechanical Damage

Seismic analysis (CRWMS M&O 1999d) shows that most of the rods in the WPs would fail from a very severe earthquake (a once per million years event) but no rods would fail for less severe and moderate frequency seismic events. This is consistent with studies (Witte et al. 1989, p. 194) of rod damage during transportation accidents that concluded that 63 g accelerations are needed to fail the rods in the shipping container (or WP). This also indicates that rock drops onto an intact WP will not cause rod failure. Therefore, the seismic failures have been included in the analysis as a disruptive event.

The analysis of seismic events is included in the TSPA-SR. Based on the analysis (CRWMS M&O 1999d), seismic events with a frequency of 1.1×10^{-6} events/year would break most of the fuel. Such events are sampled, and, when such an event occurs, all cladding is failed and to be available for unzipping.

CRWMS M&O 1999d (Section 6.2) also considered the effect of a rubble bed consisting of rocks from a drift collapse on bare fuel rods (no WP or possible drip shield protection). The analysis showed that the bare fuel assemblies would fail under the static loading of the rocks. The potential for rubble bed damage does not occurring until well after the 10,000 year period considered for the regulatory consideration. For longer time periods leading to estimating the peak dose, rubble bed damage to the cladding can not be neglected. A mechanical damage analysis has that cladding perforation from rockfall starting to occur when 50% of the surface area (patches) of the waste package is open. The fraction of rods failed then increases linearly with increased WP surface opening (patches). When 100% of the container patches are open, 100% of the cladding would have perforated from tuff static loading. This is predicted to occur after 100,000 years and might affect the peak dose. This mechanism will fail cladding in WPs that are in zones without dripping and therefore do not fail from localized corrosion. This analysis is summarized in Attachment I, line 114.

The fraction of fuel damaged by handling errors at the YMP facilities is estimated as part of the mechanical damage issue. The percent of rods damaged from handling at reactors is estimated as follows. From CRWMS M&O 2000a, Table 8, there have been 10 damaged assemblies out of a total of 21,810 assemblies. The PWR assemblies average 221 rods/assembly and 2.2 failed rods per failed assembly (CRWMS M&O 2000a, Section 6.8.2). The fraction of rods failed from handling at reactors is $4.56 * 10^{-6}$ from (10 * 2.2 /(21,810 * 221)). This is a very small fraction when compared to reactor damaged fuel. If the YMP operators were ten times more prone to accidents than the reactor operators, the fraction of fuel damaged from handling ($4.56 * 10^{-5}$), still small compared to other sources and can be neglected. Fuel damaged from handling at YMP has been neglected.

6.4.2 DHC and FEP Issues

Delayed hydride cracking (DHC) of existing cracks is analyzed (CRWMS M&O 2000a, Section 6.10.2) using the distribution of stresses shown in Figure 1. Stress intensity factors are calculated to have a mean of 0.47 MPa-$m^{0.5}$ (range 0.002 to 2.7 MPa-$m^{0.5}$), which is below the threshold stress intensity factors that are in the range of 5 to 12 MPa-$m^{0.5}$. Therefore, crack propagation by DHC is not expected. These stress intensities are also below those needed to produce embrittlement failures ($K_I < K_{IC}$). Failure of the cladding by hydride reorientation is unlikely and has not been included in the abstraction for the TSPA-SR analysis. Stresses and temperatures are too low for reorientation to occur. Even if the material did reorient, it will maintain sufficient strength such that failure would not be expected.

Various AMRs have ruled out many cladding failure modes. CRWMS M&O 2000b outlines the Features, Events, and Processes (FEPs) that have been excluded from this analysis. CRWMS M&O 2000c describes the various corrosion mechanisms that are not expected to fail the cladding, considering the expected in-package chemistry predicted in CRWMS M&O 2000i. CRWMS M&O 2000l describes the various hydride mechanisms that are not expected to fail the cladding. This Summary and Abstraction AMR only addresses the cladding failure mechanisms that are expected to contribute to radionuclide release from CSNF.

6.5 FAST RELEASE OF RADIONUCLIDES

The release of radionuclides from the fuel rod occurs in three stages, (1) release of true gap inventory, (2) fast release from initial UO_2/water reaction and (3) wet unzipping (tearing of the cladding). Sections 6.1 through 6.4 discuss the potential of failing (perforating) the cladding. This section addresses the release of radionuclides through the initial cladding failure. Section 6.6 analyzes the tearing open (unzipping) of the cladding and the release of radionuclides from the bulk fuel matrix.

6.5.1 Fast Release Abstraction

The true gap inventory (iodine, cesium, and noble gasses) is released in proportion to the fission gas release fractions (CRWMS M&O 2000d, p. 82). The release of iodine is the same fraction as the noble fission gas release fraction of 4.2% (CRWMS M&O 2000a, Table 12). Cesium gap inventory is 1/3 of the fission gas release fraction or 1.4%.

The fast release refers to the radionuclides that are released with the initial fuel dissolution before the cladding starts to unzip. Wilson (1985, 1987, 1990) reports releases of various radionuclides from fuel rod samples. The samples included intact and defected fuel rod sections and bare fuel. Wilson exposed the samples to water and measured the amounts of various radionuclides that were released during the exposure period. The first measurements were made in about 200 days. The samples were again exposed, and the measurements were repeated after an additional exposure of similar length. The fast release from the uranium pellet through slits and holes in the cladding is estimated by calculating the release rate from Wilson's eight experiments and extrapolating this release rate until the larger gaps are closed by secondary phases (approximately 50 years). Figure 17a presents a uniform distribution of fast release fraction between 0 and 0.4% (mean and median value = 0.2%) which is used in the TSPA-SR abstraction. This linear fit is reasonably bounding, over-predicting the fast release fraction for the lower Cumulative Distribution Function (CDF, equivalent to 1-CCDF) samplings. The cesium and iodine true gap inventories are added to this fuel matrix fast release fraction.

6.5.2 Fast Release Analysis

The purpose of this section is to estimate the fast release inventory. The current conceptual analysis of release from a breached fuel rod considers that the radionuclide inventory may be divided into three parts: a true gap inventory, a fast release inventory, and a delayed release inventory.

The true gap inventory is the portion of the few elements (e.g., Cs, I and noble gasses) that segregate to the gap during reactor operation. In the TSPA-SR treatment, this inventory is immediately released upon cladding and WP failure.

The fast release inventory results from the process of plugging the cracks and gaps in the fuel rod. A substantial length of the fuel rod may be wetted, and uranium dioxide in the wetted length will be converted to a hydroxide (e.g., metaschoepite). As a result, the volume of solid material increases. When the cracks and gaps are fully plugged with reaction products, the conversion process slows to insignificant rates. However, alteration of uranium dioxide will make other radionuclides available for release. In the TSPA-SR treatment, the fast release inventory should be made available for release during the first time step. In total system performance assessment, the true gap and fast release inventories are made available for release during the first time step.

The delayed release inventory is the remainder of the inventory in the fuel rod. This is released during cladding unzipping.

The fast release fraction of radionuclides is initially released before the plugging of the gap between the cladding and fuel pellets is calculated here. The treatment can be developed on the basis of data for ^{99}Tc release as measured by Wilson (1985, 1987, 1990). Wilson's experiments included intact and defected fuel rod sections and bare fuel. Only the results for defected fuel rods were considered. Results for bare fuel are not relevant because it has no protection by cladding; results for intact fuel rods are not relevant because the fuel is not exposed. In Wilson's experiments, the cladding of the defected samples had either one slit or two holes.

To estimate the fast release fraction, Wilson's results were analyzed by an approach that is shown schematically in Figure 16. The period from time 0 to time t_1 corresponds to Wilson's first exposure cycle. During this period, ^{99}Tc is released at rate R_1, which is the measured release rate for this cycle. The period from time t_1 to time t_2 corresponds to the second exposure cycle, and during this period ^{99}Tc is released at rate R_2, which is the measured release rate for the second cycle. The rate of release during the second cycle of testing was often smaller than that during the first cycle. At later times, the release rate decreases linearly from a rate of R_2 at time t_2 to a rate of zero at time t_{pl}, which is the time for complete plugging of the cracks by metaschoepite. Narrow cracks will plug quickly because they can be filled with a small amount of metaschoepite, but wide cracks will take longer to plug because they require a larger amount of metaschoepite. The gradual decrease in release rate thus corresponds to progressive plugging of cracks of different widths. In all cases, the release rate is expressed as a fraction of the total inventory, so it has the units of reciprocal time (e.g, yr^{-1}) and is not expressed as an amount of material per unit time (e.g., mol/yr). The analysis described above was repeated for each of Wilson's fuel rod samples, and the fast release fraction F was calculated as

$$F = R_1 t_1 + R_2 (t_2 - t_1) + [R_2 (t_{pl} - t_2)/2] \qquad \text{Eq. 6.5-1}$$

where the variables are as defined above. A cumulative distribution function is determined in the following paragraphs based on the values of F from the eight (8) tests by Wilson (1985, 1987, 1990).

The fast release fractions were calculated on the basis of measurements of ^{99}Tc. Of the releases tabulated by Wilson (1985, Tables 7 through 13, total measured release divided by 10^{-5} inventory for slit defect and holes defect), ^{99}Tc has the second-largest release as a fraction of inventory. The only radionuclide with a larger release fraction is ^{137}Cs. However, ^{137}Cs would be expected to have a substantial true gap inventory, so its measured releases would be larger than the fast release inventory.

Of the variables used in Equation 6.5-1, all but t_{pl} can be obtained from the data tabulated in Table 11. The value of t_{pl} may be estimated from photomicrographs of the fuel. Wilson (1990, p. 2.7, Figure 2.3) provided a photomicrograph of a cross section of one of his fuel samples. The widest crack of interest is the middle section of the nearly diametral crack. A few cracks appear even wider. However, their irregular shapes and variable widths indicate that these are not unusually wide cracks but rather cracks that appear wide because there is a small dihedral angle between the crack and the plane of the cross section. The middle section of the nearly diametral crack in the photomicrograph (Wilson 1990, p. 2.7, Figure 2.3) has a width of about 0.8 mm in the print provided in the document. Since the magnification in the print is 14.5×, the actual crack width w is about $w = 55$ μm.

CRWMS M&O (2000d, Equation 16) gives the following equation for the forward reaction rate of spent fuel in alkaline water:

$$\log_{10} Dr = 4.69 - \frac{1085}{T} - 0.12 \cdot pCO_3 - 0.32 \cdot pO_2 \qquad \text{Eq. 6.5-2}$$

where Dr is the reaction rate in mg/m^2·day, pCO_3 is the negative of the common logarithm of the total carbonate concentration in mol/L, and pO_2 is the negative of the common logarithm of the oxygen partial pressure.

For exposure of spent fuel in a repository, it is reasonable to approximate the environment by J-13 water in equilibrium with air at 25 °C. This is the same water chemistry as is used in calculating the unzipping speed. The bicarbonate concentration of J-13 water is 128.9 mg/L (CRWMS M&O 2000g, Table 1.1, MO0006J13WTRCM.000). Using the molar masses of H (1.00794 g/mol), C (12.011 g/mol) and O (15.9994 g/mol) (Lide 1995, inside front cover), one finds that the concentration of carbonate is 0.1289 g/L / (1.00794 g/mol + 12.011 g/mol + 3·15.9994 g/mol) = $2.11 \cdot 10^{-3}$ mol/L, and thus $pCO_3 = -\log_{10}(2.11 \cdot 10^{-3}) = 2.68$. In a standard atmosphere, the fraction of O_2 is 0.2095 (Weast and Astle 1980, p. F-208), so $pO_2 = -\log_{10}(0.2095) = 0.679$. By applying Equation 6.5-2, one obtains $Dr = 3.26$ mg/m^2·day. The density ρ of UO_2 is $\rho = 10970$ kg/m^3 (Lide 1995, p. 4-94). By dividing Dr by ρ, one finds that $Dr / \rho = 0.297$ nm/day.

Wet oxidation of the fuel produces metaschoepite. The molar volume of metaschoepite ($UO_3 \cdot 2H_2O$) is $v_{ms} = 64.5$ cm^3/mol (see Assumption 5.6.4). The molar volume of UO_2 is $v_{UO2} = 24.6$ cm^3/mol; this follows from the density (10970 kg/m^3) and molar masses ([238.0289 + 2·15.9994] g/mol) reported by Lide (1995, inside front cover and p. 4-94). Therefore, oxidation of a layer of UO_2 yields a layer of metaschoepite that is (v_{ms} / v_{UO2}) times as thick as the original layer. Since the original UO_2 is consumed, the surface moves by $((v_{ms} / v_{UO2}) - 1)$ times the thickness of the original layer.

The reaction rates predicted by Equation 6.5-2 are for a microscopically smooth surface. In contrast, the surfaces of cracks will be rough, so the exposed surface area will be larger, and the oxidation rate will be higher. The ratio R of the actual surface area to the apparent surface area is estimated as $R = 3$ (CRWMS M&O 2000d, p. 82).

By combining the results above, one obtains the plugging time t_{pl} as

$$t_{pl} = \frac{w\rho}{2(v_{ms} / v_{UO2} - 1)RDr} \qquad \text{Eq. 6.5-3}$$

The factor of 2 is present because oxidation occurs on both sides of the crack. Using the values above, one finds that $t_{pl} = 1.9 \cdot 10^4$ day (about 50 years).

The data from Table 11 are put into the notation of this section as follows. The values for first cycle ^{99}Tc release (10^{-5} of sample inventory) are $R_1 t_1$. The values for second cycle ^{99}Tc release (10^{-5} of sample inventory) are $R_2(t_2 - t_1)$. The first cycle time (days) and second cycle time (days) are t_1 and $t_2 - t_1$, respectively. From these values, R_2 and t_2 can be calculated. Using the data in Table 11, the results in Table 12 are obtained.

Using the approach described above, the fast release fraction was calculated for each of Wilson's eight samples. The results were plotted as an experimental Cumulative Distribution Function (CDF) in Figure 17a.

The CDF for the fast release fraction is generally expected to overestimate the actual fast release fraction for two reasons. First, Wilson's tests are for short samples rather than full-length fuel rods. In full-length rods, transport limitations may reduce the fraction released. Transport limitations are discussed in more detail below. Second, some preferential release of ^{99}Tc is expected. Wilson (1985, p. 36) states, "It is likely that ^{99}Tc partitions to the grain boundaries in the hotter central portions of the fuel. As grain boundary attack (which is clearly visible in Figure 3 of Wilson 1985) progresses in these regions, enhanced ^{99}Tc release would then be observed." For these reasons, it is expected that the recommended CDF gives a reasonably bounding estimate of the fast release fraction.

In determining the fast release fraction, the CDF is determined from experiments on short rod sections. For total system performance assessment, the same CDF applies to full-length rods. This treatment is clearly reasonably bounding, but it may be thought to be overly conservative. To determine whether it is overly conservative, it is helpful to compare the fuel rod length to the characteristic diffusion distance, $2(Dt)^{1/2}$ where D is the diffusion coefficient and t is the time allowed for diffusion. For strong electrolytes dissolved in water at 25 °C, diffusion coefficients are typically on the order of 10^{-9} m^2/s (Weast and Astle 1980, p. F-62). The diffusion time may be approximated by the plugging time $t_{pl} = 1.9 \cdot 10^4$ day $= 1.65 \cdot 10^9$ s. The diffusion distance is then $2(Dt)^{1/2} = 2.6$ m. Since this distance is comparable to the active length of a fuel rod, it is reasonable to expect that, if the entire length of the fuel rod is saturated, the entire length will contribute to radionuclide releases. Additional conservatism will result if only part of the rod is saturated. However, information on rod saturation is not available, so credit cannot be taken for partial saturation.

6.6 CLADDING UNZIPPING AND FUEL DISSOLUTION

Under wet conditions, the fuel matrix reacts with moisture at the intrinsic fuel matrix dissolution rate and precipitates locally as metaschoepite. This secondary phase isolates most of the fuel from the moisture but the fuel in the split cladding region continues to react with moisture, thus increasing in volume and forcing the split further along the cladding. Such alteration results in significant volume expansion, and the cladding breach will eventually propagate from its original location to the ends of the fueled length. Propagation of a cladding breach is termed "unzipping" which is used interchangeably with "splitting".

As discussed in Section 6.6.1 below, the reaction front is not necessarily planar. However, since fuel rods are long and thin, the reaction front can be approximated by a planar front that propagates at some multiple of the intrinsic fuel matrix dissolution rate.

To determine the inventory of radionuclides that is available for release from the entire repository, it is necessary to have a means for predicting the fraction of breached waste packages, the fraction of fuel rods with cladding breaches, and the speed of propagation of a cladding split. This section provides a mathematical framework for describing these processes in a way that is computationally efficient. The approach is intended for use in total system performance assessments.

Table 11. Inputs on ^{99}Tc Releases

Sample	Source	First Cycle ^{99}Tc Release		Second Cycle ^{99}Tc Release		Location[d]	First Cycle Time (days)	Second Cycle Time (days)	Location[d]
		(nCi)	(10^{-5} of Inv.)	(nCi)	(10^{-5} of Inv.)				
H-6-12	Wilson (1985)	28.2+5.4[b]	12.1×33.6/50.8[c]	15.8+1.4[b]	12.1×17.2/50.8[c]	Table 12	252	128	Table 3
J-8-24	Wilson (1985)	4.5+1.4[b]	6.7×5.9/27.7[c]	18.0+3.8[b]	6.7×21.8/27.7[c]	Table 12	244	128	Table 3
C5C-E	Wilson (1987)	25	2.8	18.5	2.1	Table 13	223	202	Table A.3
I9-19	Wilson (1987)	73	15.3	32	6.6	Table 13	181	195	Table A.7
C5C-C	Wilson (1987)	--	0.5[a]	--	0.5[a]	Table 13	223	202	Table A.4
I9-12	Wilson (1987)	--	0.5[a]	--	0.5[a]	Table 13	181	195	Table A.8
C5B-D	Wilson (1990)	12.7	1.4	--	0.5[a]	Table 3.8	174	181	Table A.5
C5B-B	Wilson (1990)	18.9	2.2	--	0.5[a]	Table 3.8	174	181	Table A.6

Sample	Defect Type	Location[d]
H-6-12	Slit	Table 3
J-8-24	Holes	Table 3
C5C-E	Slit	Table 1
I9-19	Slit	Table 1
C5C-C	Holes	Table 1
I9-12	Holes	Table 1
C5B-D	Slit	Table 2.1
C5B-B	Holes	Table 2.1

NOTES: Inv. = Sample inventory.
-- = Not reported.
[a] Release was below detection limit. The value used here ($5 \cdot 10^{-6}$) is half of the detection limit (10^{-5}) (Wilson (1985, p. 35).
[b] Total was not reported.
[c] Expression is (release for both cycles divided by 10^{-5} of inventory)×(release for cycle 1 in nCi)/(release for both cycles in nCi)
[d] Location refers to the Table in the Reference Source identified in the second column of this Table 11 (Wilson 1985, 1987 and 1990)

Table 12. Fast Release Fractions for Defected Samples

Sample	Fast Release Fraction
H-6-12	0.00311
J-8-24	0.00392
C5C-E	0.00102
I9-19	0.00338
C5C-C	0.00024
I9-12	0.00025
C5B-D	0.00028
C5B-B	0.00029

DTN: MO0011SPACMU07.049

The various subsections have different emphases. Section 6.6.1 summarizes the abstraction for fuel rod unzipping. That abstraction uses the intrinsic dissolution rate, so Section 6.6.2 restates the equations for dissolution rate that were developed in CRWMS M&O 2000d. The general formalism for unzipping described in Section 6.6.3 is intentionally abstract and general. It is applicable to essentially any combination of waste package and waste form analysis. In Section 6.6.4, the treatment is made more specific. It is applied to a particular analysis of fuel rod unzipping, and simplifications to the general formalism are discussed. In Section 6.6.5, the specific treatment of Section 6.6.4 is summarized for many waste packages. Finally, in Section 6.6.6, the results of Section 6.6.5 are simplified for a system with only one waste package. This form is useful in implementing a performance assessment.

6.6.1 Wet Unzipping Abstraction

Fuel rods with perforated cladding are expected to remain intact until the WP breaches and permits air and moisture to enter. While the humidity is low, dry unzipping could occur. Since the WP is expected to remain intact for at least 200 years, the fuel temperatures will be too low for dry unzipping (fuel conversion to U_3O_8) to occur. Wet unzipping of failed rods is analyzed to start when the WP breaches. Rods that fail after WP breach immediately start to unzip. The fuel matrix is dissolved at the intrinsic dissolution rate that is evaluated for the current temperature and in-package chemistry. The dissolved UO_2 precipitates locally as metaschoepite. This secondary phase isolates most of the fuel from the moisture and increases in volume compared to UO_2. In time, the cladding in the reaction region is torn as the reaction continues. This section uses three different approaches to determine the propagation speed for the split.

Conservative Treatment–When uranium dioxide fuel reacts to form metaschoepite, the volume of the material increases. From the principle of conservation of matter (see Assumption 5.6.6), it follows that

$$\frac{\pi r_x^2}{v_x} = \frac{\pi r_u^2}{v_u} \qquad \text{(Eq. 6.6-01)}$$

where r_x is the radius of the fuel after alteration, v_x is the molar volume of metaschoepite, r_u is the radius of the fuel before alteration, and v_u is the molar volume of uranium dioxide. From Equation 6.6-01, it follows that

$$\frac{r_x}{r_u} = \sqrt{\frac{v_x}{v_u}} \qquad \text{(Eq. 6.6-02)}$$

Under Assumption 5.6.8.a, when a length of fuel cladding splits, it no longer protects the enclosed fuel from water. As a result, fuel alteration proceeds uniformly around the full circumference of the fuel stack. As the split propagates, recently exposed sections of fuel retain a large core of unaltered fuel, whereas sections that were exposed earlier have less unaltered fuel. It follows that, at each end of the split, the interface between the regions of unaltered and altered fuel is a cone. A schematic longitudinal cross section of a partially altered fuel rod is shown in Figure 17b. In this figure, the surface of the fuel stack is shown by the dotted lines. The current alteration front is $\angle BAC$; the alteration front at some later time is $\angle B'DC'$.The cone propagates, base first, from the point where the split initiated toward the end of the rod. Propagation of the alteration front from $\angle BAC$ to $\angle B'DC'$ corresponds to an advance of the split by a distance Lr_u. However, alteration proceeds normal to the alteration front, so the time required to advance the split by a distance Lr_u is the distance DE divided by the alteration rate f. From the geometry of Figure 17b, it can be seen that $\angle ABD = \tan^{-1}L$, and therefore the distance DE is $r_u \sin(\tan^{-1}L)$. It follows that ratio of the split propagation rate R to the alteration rate is

$$\frac{R}{f} = \frac{L}{\sin(\tan^{-1} L)} \qquad \text{(Eq. 6.6-03)}$$

The only remaining step is to determine L, which can be derived from the apex angle for a split. Upon alteration, the circumference of fuel stack increases from $2\pi r_u$ to $2\pi r_x$. If, following Assumption 5.6.7, the split takes up all of the increase in circumference, the width of the split w after complete alteration is

$$w = 2\pi\left(\frac{r_x}{r_u} - 1\right) r_u \qquad \text{(Eq. 6.6-04)}$$

Let θ be the apex angle of the split. From Figure 17b, the length of tapered part of the split is Lr_u. Then it follows that

$$w = 2Lr_u \tan(\theta/2) \qquad \text{(Eq. 6.6-05)}$$

From Equations 6.6-04 and 6.6-05, it follows that

$$L = \frac{\pi(r_x/r_u - 1)}{\tan(\theta/2)} \qquad \text{(Eq. 6.6-06)}$$

The ratio of the splitting rate to the alteration rate R/f, can be obtained by combining Equations 6.6-02, 6.6-06, and 6.6-03. As is discussed in Section 6.5.2, the molar volumes are v_x = 64.5 cm^3/mol and v_u = 24.6 cm^3/mol. By applying Equation 6.6-02, it follows that $r_x/r_u = 1.619$.

The value of θ may be obtained from photomacrographs of oxidized fuel rods. Figure 10 of Einziger and Strain (1986) shows such a fuel rod. The rod has a double-ended split, and the image of the split measures 56 mm long and 12.5 mm wide. This corresponds to an apex angle of at least $\theta = 2\tan^{-1}(12.5/56) = 0.439$ rad. The actual angle is probably larger than this because the photograph was taken from an angle that would make the split appear narrower than it actually is.

However, the photograph provided by Einziger and Strain is of a sample that was oxidized at 360°C, whereas wet fuel oxidation will occur at or near room temperature. Lowry et al. (1981, Figures 22, 29, 32, 34, 39, 41) have plotted the total strain for tensile tests on irradiated Zircaloy fuel cladding as a function of temperature. These figures show some temperature dependence, but the ratio of the total strain at 360°C to that at room temperature is less than two. Walker and Kass (1974, Figures 3 and 4) reported the fracture toughness K_{IC} of irradiated samples of Zircaloy-4 from rolled and annealed plates. They found that the ratio of K_{IC} at 360°C to that at room temperature is about two. In view of these results, it is reasonable to use an apex angle of 0.220 rad rather than 0.439 rad (see Assumption 5.6.9).

Using r_x/r_u and θ as given above, Equation 6.6-06 yields L = 17.6. Finally, from Equation 6.6-03, R/f = 17.7. The value of 18 for R/f is used as the 10% value in the CCDF. Because of the large uncertainty in the calculation of unzipping velocities, the lower limit of the CCDF is assigned a value of R/f = 180.

Intermediate Treatment–An alternative to the treatment above is to use Assumption 5.6.8.b: once the cladding is split, water has access to the surface of the fuel only where the fuel is exposed by the split.

The interface between the altered and unaltered regions is easy to represent if the split is narrow; in that case the interface can be approximated by a cone with its axis along the split. The apex of the cone is at the tip of the split. The cone propagates along the fuel rod, apex first.

In this treatment, Equations 6.6-01, 6.6-02, 6.6-04, 6.6-05 and 6.6-06 are still applicable. However, the geometry of the alteration front is different. Figure 17c shows the modified geometry in cross section, with the split at the bottom of the figure. As in Figure 17b, the dotted lines indicate the surface of the fuel. In cross section, the current interface between altered and unaltered fuel is $\overline{AC}$; the entire surface is a cone with its apex at C and its axis along $\overrightarrow{CC'}$. The interface at some later time is $\overline{BC'}$. To advance the interface from $\overline{AC}$ to $\overline{BC'}$ requires propagation of the split by a distance Lr_u. Since alteration proceeds normal to the alteration front, the depth of alteration for this amount of split propagation is BD. But $\angle ACB = \tan^{-1}(L/2)$, so the distance BD is $2r_u \sin(\tan^{-1}(L/2))$. It follows that

$$\frac{R}{f} = \frac{L}{2\sin(\tan^{-1}(L/2))} \qquad \text{(Eq. 6.6-07)}$$

The values for r_x / r_u and L obtained for the conservative treatment apply here as well. However, L must be used in Equation 6.6-07 rather than in Equation 6.6-03. The result from Equation 6.6-07 is that $R/f = 8.8$.

Lower-bound Treatment–A third alternative is to use Assumption 5.6.8.c, which states that oxidation occurs only on the circular end of the fuel stack. Under this treatment, the oxidation front is planar. Accordingly, $R/f = 1$.

To represent the three different treatments above, a triangular distribution is recommended. The lower limit of the distribution is at $R/f = 1$, the mode is at $R/f = 9$, and the upper limit is at $R/f = 18$. The values for the mode and upper limit are the values given above after rounding to the nearest integer. As is discussed in Section 6.6.2 below, the alteration rate f is six times the intrinsic dissolution rate. To account for time-dependence of the water chemistry and temperature, f should be evaluated at each time step. Section 6.6.6 gives equations for determining the rate at which fuel is exposed as a result of unzipping. These equations take into account the effect of having fuel rods fail at different times.

6.6.2 Intrinsic Dissolution Abstraction

The intrinsic dissolution rate is used in the unzipping calculations to determine the reaction rate velocity. The intrinsic dissolution equation is to be applied at each TSPA-SR simulation time step and is to be based on the local chemical conditions. At some times the pH could be basic and at other times it could be acidic (CRWMS M&O 2000i). The abstraction is therefore divided into regions of pH greater than and less than a neutral pH (pH = 7). CRWMS M&O 2000d (p. 82) develops the intrinsic dissolution equations that are recommended for TSPA-SR.

For basic conditions (pH > 7),

$$\mathrm{Log}_{10}\, Dr = a_0 + a_1 / \mathrm{Tk} + a_2 \cdot \mathrm{pCO_3} + a_3 \cdot \mathrm{pO_2} \qquad \text{(Eq. 6.6-1)}$$

where $a_0 = 4.69$, $a_1 = -1085$, $a_2 = -0.12$, and $a_3 = -0.32$.

For acid conditions (pH < 7),

$$\mathrm{Log}_{10}\, Dr = a_0 + a_1 / \mathrm{Tk} + a_3 \cdot \mathrm{pO_2} + a_4 \cdot \mathrm{pH} \qquad \text{(Eq. 6.6-2)}$$

where $a_0 = 7.13$, $a_1 = -1085$, $a_3 = -0.32$, and $a_4 = -0.41$.

Equations 6.6-1 and 6.6-2 may be combined in the following form:

$$\mathrm{Log10(Dr)} = a_0 + a_1/\mathrm{Tk} + a_2 \cdot \mathrm{pCO_3} + a_3 \cdot \mathrm{pO_2} + a_4 \cdot \mathrm{pH} \qquad \text{(Eq. 6.6-3)}$$

where Tk = absolute temperature (K)
$\mathrm{pCO_3}$ = –Log10 (molar concentration of $\mathrm{CO_3}$--)
$\mathrm{pO_2}$ = –Log10 (partial pressure in atmospheres of $\mathrm{O_2}$)
Dr = intrinsic dissolution rate = mg /$\mathrm{m^2}$·d.

The coefficients for these equations are summarized in Table 13. This function is used in the TSPA-SR. The uncertainty in the intrinsic dissolution rate is applied to the coefficient a_0. The value of a_0 is uniformly distributed by + or – 1.0. This is equivalent to a log uniform distribution of the intrinsic dissolution rate by a multiple of ten (10). CRWMS M&O 2000d recommended an uncertainty of 1.5 orders of magnitude. An inspection of the test results shown in CRWMS M&O 2000d (Table 1) suggests a much smaller range. Three tests under identical conditions (Runs 1,2 3) varied by only 18% from the mean. There is also an independent uncertainty of a factor of six (6) associated with the unzipping velocity in the use of the intrinsic dissolution rate. Figure 18 (CRWMS M&O 2000d, p. 55) shows the dependency of the intrinsic dissolution on temperature and pH for constant O_2 and CO_2 gas pressure. As the pH increases, the carbonate speciation shifts from H_2CO_3 to CO_3^{--}. The lines of Figure 18 are sloped for pH>7 even though $a_4 = 0$ because of the increase in CO_3^{--} in the water. In the TSPA-SR, each of the variables could vary with time.

Table 13. Intrinsic Dissolution Equation and Terms

	a_0	a_1	a_2	a_3	a_4
pH>7	4.69	-1085	-0.12	-0.32	0
pH<=7	7.13	-1085	0	-0.32	-0.41

CRWMS M&O 2000d, p. 55

Both the intrinsic dissolution tests and the equations given above are based on tests for individual grains of UO_2. The unzipping analyzed in TSPA-SR occurs on the pellet surface and the rate in $mg/m^2 \cdot d$ is converted to a reaction rate velocity of cm/yr. A grain boundary penetration factor of six (6) from Gray and Wilson 1995 (p. 4.2) is applied to the intrinsic dissolution rate to account for water penetration into grain boundaries. An additional factor for surface area due to cracks in the spent fuel pellet or surface roughness should not be used. According to Assumption 5.6.5, cracks will be filled in by precipitates. Also, a reaction front on an initially rough surface will reduce the peaks faster than the valleys because of the peaks' higher surface area, so the reaction front will tend to become smooth.

Figure 19 is an example of unzipping times as a function of temperature for a constant chemistry of approximate J-13 water, and Figure 20 shows the dependency on pH at a fixed temperature of 35 °C. In the TSPA-SR, both in-package chemistry and temperature are changing with time and the unzipping velocity is evaluated within the TSPA-SR analysis itself.

6.6.3 General Formalism for Wet Unzipping

Each fuel rod can be classified as either intact, unzipping, or exhausted. "Intact" is used broadly to denote those rods whose fuel is protected from alteration, thus the intact fraction includes all rods in intact waste packages and all rods with intact cladding in breached waste packages. "Unzipping" denotes rods that are in the process of alteration, that is those rods that are in breached waste packages and have breached cladding but are not yet fully unzipped. "Exhausted" refers to those rods that were breached so long ago that they are fully unzipped, that is the split has propagated all the way to the ends of the fueled region of the rod.

For convenience, the "time of emplacement" will be taken as "time = zero" and "time since emplacement" will simply be called "time." The waste package and waste form analysis must provide the following three functions. Let $W(t)$ be the fraction of waste packages breached at some time t. For a particular waste package that breached at time t_w, let $f_b(t, t_w)$ be the fraction of fuel rods that are breached at time t. "Breached" fuel rods are those that are either unzipping or exhausted, so $f_b(t, t_w) = 0$ for $t < t_w$. Let $v(t)$ be the unzipping speed for a breached fuel rod in a breached waste package at time t. The method described here applies only for $t \geq 0$.

To describe the instantaneous state of unzipping for the entire group of waste packages, define $f_i(t)$, $f_u(t)$, and $f_e(t)$ which are the fractions of the fuel rods that are intact, unzipping, and exhausted, respectively, at time t. These functions are not applied to individual waste packages; rather, they describe all the rods in the entire group of waste packages. Note that the unzipping fraction includes rods with a variety of split lengths, from very short to nearly the entire fueled length. No distinction among these rods is made on the basis of split length. None of the functions $f_i(t)$, $f_u(t)$, and $f_e(t)$ is specified in advance; they are all derived from $W(t)$, $f_b(t, t_w)$, and $v(t)$. Note, however, that $f_i(t) + f_u(t) + f_e(t) = 1$ for any time t, so only two of $f_i(t)$, $f_u(t)$, and $f_e(t)$ are independent.

The first of these functions to be derived is $f_i(t)$. Initially:

$$f_i(0) = 1 - W(0) f_b(0,0) \qquad \text{(Eq. 6.6-4)}$$

Equation 6.6-4 follows because, out of the entire set of rods, the fraction that is breached rods in breached waste packages at the time of emplacement is $W(0)f_b(0, 0)$; all other rods are "intact" in the sense defined above. At later times, there may be additional breached waste packages and breached rods. The fraction that remains intact at time t will be:

$$f_i(t) = 1 - W(0) f_b(t,0) - \int_0^t \frac{dW(\tau)}{d\tau} f_b(t,\tau) d\tau \qquad \text{(Eq. 6.6-5)}$$

Equation 6.6-5 is justified as follows. The first term (1) corresponds to the entire set of rods. The second term corresponds to those rods that are in defective waste packages (i.e., the WPs have failed at the time of emplacement) and the rods either are breached at emplacement or breach after emplacement but before time t. The third term corresponds to rods in the waste packages that breach after emplacement. During a given infinitesimal time interval from τ to $\tau + d\tau$, the fraction of waste packages that breach is $(dW(\tau) / d\tau)\, d\tau$. At some later time t, the fraction of breached rods in these packages is $f_b(t, \tau)$. The integral takes into account all waste package failure times up to time t.

The amount of fuel altered could be determined by solving a partial differential equation for the distribution of split lengths as a function of time, but this approach is computationally costly. A more efficient approach is derived here. Figure 21 is a schematic plot of the alteration rate as a function of time for two individual fuel rods in a breached waste package. For the time scales of interest in performance assessment, the radionuclide inventory can be divided into two parts: the gap inventory and the fuel matrix inventory. The alteration of both parts is shown schematically in Figure 21. The cladding of rod A breaches at time t_{0A}. There is a pulse of alteration at this time; the pulse corresponds to the gap inventory. The fuel matrix inventory takes much longer to

alter; fuel matrix alteration begins at time t_{0A} and continues until time t_{1A}, when the fuel rod is fully unzipped (exhausted) and the fuel matrix is fully altered. The fuel matrix alteration rate is time-dependent because the conditions (e.g., temperature and water chemistry) inside the waste package are time-dependent. The alteration of the fuel in rod B is similar, but the cladding of rod B breaches later, at time t_{0B}. Since the fuel matrix alteration rate is decreasing with increasing time, alteration of the entire inventory in rod B takes longer, and the rod is not exhausted until time t_{1B}. The alteration rate for an entire waste package will be a superposition of the alteration rates for each rod.

Let $F_g(t)$ be the fraction of the total gap inventory (for the entire group of waste packages) that has been altered at time t. The gap inventory is altered immediately if the waste package and fuel cladding are both breached, and thus the altered fraction can be written as follows

$$F_g(t) = 1 - f_i(t) \qquad \text{(Eq. 6.6-6)}$$

The following approach can be used to determine the fraction of the fuel matrix inventory that has been altered. Before significant numbers of waste packages begin to breach, the heat output of the packages will have become fairly small, so the temperatures and in-package chemical environment will be fairly uniform. Therefore, it is a reasonable approximation to use a single unzipping speed for all the fuel rods in the entire group of WPs. In light of that approximation, define the function $h(t)$ as:

$$h(t) = \int_0^t v(\tau) d\tau \qquad \text{(Eq. 6.6-7)}$$

where $v(\tau)$ is the speed of unzipping at time τ. Note that $h(0) = 0$ because the interval of integration will have zero length. The function h is referred to as the "propagation distance". As an alternative to Equation 6.6-7, changes in $h(t)$ may be expressed in differential form:

$$\frac{d}{dt} h(t) = v(t) \qquad \text{(Eq. 6.6-8)}$$

For simplicity, the initial cladding damage always occurs at the center of the fueled region. The split will then propagate to both ends of the fueled length. This gives the fastest alteration rate: If the split starts at the center, the rod is exhausted when each end of the split has propagated by a distance of L / 2, where L is the length of the fueled region. In contrast, if the split starts somewhere besides the center, the split must propagate farther in one direction, and thus for a longer time, before the rod is exhausted.

The time for unzipping of fuel rods A and B is shown schematically in Figure 22, where the propagation distance h is plotted as a function of time. For the purposes of this illustration, it is presumed that rod A is failed at the time of emplacement and is in a waste package that is breached at emplacement. (This will presumably be an extremely rare occurrence.) In this case $t_{0A} = 0$. As can be seen from Figure 22, rod A starts unzipping at time t_{0A}, when $h = 0$, and is exhausted at time t_{1A}, when $h = L / 2$. This is readily understandable in light of the definition of $h(t)$ in Equation 6.6-7. The situation for rod B is slightly more complicated. The fuel in rod B is not exposed for alteration until time t_{0B}; this is the time when both the waste package and

cladding are breached. At this time, rod A is already partially unzipped. As is shown in Figure 22 for rod A, $h(t_{0B}) = c$. Both rods then unzip at the same rate, since there is a single unzipping speed for all rods. At time t, the distance that the split has propagated from the center of rod A is $h(t)$ (for $t_{0A} \le t \le t_{1A}$), but the distance that the split has propagated from the center of rod B is $h(t) - c$ (for $t_{0B} \le t \le t_{1B}$). Thus, rod B is exhausted when h reaches $L / 2 + c$.

The discussion above also sheds additional light on the nature of h. In an actual rod, splitting initiates at some time, the split propagates until it reaches the ends of the fueled region, and splitting stops. In contrast, $h(t)$ increases without limit. Thus, $h(t)$ is the propagation distance for an infinitely long rod that starts splitting at the time of emplacement.

The invariance of the unzipping speed has an important implication: It is not necessary to track the propagation of splits in individual rods or even the state of individual waste packages. The fraction of matrix alteration can be deduced from $f_i(t)$ and $v(t)$ alone, as is shown below.

The first step in determining the fraction of matrix alteration is to define a function h^{-1}, which is the inverse function of h, that is:

$$h^{-1}(h(t)) = t \text{ for } t \ge 0 \qquad \text{(Eq. 6.6-9)}$$

The physical meaning of h^{-1} is straightforward. Given a time $t \ge 0$, $h(t)$ is the distance that the split has propagated at that time. Given a propagation distance $x \ge 0$, $h^{-1}(x)$ is the time at which that propagation distance is reached.

Consider a time t that is sufficiently large that some rods are exhausted. The exhausted rods became exhausted by breaching at some earlier time and having the split propagate by a distance of $L / 2$ to the ends of the fueled region. At the time t in question, the propagation distance is $h(t)$. The rods that are exhausted at time t are therefore exactly those that were breached (either exhausted or unzipping at the earlier time) when the propagation distance was $h(t) - L / 2$. But a propagation distance of $h(t) - L / 2$ corresponds to a time of $h^{-1}(h(t) - L / 2)$. Therefore:

$$\begin{aligned} f_e(t) &= 1 - f_i(h^{-1}(h(t) - L/2)) \text{ for } t \ge h^{-1}(L/2) \\ &= 0 \text{ for } t < h^{-1}(L/2) \end{aligned} \qquad \text{(Eq. 6.6-10)}$$

because $1 - f_i$ is the fraction of breached rods. For times earlier than $h^{-1}(L / 2)$, there are no exhausted rods because there has not been enough time for any split to propagate by a distance of $L / 2$.

Given the fraction of intact rods and the fraction of exhausted rods, the fraction of unzipping rods follows:

$$f_u(t) = 1 - f_i(t) - f_e(t) \qquad \text{(Eq. 6.6-11)}$$

Let $F_m(t)$ be the fraction of the total fuel matrix inventory that has been altered at time t. At the time of emplacement ($t = 0$), $F_m(0) = 0$. At later times, some of the fuel may be altered. Let n be the total number of fuel rods in all the waste packages and let A be the cross-sectional area of one

fuel rod. The total volume of fuel is ALn. In each unzipping rod, the rate at which fuel is being altered is $2Av(t)$. But there are $nf_u(t)$ unzipping rods, so:

$$\frac{dF_m(t)}{dt} = \frac{2Av(t)nf_u(t)}{ALn} = \frac{2}{L}v(t)f_u(t) \qquad \text{(Eq. 6.6-12)}$$

Since $F_m(0) = 0$, integration of Equation 6.6-12 yields:

$$F_m(t) = \frac{2}{L}\int_0^t v(\tau)f_u(\tau)d\tau \qquad \text{(Eq. 6.6-13)}$$

6.6.4 Application to a Specific Analysis of Unzipping

The general formalism presented in Equations 6.6-4 through 6.6-13 is quite general, but it is still computationally costly to implement. In particular, Equation 6.6-5 requires evaluation of an integral whenever a value of $f_i(t)$ is needed. To simplify the implementation, this section applies the general formalism to a particular analysis for unzipping.

In place of the general function $f_b(t, t_w)$ for the fraction of fuel rods that are breached, define a new function $f_b(t - t_w)$ where t is the time since emplacement and t_w is the time of waste package breach. This function can be used in the general formalism above by replacing Equations 6.6-4 and 6.6-5 above with the following equations:

$$f_i(0) = 1 - W(0)f_b(0) \qquad \text{(Eq. 6.6-14)}$$

$$f_i(t) = 1 - W(0)f_b(t) - \int_0^t \frac{dW(\tau)}{d\tau} f_b(t-\tau)d\tau \quad \text{for } t \geq 0 \qquad \text{(Eq. 6.6-15)}$$

Even with this simplification, Equation 6.6-15 includes a convolution integral, and a complete evaluation of the integral is necessary whenever $f_i(t)$ is needed. However, the form of f_b that has been proposed for performance assessment is particularly simple:

$$\begin{aligned} f_b(z) &= 0 \text{ for } z < 0 \\ &= a_0 + a_1 z \text{ for } 0 \leq z \leq \frac{1-a_0}{a_1} \\ &= 1 \text{ for } z > \frac{1-a_0}{a_1} \end{aligned} \qquad \text{(Eq. 6.6-16)}$$

As in the general formulation, fuel rods in an intact waste package are not considered to be "breached," regardless of the condition of the cladding. In Equation 6.6-16, a_0 and a_1 are positive constants; a_0 is the fraction of fuel rods that are breached when the waste package breaches. Rods that breach by short-term processes (such as creep rupture) may be included in this set because these processes will be essentially complete before significant numbers of waste packages breach. The constant a_1 gives the rate of change of the fraction of breached rods after the waste package is breached. This constant describes processes such as localized corrosion of

the cladding. The fraction of breached rods cannot exceed 1. In general, the values of a_0 and a_1 will reflect the abstraction of the cladding degradation analysis, and their values will vary from one realization to the next. Note that $f_b(z)$ is continuous at $z = (1-a_0)/a_1$, but it is discontinuous at $z = 0$ because all the rods that were perforated earlier are suddenly considered as "breached". However, $f_b(z)$ is generally not of interest for $z < 0$, so the discontinuity will not cause difficulty.

The form of Equation 6.6-16 allows for further simplification of Equation 6.6-15, but it requires separate consideration of the different time intervals listed in Equation 6.6-16. For $0 \le t \le (1-a_0)/a_1$:

$$\begin{aligned} f_i(t) &= 1 - W(0) f_b(t) - \int_0^t \frac{dW(\tau)}{d\tau}[a_0 + a_1(t-\tau)]d\tau \\ &= 1 - W(0) f_b(t) - (a_0 + a_1 t)\int_0^t \frac{dW(\tau)}{d\tau}d\tau + a_1 \int_0^t \frac{dW(\tau)}{d\tau}\tau d\tau \\ &= 1 - W(0) f_b(t) - (a_0 + a_1 t)[W(t) - W(0)] + a_1 \int_0^t \frac{dW(\tau)}{d\tau}\tau d\tau \\ &= 1 - W(0) f_b(t) - f_b(t)[W(t) - W(0)] + a_1 \int_0^t \frac{dW(\tau)}{d\tau}\tau d\tau \\ &= 1 - f_b(t) W(t) + a_1 \int_0^t \frac{dW(\tau)}{d\tau}\tau d\tau \end{aligned}$$

(Eq. 6.6-17)

Equation 6.6-17 can then be differentiated with respect to time:

$$\begin{aligned} \frac{df_i(t)}{dt} &= -f_b(t)\frac{dW(t)}{dt} - \frac{df_b(t)}{dt}W(t) + a_1 \frac{dW(t)}{dt}t \\ &= -a_0 \frac{dW(t)}{dt} - a_1 t \frac{dW(t)}{dt} - a_1 W(t) + a_1 t \frac{dW(t)}{dt} \\ &= -a_0 \frac{dW(t)}{dt} - a_1 W(t) \end{aligned}$$

(Eq. 6.6-18)

Equation 6.6-18 applies for all t such that for $0 \le t \le (1-a_0)/a_1$.

For convenience, define:

$$t_c = \frac{1-a_0}{a_1} \qquad \text{(Eq. 6.6-19)}$$

From Equations 6.6-15 and 6.6-16 it follows that, for $t = {}^{99}\text{Tc} + t_x$, where $t_x > 0$:

$$
\begin{aligned}
f_i(t) &= 1 - W(0) f_b(t) - \int_0^{t_x} \frac{dW(\tau)}{d\tau} f_b(t-\tau) d\tau \; - \int_{t_x}^{t} \frac{dW(\tau)}{d\tau} f_b(t-\tau) d\tau \\
&= 1 - W(0) - \int_0^{t_x} \frac{dW(\tau)}{d\tau} d\tau \; - \int_{t_x}^{t} \frac{dW(\tau)}{d\tau} (a_0 + a_1(t-\tau)) d\tau \\
&= 1 - W(0) - [W(t_x) - W(0)] - (a_0 + a_1 t) \int_{t_x}^{t} \frac{dW(\tau)}{d\tau} d\tau \; + a_1 \int_{t_x}^{t} \frac{dW(\tau)}{d\tau} \tau d\tau \\
&= 1 - W(t_x) - (a_0 + a_1 t)[W(t) - W(t_x)] + a_1 \int_{t_x}^{t} \frac{dW(\tau)}{d\tau} \tau d\tau
\end{aligned}
$$

(Eq. 6.6-20)

In writing Equation 6.6-20, the interval of integration from Equation 6.6-15 has been divided in two. These intervals reflect the differing forms of f_b in different regions.

By differentiating Equation 6.6-20, one obtains:

$$
\begin{aligned}
\frac{df_i(t)}{dt} &= -\frac{dW(t_x)}{dt} - (a_0 + a_1 t)\frac{dW(t)}{dt} + (a_0 + a_1 t)\frac{dW(t_x)}{dt} - a_1 W(t) + a_1 W(t_x) \\
&\quad + a_1 t \frac{dW(t)}{dt} - a_1 t_x \frac{dW(t_x)}{dt} \\
&= -a_0 \frac{dW(t)}{dt} + (a_0 + a_1 t - 1 - a_1 t_x)\frac{dW(t_x)}{dt} - a_1 W(t) + a_1 W(t_x) \\
&= -a_0 \frac{dW(t)}{dt} - a_1 W(t) + a_1 W(t_x)
\end{aligned}
$$

(Eq. 6.6-21)

In carrying out the differentiation, it is important to recognize that t_x is a function of t; $t_x = t - t_c$. To obtain the last line of Equation 6.6-21, note that $a_1 t_x = a_1(t - t_c) = a_1 t - (1 - a_0)$, so $a_0 + a_1 t - 1 - a_1 t_x = 0$. Equation 6.6-21 applies for $t > t_c$.

6.6.5 Unzipping Abstraction Summary for Many Waste Packages

This section summarizes the results of Sections 6.6.3 and 6.6.4 in a concise form for guidance in implementing a performance assessment. First, the inputs and outputs are defined. Next, the initial state of degradation is expressed in terms of the inputs. Finally, the method for determining changes in state of degradation is given.

Definition of Inputs and Outputs–The following inputs are required:

t Time since emplacement.

L Fueled length of rod.

$W(t)$ Fraction of waste packages breached at time t. $W(t)$ will be provided by a analysis of waste package degradation and will vary from one realization to the next.

$v(t)$ Unzipping speed at time t. $v(t)$ will be provided by a analysis of fuel rod unzipping and will vary from one realization to the next.

$f_b(t-t_w)$ Fraction of breached fuel rods at time t for a particular waste package that breached at time t_w. The function is defined by the following equation:

$$f_b(z) = 0 \text{ for } z < 0$$
$$= a_0 + a_1 z \text{ for } 0 \le z \le \frac{1-a_0}{a_1}$$
$$= 1 \text{ for } z > \frac{1-a_0}{a_1}$$

(Eq. 6.6-22)

The constant a_0 is the fraction of fuel rods that are breached when the waste package breaches. Rods that breach by short-term processes (such as creep rupture) may be included in this set because these processes will be essentially complete before significant numbers of waste packages breach. The constant a_1 gives the rate of change of the fraction of breached rods after the waste package is breached. This constant describes processes such as localized corrosion of the cladding. The values of a_0 and a_1 will reflect the cladding degradation analysis, and their values will vary from one realization to the next.

The following outputs are produced:

$h(t)$ Split propagation distance at time t.

$f_i(t)$ Fraction of "intact" fuel rods at time t. $f_i(t)$ is an average over all the rods in the entire group of waste packages. "Intact" means rods whose fuel is protected from alteration, thus the intact fraction includes all rods in intact waste packages and all rods with intact cladding in breached waste packages.

$f_u(t)$ Fraction of unzipping fuel rods at time t. $f_u(t)$ is an average over all the rods in the entire group of waste packages. No distinction among these rods is made on the basis of split length.

$f_e(t)$ Fraction of exhausted (fully unzipped) fuel rods at time t. $f_e(t)$ is an average over all the rods in the entire group of waste packages.

$F_g(t)$ Fraction of fuel gap inventory altered at time t.

$F_m(t)$ Fraction of fuel matrix inventory altered at time t.

Initial State of Degradation–The initial state of degradation (t = 0) is given by the following equations:

$$h(0) = 0 \quad \text{(Eq. 6.6-23)}$$

$$f_i(0) = 1 - W(0) f_b(0) \quad \text{(Eq. 6.6-24)}$$

$$f_u(0) = W(0) f_b(0) \quad \text{(Eq. 6.6-25)}$$

$$f_e(0) = 0 \quad \text{(Eq. 6.6-26)}$$

$$F_g(0) = W(0) f_b(0) \quad \text{(Eq. 6.6-27)}$$

$$F_m(0) = 0 \quad \text{(Eq. 6.6-28)}$$

Changes in State of Degradation–Changes in the state of degradation are calculated by the following method. First, values of h and f_i are calculated at a new value of time by integrating the following rates of change:

$$\frac{d}{dt} h(t) = v(t) \quad \text{(Eq. 6.6-29)}$$

$$\begin{aligned} \frac{d}{dt} f_i(t) &= -a_0 \frac{dW(t)}{dt} - a_1 W(t) \text{ for } 0 \le t \le \frac{1-a_0}{a_1} \\ &= -a_0 \frac{dW(t)}{dt} - a_1 W(t) + a_1 W\left(t - \frac{1-a_0}{a_1}\right) \text{ for } t > \frac{1-a_0}{a_1} \end{aligned} \quad \text{(Eq. 6.6-30)}$$

Values of h and f_i must be accumulated so that previous values can be looked up later. After h and f_i have been calculated for a new value of time, f_e, f_u, and F_g are calculated at that time:

$$\begin{aligned} f_e(t) &= 1 - f_i(h^{-1}(h(t) - L/2)) \text{ for } t \ge h^{-1}(L/2) \\ &= 0 \text{ for } t < h^{-1}(L/2) \end{aligned} \quad \text{(Eq. 6.6-31)}$$

$$f_u(t) = 1 - f_i(t) - f_e(t) \quad \text{(Eq. 6.6-32)}$$

$$F_g(t) = 1 - f_i(t) \quad \text{(Eq. 6.6-33)}$$

In applying Equation 6.6-31, h^{-1} is the inverse function of h, that is:

$$h^{-1}(h(t)) = t \text{ for } t \ge 0 \quad \text{(Eq. 6.6-34)}$$

The last step is to calculate changes in F_m by integrating the following rate of change:

$$\frac{dF_m(t)}{dt} = \frac{2}{L} v(t) f_u(t) \quad \text{(Eq. 6.6-35)}$$

6.6.6 Unzipping Abstraction Summary for One Waste Package

The definitions and equations in Section 6.6.5 apply with the following exceptions:

Definition of Inputs and Outputs–The following input is changed:

t_w Time of waste package breach.

$W(t)$ This function is replaced by a Heaviside step function at $t = t_w$, i.e., $\Phi(t-t_w)$. For simplicity, $W(t)$ does not appear in the equations. Instead, its value (1 for times of interest) is used directly.

Initial State of Degradation–Since fuel alteration does not occur in an intact waste package, the initial state of degradation is defined at $t = t_w$ rather than $t = 0$:

$$h(t_w) = 0 \quad \text{(Eq. 6.6-36)}$$

$$f_i(t_w) = 1 - f_b(0) \quad \text{(Eq. 6.6-37)}$$

$$f_u(t_w) = f_b(0) \quad \text{(Eq. 6.6-38)}$$

$$f_e(t_w) = 0 \quad \text{(Eq. 6.6-39)}$$

$$F_g(t_w) = f_b(0) \quad \text{(Eq. 6.6-40)}$$

$$F_m(t_w) = 0 \quad \text{(Eq. 6.6-41)}$$

Changes in State of Degradation–Equations 6.6-30 and 6.6-34 are replaced by the following equations:

$$f_i(t) = 1 - f_b(t - t_w) \quad \text{(Eq. 6.6-42)}$$

$$h^{-1}(h(t)) = t \text{ for } t \geq t_w \quad \text{(Eq. 6.6-43)}$$

6.7 STAINLESS STEEL CLADDING

As discussed in CRWMS M&O 2000a, about 1.1% of the commercial fuel was clad with Stainless Steel (SS) cladding material. This material was used in the early core designs and is no longer used. CRWMS M&O 2000k, p. 8, analyzed the expected inventory of SS clad fuel and concluded that 3.49% of the CSNF WPs would contain SS clad fuel and the average percent of fuel in these WPs with SS cladding is 29.9%. This analysis is based on loading the fuel at the

repository as it is expected to be delivered. In TSPA-SR, the SS cladding will be perforated when the WP fails and to be immediately available for unzipping. It was also discussed in Section 6.1 of CRWMS M&O 2000a that failed rods from reconstituted assemblies were loaded into assembly size cans for pool storage and later disposal. These cans will be analyzed as SS clad and will be available for unzipping as soon as the WP fails (no credit for the can itself). This group was analyzed to be 10% of the SS assemblies or about 200 cans. This raised the fraction of stainless steel assemblies from 29.9% to 32.9%. This is summarized in Attachment I, Rows 109 and 110.

7. CONCLUSIONS

The purpose of this AMR is to develop the summary cladding degradation abstraction that is consistent with and used in the TSPA-SR. This summary is also submitted to the Waste Form PMR. The methodology developed for this AMR is consistent with ASTM Standard C1174-97 (ASTM 1998). Earlier TSPAs analyzed the waste form as bare UO_2 which was available for dissolution at the intrinsic dissolution rate. Water in the WP quickly became saturated with many of the radionuclides, limiting their release rate. In TSPA-VA cladding was analyzed as part of the waste form and limited the amount of fuel available at any time to dissolve. The major components of cladding failure were failure in reactor operation, mechanical failure from rocks and general corrosion of patches. The current analysis considers rod perforations from failure from reactor operation, creep and stress corrosion cracking (SCC) failures, localized corrosion from fluorides, and mechanical failure from static loading of rocks or seismic events as mechanisms for perforating the cladding. All stainless steel cladding is perforated. The second phase of the analysis is the release of radionuclides through the fast release and unzipping of the cladding from the reaction of water and UO_2. The unzipping starts in the middle of the cladding and progress toward each end. This unzipping is driven by the intrinsic dissolution rate, which is dependent on the local temperature and chemistry. The following is a summary of the components used in TSPA-SR. Attachment I is a table of the numerical values. This information is also given in DTN: MO0011SPACMU07.049.

Cladding Condition as Received

The groups of WPs represented in the TSPA-SR have an initial percent of rods failed defined by:

Lower limit	=	0.0155 %
Median	=	0.0948 %
Upper limit	=	1.285 %

This failure rate is based on historical data on reactor operation and includes an uncertainty factor of 4. It also includes failure from dry storage, handling, and transportation. This percentage of rods is available for radionuclide release through fast release and unzipping when the WP fails. This information is summarized in Attachment I, Rows 6 and 7.

Creep Strain Failure

Creep is analyzed using the Modified Murty creep correlation. The resulting rod failure distribution is displayed in Figure 13 and given in Rows 40 through 51 of Attachment I. In TSPA-SR, for each realization, the peak WP surface temperature is established and a triangular distribution of the rod fraction is interpolated from the table given in Attachment I, Rows 40 through 52. With the current repository design having WP peak surface temperatures below 227°C, creep failures from either dry storage or emplacement in the repository are expected to be insignificant. The analysis shows (see Figure 14) that limiting the peak cladding temperature in the WP, after repository closure, to below 350°C will prevent cladding failure from creep damage.

The percent of failed rods from creep strain is summed with the failures from "as received" and is available to release radionuclides through fast release and unzipping when the WP fails.

Stress Corrosion Cracking Failures

Rods with a maximum stress exceeding 180 MPa are presumed to fail by Stress Corrosion Cracking (SCC). The analysis in Section 6.2.5 concludes that 0.48% of the rods might fail from this mechanism. This percent of failures is added to the as received rod failures (see lines 55 and 5 through 8 of Attachment I)

Localized Corrosion

Localized corrosion by various aggressive species of chemicals has been represented by idealized corrosion from fluoride. The resulting analysis has 2.3 rods in a WP fail for every cubic meter of water entering the WP. In the localized corrosion analysis, all the J13 water is concentrated on a 10 mm length of a single rod. All of the fluoride reacts with the 10 mm length of cladding of this single rod until the cladding fails from fluoride corrosion. Corrosion then starts on another rod. This analysis makes the rod failure fraction linearly dependent on the water ingression rate (% failed = 0.0413 * m^3 water in WP). The water ingression into the WP increases with time as additional patches on the WP fail or open. Rod failure rate also depends on the location of the WP group because of different drip rates in different repository regions. As an example, with 50 liters/year of J13 water entering the WP (2.2 ppm fluoride), 20% of the rods would fail by fluoride corrosion in 10,000 years. This information is summarized in Attachment I, Rows 57 through 59.

Mechanical Failures

A very severe seismic event which occurs with a frequency of 1.1×10^{-6} events/year fails all of the cladding and all the rods are available for fast release and unzipping when the WP fails. This is included in the TSPA-SR base case and sampled every time step. Static loading from rockfalls also fails the cladding. Failure starts when 50% of the WP patches are open and increases linearly to 100% failure when all the patches are open. This information is summarized in Attachment I, Rows 114 through 117.

Stainless Steel Cladding

The abstraction places the Stainless Steel (SS) cladding into WPs as it arrives at YMP. This results in 3.49% of the WPs contain SS cladding. These WPs contain 32.9% SS cladding which is failed and available for fast release and unzipping when the WP fails. In the TSPA-SR, WPs containing SS cladding are considered a different fuel type group with a high initial cladding failure percent (32.9%). This information is summarized in Attachment I, Rows 109 through 111.

Fast Release Fraction

When the WP fails or when the rod fails after WP failure, some of the radionuclides are immediately released. This includes the inventory of radionuclides in the gap between the fuel pellet and cladding, including that which is initially released from the early UO_2 interaction with the water. The gap release of iodine equals the fission gas release of 4.2% and cesium is one third this value or 1.4%. The fast release fraction for other radionuclides including additional cesium and iodine is an average of 0.2% (range 0 to 0.4%, uniformly distributed) from the UO_2 dissolution. This information is summarized in Attachment I, Rows 62 through 65.

Cladding Unzipping and Fuel Dissolution

The initial cladding damage occurs at the center of the fuel rod and the split (unzipping) will then propagate to both ends of the active fuel length. The unzipping velocity is a multiple of the intrinsic dissolution velocity defined by a CCDF: 100%=1, 50%=9, 10%=18, 0%=180. The intrinsic dissolution velocity is a function of the temperature and chemistry inside the WP. This relationship is given in Rows 69 to 92 of Attachment I and is included in the TSPA-SR. An example calculation with a WP with J13 type water chemistry at 40°C, predicts 4.5% unzipping of failed rods in 10,000 years.

In summary, the cladding degradation is analyzed in TSPA-SR in two stages: Cladding failure and cladding fast release and unzipping. The cladding degradation abstraction depends on the WP temperature, internal chemistry, WP surface perforation rate, and location (amount of water dripping on the WP). Uncertainties have been established for the important parameters and the results vary for each TSPA-SR realization. Typically, 2.54% of the cladding is failed from previous reactor operations and creep or SCC failures. Little additional creep or SCC failures occur under design repository conditions but creep failures could become important for a high temperature repository design. Localized corrosion depends on the water ingression rate which depends on the number of patches open or failed on the WP surface and the location of the WP in the repository. The cladding is also failed from rockfall after significant WP degradation. For a water ingression rate of 50 liters/year of J13 water into a WP, 20% of the rods in that WP fail from localized corrosion in 10,000 years. Most WPs are located in regions of little or no water ingression and do not undergo localized failure. When the WP fails, there is a fast release of radionuclides from the failed cladding gap. Then an average additional 4.5% is released from cladding unzipping in the next 10,000 years after WP failure from cladding unzipping, depending on local chemistry. With the ranges and uncertainties included in the abstraction, this analysis is valid for its intended use, analyzing cladding degradation in the TSPA-SR . This analysis and the TSPA-SR abstraction do not address the potential for damaging the cladding at

the surface facilities at YMP. The cladding degradation analysis considers the WP peak surface temperature as an independent variable, and the results are usable for a repository design with or without backfill. The analysis is sensitive to thermal loading and would have to be modified if the WP thermal loading were significantly changed.

Alternative Conceptual Analysis: The analysis by S. Cohen & Associates (1999, p. 7-1 to 7-4) is considered an alternative conceptual analysis and qualitatively agrees with this AMR. The earlier YMP TSPA's performed in 1993 and 1995 did not consider cladding, and as such are an alternative conceptual analysis that is extremely conservative because it permits all fuel to dissolve at the intrinsic dissolution rate. A solubility limit (an indirect way of considering secondary phases) is used to limit the release rate of the fuel. European site TSPAs also did not consider cladding. The European sites were both saturated and reducing environments where the UO_2 dissolution rates were so slow that cladding degradation was not considered.

The following table contains a listing of specific technical issues addressed in Revision 2 of the NRC IRSR, for Container Life and Source Term (IRSR-CLST) (NRC 1999, pp. 56-59) and the status of their resolution.

Table 14. Resolution of IRSR-CLST Issues

Technical Issue	Resolution Status
Evaluate the processes of pitting corrosion and Stress Corrosion Cracking in the presence of oxidizing chloride solutions. Evaluate the effects on cladding integrity within the WC.	Pitting is addressed in CRWMS M&O 2000c SCC is addressed in this AMR Localized corrosion by Fluoride is addressed in this AMR
Evaluate and assess creep rupture models and the validity of extrapolation to lower temperatures. Resolve issues relating to the DCCG model of creep.	Creep Rupture addressed in CRWMS M&O 2000a and this AMR
Further qualify the DHC analysis with the use of a crack-size distribution in the cladding. Assess hydrogen embrittlement in the cladding as a function of cladding temperature and assess the possibility of hydride reorientation.	DHC is quantified in CRWMS M&O 2000a, and CRWMS M&O 2000l Hydride embrittlement is addressed in CRWMS M&O 2000b Hydride reorientation is addressed in CRWMS M&O 2000l
Develop models for clad splitting for repository storage temperatures in dry air and aqueous environments.	Clad dry splitting is addressed in CRWMS M&O 2000b Wet splitting is addressed in this AMR
Assess the possibility of cladding mechanical failure during rock fall and seismic events using a fracture mechanics model.	Addressed in CRWMS M&O 1999d and this AMR
Evaluate the damage introduced during reactor operation and deterioration during transportation and dry storage that may affect the behavior under disposal conditions.	Addressed in CRWMS M&O 2000a and this AMR

DTN: MO0011SPACMU07.049

This document may be affected by technical product input information that requires confirmation. Any changes to the document that may occur as a result of completing the confirmation activities will be reflected in subsequent revisions. The status of the technical product input information quality may be confirmed by review of the DIRS database.

Model Output Data

Section 8.4 lists the DTN that has been submitted to the TDMS as a result of the analysis described in this AMR.

8. INPUTS AND REFERENCES

8.1 REFERENCES CITED

Ahn, T.M.; Cragnolino, G.A.; Chan, K.S.; and Sridhar, N. 1999. "Scientific Bases for Cladding Credit as a Barrier to Radionuclide Release at the Proposed Yucca Mountain Repository." *Scientific Basis for Nuclear Waste Management XXII, Symposium held November 30-December 4, 1998, Boston, Massachusetts, U.S.A.* Wronkiewicz, D.J. and Lee, J.H., eds. 556, 525-533. Warrendale, Pennsylvania: Materials Research Society. TIC: 246426.

Armijo, J.S.; Coffin, L.F.; and Rosenbaum, H.S. 1994. "Development of Zirconium-Barrier Fuel Cladding." *Zirconium in the Nuclear Industry: Tenth International Symposium held in Baltimore, Maryland, 21-24 June 1993.* Garde, A.M., and Bradley, E.R. eds. *ASTM STP 1245*, 3-18. Philadelphia, Pennsylvania: American Society for Testing and Materials. TIC: 246390.

Bouffioux, P. and Legras, L. 2000. "Effect of Hydriding on the Residual Cold Work Recovery and Creep of Zircaloy 4 Cladding Tubes." *International Topical Meeting on Light Water Reactor Fuel Performance, April 10-13, 2000, Park City, Utah.* Pages 111-118. La Grange Park, Illinois: American Nuclear Society. TIC: 248973.

Brach, E.W. 2000. "Issuance of Revision 1 of SFPO Director's Interim Staff Guidance Document 11." Memorandum from E.W. Brach (Spent Fuel Project Office) to SFPO Staff Members, 16 May 2000, with attachment. TIC: 248911.

Bredel, T.; Cappelaere, C.; Limon, R.; Pinte, G.; and Bouffioux, P. 2000. "Long Term Creep Behavior of Spent Fuel Cladding for Storage and Disposal." *Scientific Basis for Nuclear Waste Management XXIII, Symposium held November 29-December 2, 1999, Boston Massachusetts.* Smith, R.W. and Shoesmith, D.W., eds. *608,* 11-16. Warrendale, Pennsylvania: Materials Research Society. TIC: 249052.

Chung, H.M.; Yaggee, F.L.; and Kassner, T.F. 1987. "Fracture Behavior and Microstructural Characteristics of Irradiated Zircaloy Cladding." *Zirconium in the Nuclear Industry, Seventh International Symposium Sponsored by ASTM Committee B-10 on Reactive and Refractory Metals, Strasbourg, France, 24-27 June 1985.* Adamson, R.B. and Van Swam, L.F.P., eds. Pages 775-801. Philadelphia, Pennsylvania: American Society for Testing and Materials. TIC: 238255.

Cox, B. 1973. "Stress Corrosion Cracking of Zircaloy-2 in Neutral Aqueous Chloride Solutions at 25 C." *Corrosion, 29,* (4), 157-166. Houston, Texas: National Association of Corrosion Engineers. TIC: 248988.

Cox, B. 1990a. "Pellet-Clad Interaction (PCI) Failures of Zirconium Alloy Fuel Cladding - A Review." *Journal of Nuclear Materials, 172,* 249-292. [Amsterdam, The Netherlands]: Elsevier Science Publishers B.V. TIC: 248990.

Cox, B. 1990b. "Environmentally-Induced Cracking of Zirconium Alloys - A Review." *Journal of Nuclear Materials, 170,* 1-23. Amsterdam, The Netherlands: Elsevier Science Publishers. TIC: 234774. On Order Library Tracking Number-234774.

CRWMS M&O 1995. *Total System Performance Assessment - 1995: An Evaluation of the Potential Yucca Mountain Repository.* B00000000-01717-2200-00136 REV 01. Las Vegas, Nevada: CRWMS M&O. ACC: MOL.19960724.0188.

CRWMS M&O 1998a. "Waste Form Degradation, Radionuclide Mobilization, and Transport Through the Engineered Barrier System." Chapter 6 of *Total System Performance Assessment-Viability Assessment (TSPA-VA) Analyses Technical Basis Document.* B00000000-01717-4301-00006 REV 01. Las Vegas, Nevada: CRWMS M&O. ACC: MOL.19981008.0006.

CRWMS M&O 1998b. *Total System Performance Assessment-Viability Assessment (TSPA-VA) Analyses Technical Basis Document.* Las Vegas, Nevada: CRWMS M&O. ACC: MOL.19981008.0001; MOL.19981008.0002; MOL.19981008.0003; MOL.19981008.0004; MOL.19981008.0005; MOL.19981008.0006; MOL.19981008.0007; MOL.19981008.0008; MOL.19981008.0009; MOL.19981008.0010; MOL.19981008.0011.

CRWMS M&O 1999a. *Cladding Degradation - Abstraction and Summary Analysis Results for Input to TSPA Analyses.* TDP-WIS-MD-000005 REV 00. Las Vegas, Nevada: CRWMS M&O. ACC: MOL.19990902.0471.

CRWMS M&O 1999b. *Conduct of Performance Assessment.* Activity Evaluation, September 30, 1999. Las Vegas, Nevada: CRWMS M&O. ACC: MOL.19991028.0092.

CRWMS M&O 1999c. *Thermal Evaluation of Breached 21-PWR Waste Packages.* CAL-UDC-ME-000002 REV 00. Las Vegas, Nevada: CRWMS M&O. ACC: MOL.20000120.0447.

CRWMS M&O 1999d. *Breakage of Commercial Spent Fuel Cladding by Mechanical Loading.* CAL-EBS-MD-000001 REV 00. Las Vegas, Nevada: CRWMS M&O. ACC: MOL.19991213.0237.

CRWMS M&O 1999e. *Thermal Loading Histogram for 21-PWR (Pressurized Water Reactor) Absorber Plate Waste Packages.* Input Transmittal PA-WP-99366.T. Las Vegas, Nevada: CRWMS M&O. ACC: MOL.19991115.0138.

CRWMS M&O 2000a. *Initial Cladding Condition.* ANL-EBS-MD-000048 REV 00 ICN 01. Las Vegas, Nevada: CRWMS M&O. ACC: MOL.20001002.0145.

CRWMS M&O 2000b. *Clad Degradation – FEPs Screening Arguments.* ANL-WIS-MD-000008 REV 00. Las Vegas, Nevada: CRWMS M&O. ACC: MOL.20000525.0378.

CRWMS M&O 2000c. *Clad Degradation–Local Corrosion of Zirconium and Its Alloys Under Repository Conditions.* ANL-EBS-MD-000012 REV 00. Las Vegas, Nevada: CRWMS M&O. ACC: MOL.20000405.0479.

CRWMS M&O 2000d. *CSNF Waste Form Degradation: Summary Abstraction.* ANL-EBS-MD-000015 REV 00. Las Vegas, Nevada: CRWMS M&O. ACC: MOL.20000121.0161.

CRWMS M&O 2000e. Reference not used.

CRWMS M&O 2000f. *Thermal History of Cladding in a 21 PWR SNF WP Loaded with Average Fuel.* CAL-UDC-ME-000001 REV 00. Las Vegas, Nevada: CRWMS M&O. ACC: MOL.20000216.0105.

CRWMS M&O 2000g. *Data Qualification Report: Composition of J-13 Well Water for Use on the Yucca Mountain Project, Revision 0.* TDR-NBS-HS-000003 REV 00. Las Vegas, Nevada: CRWMS M&O. ACC: MOL.20000724.0463.

CRWMS M&O 2000h. *Abstraction of NFE Drift Thermodynamic Environment and Percolation Flux.* ANL-EBS-HS-000003 REV 00. Las Vegas, Nevada: CRWMS M&O. ACC: MOL.20000504.0296.

CRWMS M&O 2000i. *In-Package Chemistry Abstraction.* ANL-EBS-MD-000037 REV 00. Las Vegas, Nevada: CRWMS M&O. ACC: MOL.20000418.0818.

CRWMS M&O 2000j. *Comparison of Cladding Creep Rupture Models.* CAL-EBS-MD-000009 REV 00. Las Vegas, Nevada: CRWMS M&O. ACC: MOL.20000616.0248.

CRWMS M&O 2000k. *Stainless Steel in Waste Packages for TSPA-SR.* CAL-WIS-MD-000010 REV 00. Las Vegas, Nevada: CRWMS M&O. ACC: MOL.20000630.0249.

CRWMS M&O 2000l. *Hydride-Related Degradation of SNF Cladding Under Repository Conditions.* ANL-EBS-MD-000011 REV 00. Las Vegas, Nevada: CRWMS M&O. ACC: MOL.20000319.0048.

CRWMS M&O 2000m. *Creep Strain Values and Correlation for Irradiated Spent Nuclear Fuel.* Input Transmittal PA-WP-00383.T. Las Vegas, NV: CRWMS M&O. ACC: MOL20001117.0046.

CRWMS M&O 2000n. Process Control Evaluation For Supplement V: "Performance Assessment Operations. (Reference QAP-2-0 Activity Evaluation Form. Conduct of

Performance Assessment, November 9, 1999)". Las Vegas, Nevada: CRWMS M&O. ACC: MOL.20000128.0236.

Cunnane, J. 2000. Clad Degradation-Wet Unzipping: Release Rates from Breached Cladding and Potential Unzipping Velocity. Scientific Notebook 1563. ACC: MOL.20000301.1129.

Cunningham, M.E.; Simonen, E.P.; Allemann, R.T.; Levy, I.S.; Gilbert, E.R.; and Hazelton, R.F. 1987. *Control of Degradation of Spent LWR Fuel During Dry Storage in an Inert Atmosphere.* PNL-6364. Richland, Washington: Pacific Northwest Laboratory. TIC: 210249.

DOE (U.S. Department of Energy) 2000. *Quality Assurance Requirements and Description.* DOE/RW-0333P, Rev. 10. Washington, D.C.: U.S. Department of Energy, Office of Civilian Radioactive Waste Management. ACC: MOL.20000427.0422.

Dyer, J.R. 1999. "Revised Interim Guidance Pending Issuance of New U.S. Nuclear Regulatory Commission (NRC) Regulations (Revision 01, July 22, 1999), for Yucca Mountain, Nevada." Letter from J.R. Dyer (DOE/YMSCO) to D.R. Wilkins (CRWMS M&O), September 3, 1999, OL&RC:SB-1714, with enclosure, "Interim Guidance Pending Issuance of New NRC Regulations for Yucca Mountain (Revision 01)." ACC: MOL.19990910.0079.

Einziger, R.E. and Kohli, R. 1984. "Low-Temperature Rupture Behavior of Zircaloy-Clad Pressurized Water Reactor Spent Fuel Rods Under Dry Storage Conditions." *Nuclear Technology, 67,* (1), 107-123. Hinsdale, Illinois: American Nuclear Society. TIC: 216868.

Einziger, R.E. and Strain, R.V. 1986. "Behavior of Breached Pressurized Water Reactor Spent-Fuel Rods in an Air Atmosphere Between 250 and 360°C." *Nuclear Technology, 75,* (1), 82-95. Hinsdale, Illinois: American Nuclear Society. TIC: 238325.

Einziger, R.E.; Atkin, S.D.; Stellrecht, D.E.; and Pasupathi, V. 1982. "High Temperature Postirradiation Materials Performance of Spent Pressurized Water Reactor Fuel Rods Under Dry Storage Conditions." *Nuclear Technology, 57,* (1), 65-80. Hinsdale, Illinois: American Nuclear Society. TIC: 237142.

Finch, R.J.; Miller, M.L.; and Ewing, R.C. 1992. "Weathering of Natural Uranyl Oxide Hydrates: Schoepite Polytypes and Dehydration Effects." *Radiochimica Acta, 58/59,* 433-443. München, Germany: R. Oldenbourg Verlag. TIC: 238032.

Garde, A.M. 1986. *Hot Cell Examination of Extended Burnup Fuel from Fort Calhoun.* DOE/ET/34030-11. Windsor, Connecticut: Combustion Engineering. TIC: 237128.

Garde, A.M.; Smith, G.P.; and Pirek, R.C. 1996. "Effects of Hydride Precipitate Localization and Neutron Fluence on the Ductility of Irradiated Zircaloy-4." ASTM-STP-1295 *Zirconium in the Nuclear Industry: 11th International Symposium.* Bradley, E.R. and Sabol, G.P., eds. pp. 407-430. Philadelphia, Pennsylvania: American Society of Testing and Materials. TIC: 244499.

Gray, W.J. and Wilson,C.N. 1995. *Spent Fuel Dissolution Studies, FY 1991-1994.* PNL-10540. Richland, Washington: Pacific Northwest Laboratory. ACC: MOL.19980625.0338.

Henningson, P.J. 1998. *Cladding Integrity Under Long Term Disposal.* 51-1267509-00. Lynchburg, Virginia: Framatome Technologies. ACC: MOL.19990310.0103.

Hopf, J.E. 1999. *Cladding Creep Behavior of Light Water Reactor Fuel Assemblies from Fuel Pool to Dry Storage.* CMPC.0302. [Fairfax, Virginia]: BNFL Fuel Solutions. TIC: 248925.

Kaspar, G.; Peehs, M.; Steinberg, E.; and Schonfeld, H. 1985. "Experimental Investigation of Post-Pile Creep of Zircaloy Cladding Tubes." *International Conference on Structural Mechanics in Reactor Technology, Brussels, Belgium, August 19-25, 1985.* Volume C. Pages 51-57. Amsterdam, The Netherlands: North-Holland Physics Publishing. TIC: 247092.

Lide, D.R., ed. 1995. *CRC Handbook of Chemistry and Physics.* 76th Edition. Boca Raton, Florida: CRC Press. TIC: 216194.

Lowry, L.M.; Markworth, A.J.; Perrin, J.S.; and Landow, M.P. 1981. *Evaluating Strength and Ductility of Irradiated Zircaloy, Task 5. Experimental Data Final Report.* NUREG/CR-1729, Volume 1. Washington, D.C.: U.S. Nuclear Regulatory Commission. TIC: 238074.

Macheret, P. 2000. "Information on Experimental Creep Strain Values." Interoffice Correspondence from P. Macheret (CRWMS M&O) to E. Siegmann, October 20, 2000, LV.WP.PM.10/00-182, with enclosures. ACC: MOL.20001031.0258.

Manaktala, H.K. 1993. *Characteristics of Spent Nuclear Fuel and Cladding Relevant to High-Level Waste Source Term.* CNWRA 93-006. NRC-02-88-005. San Antonio, Texas: Center for Nuclear Waste Regulatory Analyses. TIC: 208034.

Mardon, J-P.; Charquet, D.; and Senevat, J. 1994. "Optimization of PWR Behavior of Stress-Relieved Zircaloy-4 Cladding Tubes by Improving the Manufacturing and Inspection Process." *Zirconium in the Nuclear Industry: Tenth International Symposium held in Baltimore, Maryland, 21-24 June 1993.* Garde, A.M., and Bradley, E.R. eds. *ASTM STP 1245,* 328-348. Philadelphia, Pennsylvania: American Society for Testing and Materials. TIC: 246390.

Matsuo, Y. 1987. "Thermal Creep of Zircaloy-4 Cladding Under Internal Pressure." *Journal of Nuclear Science and Technology, 24,* (2), 111-119. Tokyo, Japan: Atomic Energy Society of Japan. TIC: 237137.

Mattas, R.F.; Yaggee, F.L.; and Neimark, L.A. 1982. "Effect of Zirconium Oxide on the Stress-Corrosion Susceptibility of Irradiated Zircaloy Cladding." *Zirconium in the Nuclear Industry, Proceedings of the Fifth International Conference, Boston, Massachusetts, 4-7 August 1980. ASTM STP 754,* 158-170. Philadelphia, Pennsylvania: American Society for Testing and Materials. TIC: 247323.

NAC (Nuclear Assurance Corporation) 1993. *Topical Safety Analysis Report for the NAC Storable Transport Cask for use at an Independent Spent-Fuel Storage Installation, Rev. 2.* NAC T-90002. Norcross, Georgia: Nuclear Assurance Corporation. TIC: 101980.

NRC (U.S. Nuclear Regulatory Commission) 1997. *Standard Review Plan for Dry Cask Storage Systems.* NUREG-1536. Washington, D.C.: U.S. Nuclear Regulatory Commission. TIC: 232373.

NRC (U.S. Nuclear Regulatory Commission) 1999. *Issue Resolution Status Report Key Technical Issue: Container Life and Source Term.* Rev. 2. Washington, D.C.: U.S. Nuclear Regulatory Commission. TIC: 245538.

NRC (U.S. Nuclear Regulatory Commission) 2000a. "ISG-11 - Storage of High Burnup Spent Fuel." Interim Staff Guidance - 11. Washington, D.C.: U.S. Nuclear Regulatory Commission. Accessed March 21, 2000. TIC: 247227. http://www.nrc.gov/OPA/reports/isg11.htm

NRC (U.S. Nuclear Regulatory Commission) 2000b. *Issue Resolution Status Report Key Technical Issue: Total System Performance Assessment and Integration.* Rev. 2. Washington, D.C.: U.S. Nuclear Regulatory Commission. TIC: 247614.

Nuclear Assurance Corporation. 1999. *NAC-MPC Safety Analysis Report for the NAC Multi-Purpose Canister System.* Docket No. 72-1025, Rev. 2. Norcross, Georgia: Nuclear Assurance Corporation. TIC: 245218.

NUTECH 1989. *Topical Report for the NUTECH Horizontal Modular Storage System for Irradiated Nuclear Fuel, NUHOMS®-24P.* NUH-002, Revision 1A. Volume 1. San Jose, California: NUTECH Engineers. TIC: 243591.

Peehs, M. 1998. *Assessment of Dry Storage Performance of Spent LWR Fuel Assemblies with Increasing Burn-Up.* Erlangen, Germany: Bereich Energieerzeugung. TIC: 245171.

Pescatore, C. and Cowgill, M. 1994. *Temperature Limit Determination for the Inert Dry Storage of Spent Nuclear Fuel.* EPRI TR-103949. Palo Alto, California: Electric Power Research Institute. TIC: 102933.

Pescatore, C.; Cowgill, M.G.; and Sullivan, T.M. 1990. *Zircaloy Cladding Performance Under Spent Fuel Disposal Conditions Progress Report May 1 - October 31, 1989.* BNL 52235. Upton, New York: Brookhaven National Laboratory. ACC: NNA.19900710.0055.

Rothman, A.J. 1984. *Potential Corrosion and Degradation Mechanisms of Zircaloy Cladding on Spent Nuclear Fuel in a Tuff Repository.* UCID-20172. Livermore, California: Lawrence Livermore National Laboratory. ACC: NNA.19870903.0039.

S. Cohen & Associates 1999. *Effectiveness of Fuel Rod Cladding as an Engineered Barrier in the Yucca Mountain Repository.* McLean, Virginia: S. Cohen & Associates. TIC: 246541.

Sanders, T.L.; Seager, K.D.; Rashid, Y.R.; Barrett, P.R.; Malinauskas, A.P.; Einziger, R.E.; Jordan, H.; Duffey, T.A.; Sutherland, S.H.; and Reardon, P.C. 1992. *A Method for Determining the Spent-Fuel Contribution to Transport Cask Containment Requirements.* SAND90-2406. Albuquerque, New Mexico: Sandia National Laboratories. TIC: 232162.

Spilker, H. and Fleisch, J. 1986. "Dry Storage Demonstrations of Castor I and TN-1300 Casks." *Proceedings, Third International Spent Fuel Storage Technology Symposium/Workshop, April 8-10, 1986, Seattle, Washington, USA. 1,* S-1 to S-19. Washington, D.C.: U.S. Department of Energy, Office of Civilian Radioactive Waste Management. TIC: 227157.

Tasooji, A.; Einziger, R.E.; and Miller, A.K. 1984. "Modeling of Zircaloy Stress-Corrosion Cracking: Texture Effects and Dry Storage Spent Fuel Behavior." *Zirconium in the Nuclear Industry, Sixth International Symposium, Vancouver, British Columbia, June 28- July 1, 1982.* Franklin, D.G. and Adamson, R.B., eds. *ASTM STP 824,* 595-626. Philadelphia, Pennsylvania: American Society for Testing and Materials. TIC: 241417.

Van Swam, L.F.; Strasser, A.A.; Cook, J.D.; and Burger, J.M. 1997. "Behavior of Zircaloy-4 and Zirconium Liner Zircaloy-4 Cladding at High Burnup." *Proceedings of the 1997 International Topical Meeting on LWR Fuel Performance, Portland, Oregon, March 2-6, 1997.* Pages 421-431. La Grange Park, Illinois: American Nuclear Society. TIC: 232556.

Walker, T.J. and Kass, J.N. 1974. "Variation of Zircaloy Fracture Toughness in Irradiation." *Zirconium in Nuclear Applications, A Symposium, 21-24 August 1973, Portland, Oregon.* ASTM Special Technical Publication 551. Pages 328-354. Philadelphia, Pennsylvania: American Society for Testing and Materials. TIC: 247106.

Weast, R.C. and Astle, M.J., eds. 1980. *CRC Handbook of Chemistry and Physics.* 61st Edition. Boca Raton, Florida: CRC Press. TIC: 242182.

Wilson, C.N. 1985. *Results from NNWSI Series 1 Spent Fuel Leach Tests.* HEDL-TME-84-30. Richland, Washington: Hanford Engineering Development Laboratory. TIC: 210347.

Wilson, C.N. 1987. *Results from Cycles 1 and 2 of NNWSI Series 2 Spent Fuel Dissolution Tests.* HEDL-TME-85-22. Richland, Washington: Hanford Engineering Development Laboratory. TIC: 202294.

Wilson, C.N. 1990. *Results from NNWSI Series 3 Spent Fuel Dissolution Tests.* PNL-7170. Richland, Washington: Pacific Northwest Laboratory. ACC: NNA.19900329.0142.

Witte, M.C.; Chun, R.C.; and Schwartz, M.W. 1989. "Dynamic Impact Effects on Spent Fuel Assemblies." *9th International Symposium on the Packaging and Transportation of Radioactive Materials, Washington, D.C., June 11-16, 1989. 1,* 186-194. Oak Ridge, Tennessee: Oak Ridge National Laboratory. TIC: 240741.

Yau, T. L. 1984. "Zirconium Versus Corrosive Species in Geothermal Fluids." Paper 140 of *Corrosion 84.* Houston, Texas: National Association of Corrosion Engineers. TIC: 238987.

Yau, T.L. and Webster, R.T. 1987. "Corrosion of Zirconium and Hafnium." In *Corrosion,* Volume 13, Pages 707-721 of *ASM Handbook.* Formerly 9th Edition, Metals Handbook. [Materials Park, Ohio]: ASM International. TIC: 240704.

8.2 CODES, STANDARDS, REGULATIONS AND PROCEDURES

64 FR 8640. Disposal of High-Level Radioactive Wastes in a Proposed Geologic Repository at Yucca Mountain, Nevada. Readily Available

AP-2.13Q, Rev. 0, ICN 4. *Technical Product Development Planning.* Washington, D.C.: U.S. Department of Energy, Office of Civilian Radioactive Waste Management. ACC: MOL.20000620.0067.

AP-2.21Q, Rev. 0, ICN 0. *Quality Determinations and Planning for Scientific, Engineering, and Regulatory Compliance Activities.* [Washington, D.C.]: U.S. Department of Energy, Office of Civilian Radioactive Waste Management. ACC: MOL.20000802.0003.

AP-3.10Q, Rev. 2, ICN 3. *Analyses and Models.* Washington, D.C.: U.S. Department of Energy, Office of Civilian Radioactive Waste Management. ACC: MOL.20000918.0282

AP-3.15Q, Rev. 2, ICN 0. *Managing Technical Product Inputs.* Washington, D.C.: U.S. Department of Energy, Office of Civilian Radioactive Waste Management. ACC: MOL.20001109.0051.

AP-SI.1Q, Rev. 2, ICN 4, ECN 1. *Software Management.* Washington, DC: U.S. Department of Energy, Office of Civilian Radioactive Waste Management. ACC: MOL.20001019.0023.

AP-SV.1Q, Rev. 0, ICN 2. *Control of the Electronic Management of Information.* Washington, DC: U.S. Department of Energy, Office of Civilian Radioactive Waste Management. ACC: MOL.20000831.0065.

ASTM C 1174-97. 1998. *Standard Practice for Prediction of the Long-Term Behavior of Materials, Including Waste Forms, Used in Engineered Barrier Systems (EBS) for Geological Disposal of High-Level Radioactive Waste.* West Conshohocken, Pennsylvania: American Society for Testing and Materials. TIC: 246015.

NLP-2-0, Rev. 5, ICN 1. *Determination of Importance Evaluations.* Las Vegas, Nevada: CRWMS M&O. ACC: MOL.20000713.0360.

QAP-2-0, Rev. 5, ICN 1. *Conduct of Activities.* Las Vegas, Nevada: CRWMS M&O. ACC: MOL.19991109.0221.

QAP-2-3, Rev. 10. *Classification of Permanent Items.* Las Vegas, Nevada: CRWMS M&O. ACC: MOL.19990316.0006.

YAP-SV1.Q, Rev. 0, ICN 1. *Control of the Electronic Management of Data.* Las Vegas, Nevada: Yucca Mountain Site Characterization Office. ACC: MOL.19991008.0209.

8.3 SOURCE DATA

MO0001SPAICC48.037. Initial Cladding Condition for CSNF. Submittal date: 01/27/2000.

MO0006J13WTRCM.000. Recommended Mean Values of Major Constituents in J-13 Well Water. Submittal date: 06/07/2000. Submit to RPC URN-0532

SN0001T0810599.008. Stainless Steel in Waste Packages for TSPA-SR (Total System Performance Assessment-Site Recommendation). Submittal date: 01/18/2000.

SN0001T0872799.006. In-Drift Thermodynamic Environment and Percolation Flux. Submittal date: 01/27/2000.

8.4 OUTPUT DATA, LISTED BY DATA TRACKING NUMBER

MO0011SPACMU07.049. Clad Degradation – Summary and Abstraction. Submittal date: 11/27/2000.

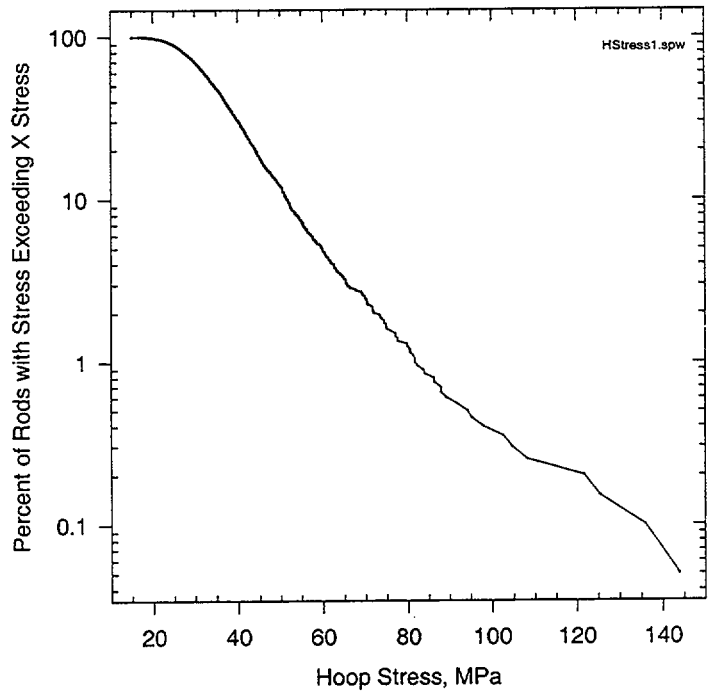

Figure 1. CCDF for Rod Stress as Received (Room Temperature)

(DTN: MO0011SPACMU07.049)

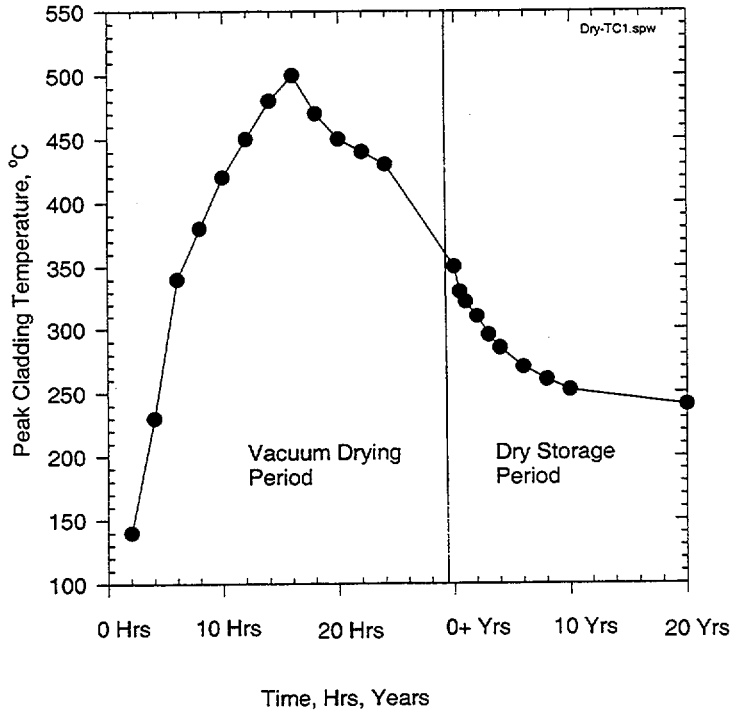

Figure 2. Maximum Cladding Temperature Profile for Vacuum Drying and Dry Storage

(DTN: MO0011SPACMU07.049)

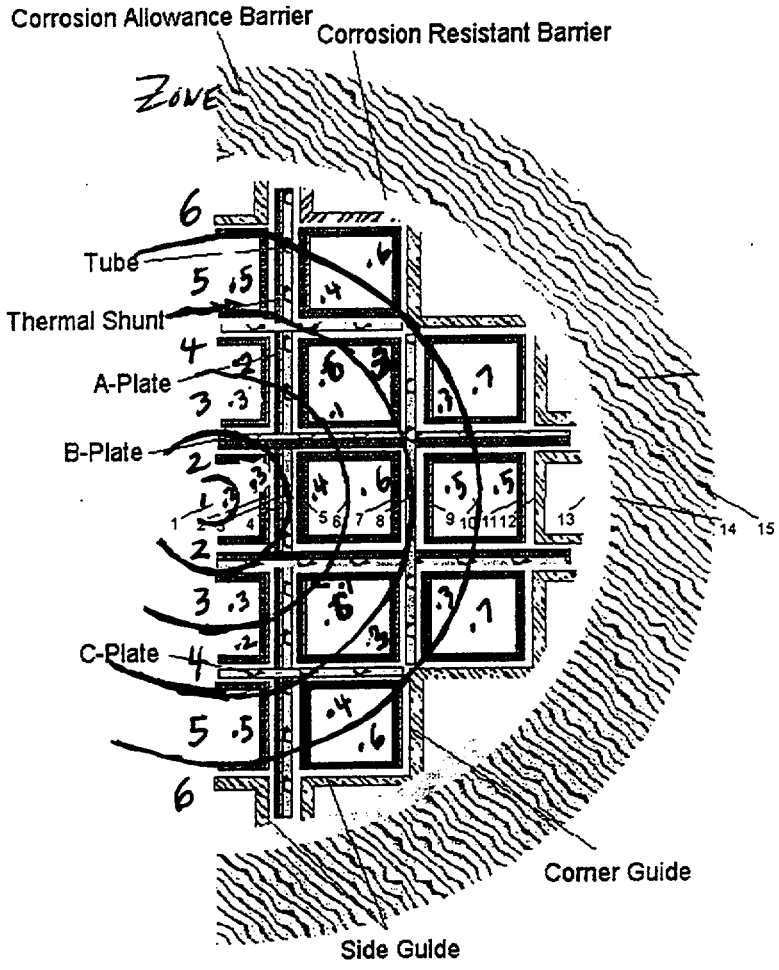

1	Mid-fuel Assembly (c01i000)	9	Inside Tube (s07i000)
2	Inside Tube (s01o000)	10	Mid-fuel Assembly (c07o000)
3	Inside A – Plate (b01o000)	11	Inside Tube (s07o000)
4	Outside A – Plate (a01o000)	12	Inside Side Guide (g07i000)
5	Inside Tube (s04i000)	13	Inside Alloy 22 Inner Barrier (i07i000)
6	Mid-fuel Assembly (c04o000)	14	Outside Alloy 22 Inner Barrier (i07o000)
7	Inside Tube (s04o000)	15	Outside A516 Outer Barrier (o07o000)
8	Mid-plate (b04i000)		

Figure 3. Nodal Locations and Zones for the 21 Assembly PWR Waste Package

(DTN: MO0011SPACMU07.049)

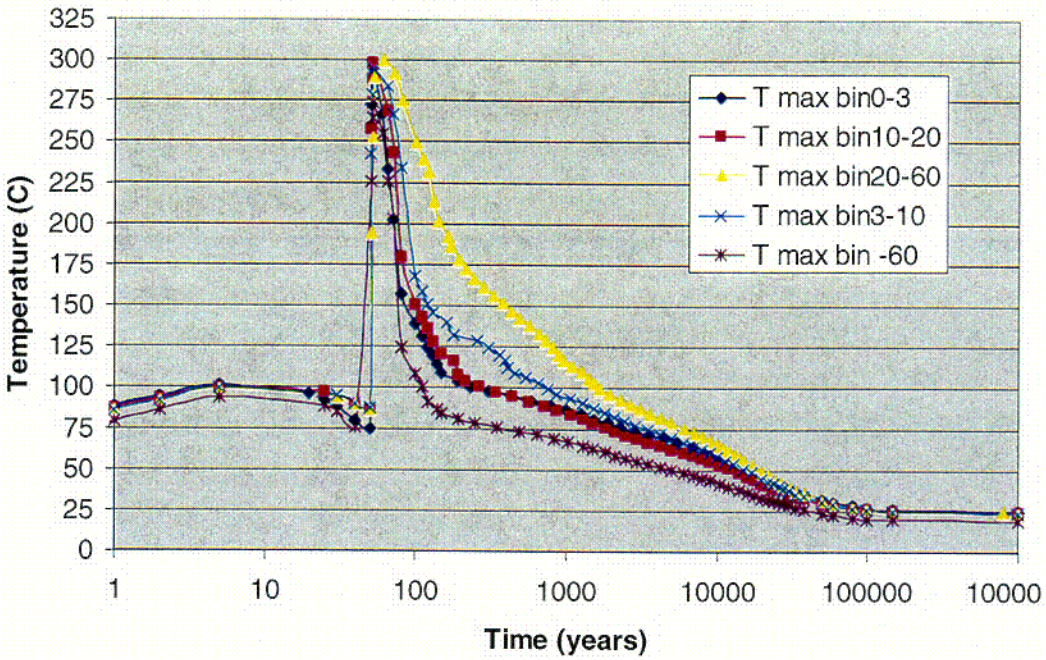

Figure 4. Maximum Temperature Distribution of the 5 Bins of WPs

(DTN: SN0001T0872799.006)

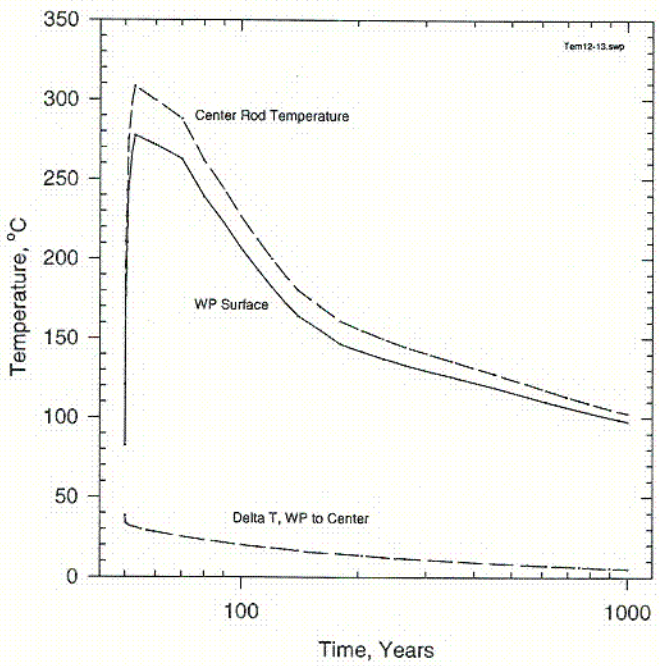

Figure 5. Temperature Histories for WP Surface and Center Rod

(DTN: MO0011SPACMU07.049)

C01

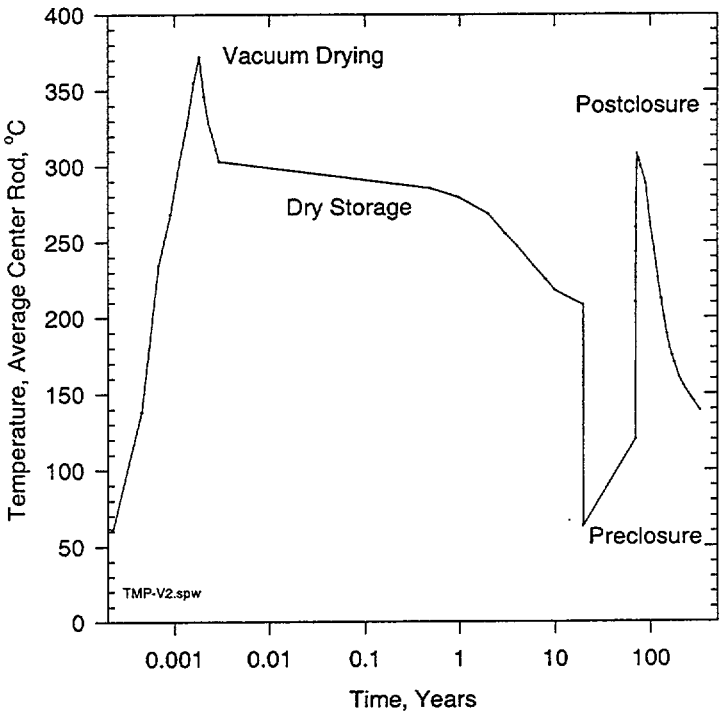

Figure 6. Average Center Rod Temperature History for Creep and SCC Analysis

(DTN: MO0011SPACMU07.049)

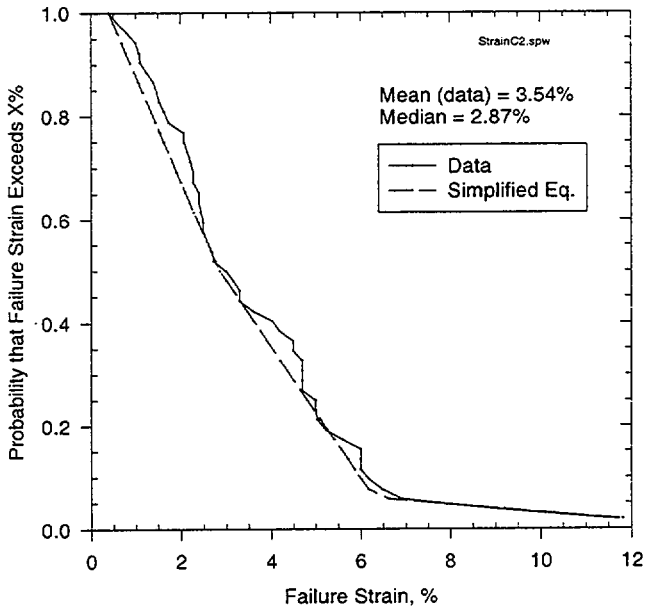

Figure 7. CCDF for Creep Strain Failure Criterion

(DTN: MO0011SPACMU07.049)

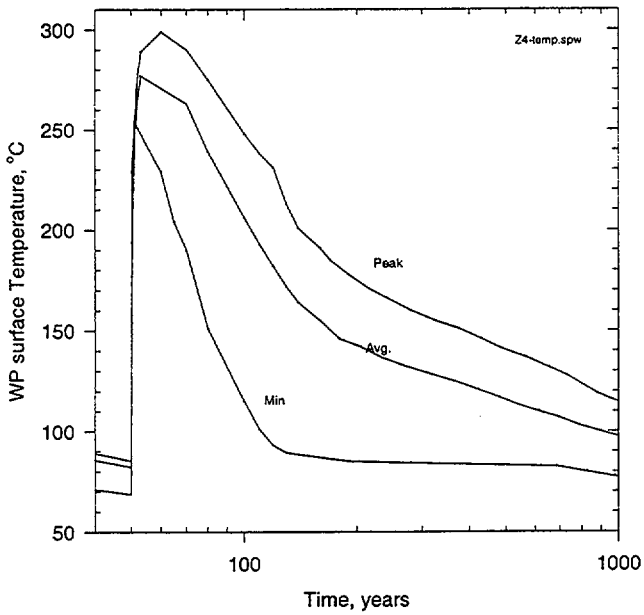

Figure 8. Minimum, Maximum, and Average Temperatures for Bin 4

(DTN: SN0001T0872799.006)

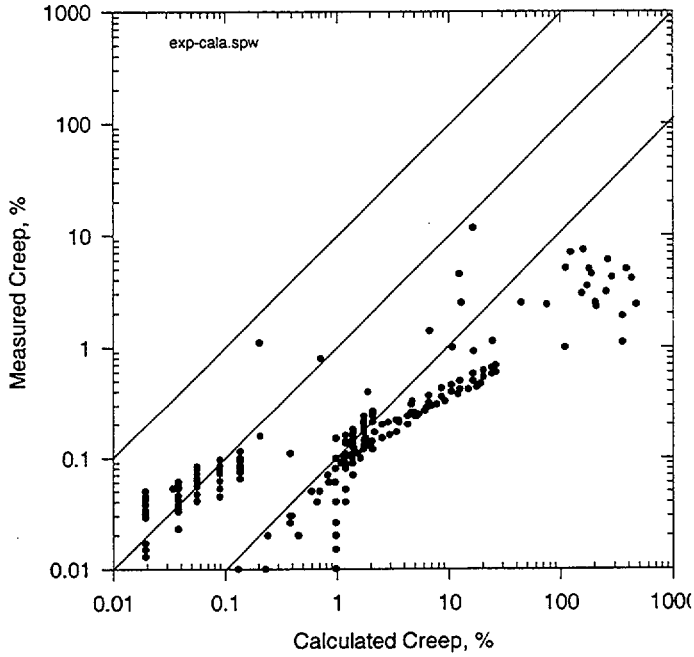

Figure 9. Comparison of Measured and Murty Creep Strain

(DTN: MO0011SPACMU07.049)

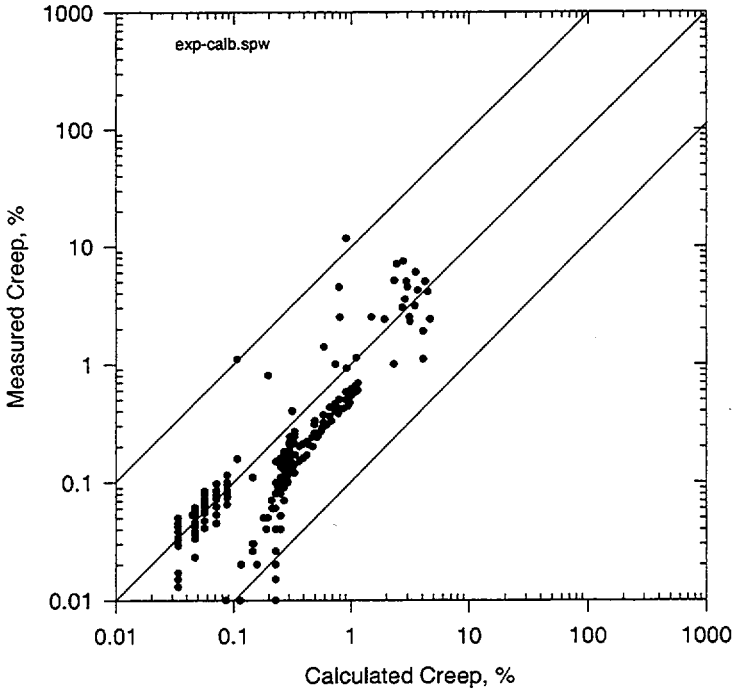

Figure 10. Comparison of Measured and Modified Murty Creep Strain

(DTN: MO0011SPACMU07.049)

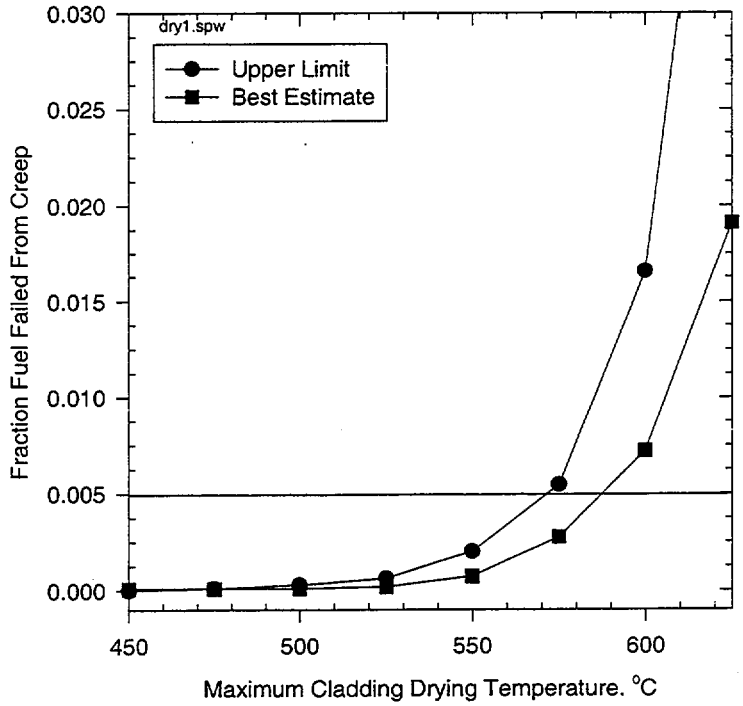

Figure 11. Creep Failure vs. Maximum Cladding Vacuum Drying Temperature

(DTN: MO0011SPACMU07.049)

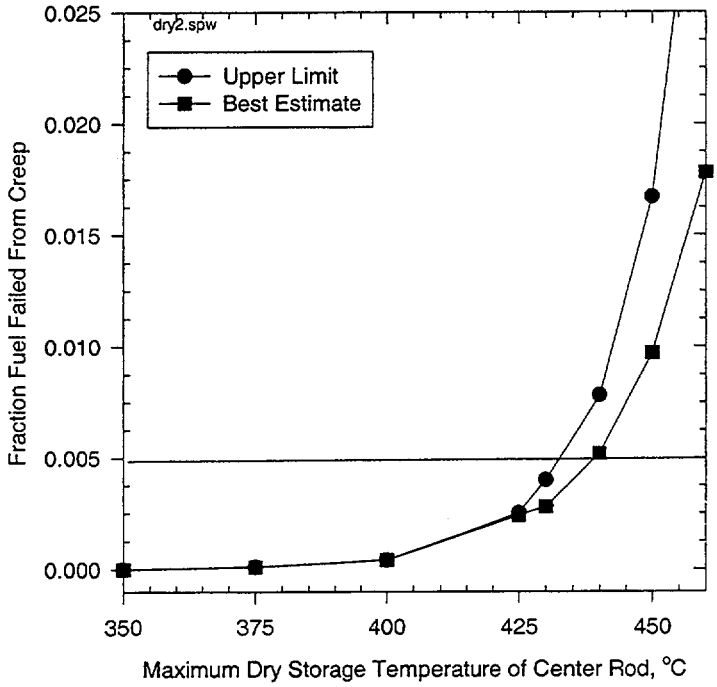

Figure 12. Creep Failure vs. Maximum Cladding Dry Storage Temperature

(DTN: MO0011SPACMU07.049)

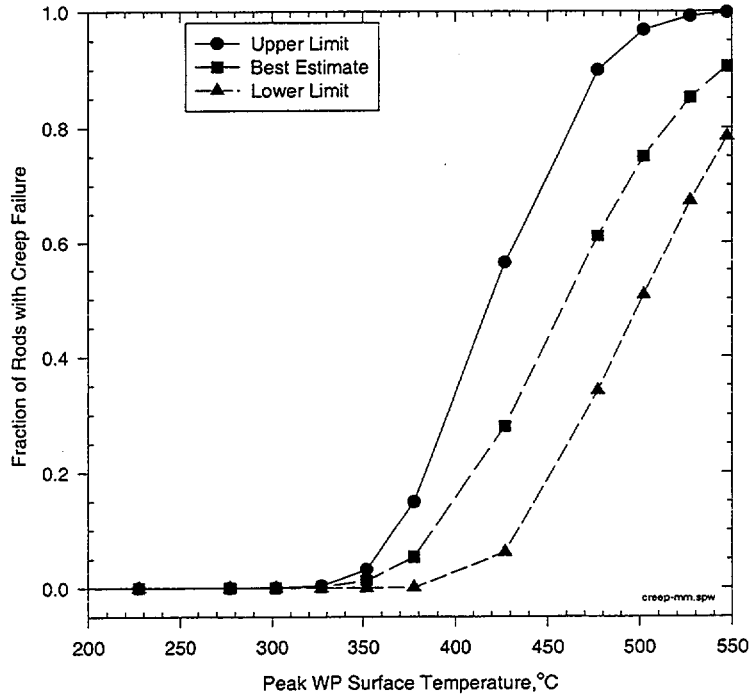

Figure 13. Creep Failure Fraction as a Function of Peak WP Surface Temperature

(DTN: MO0011SPACMU07.049)

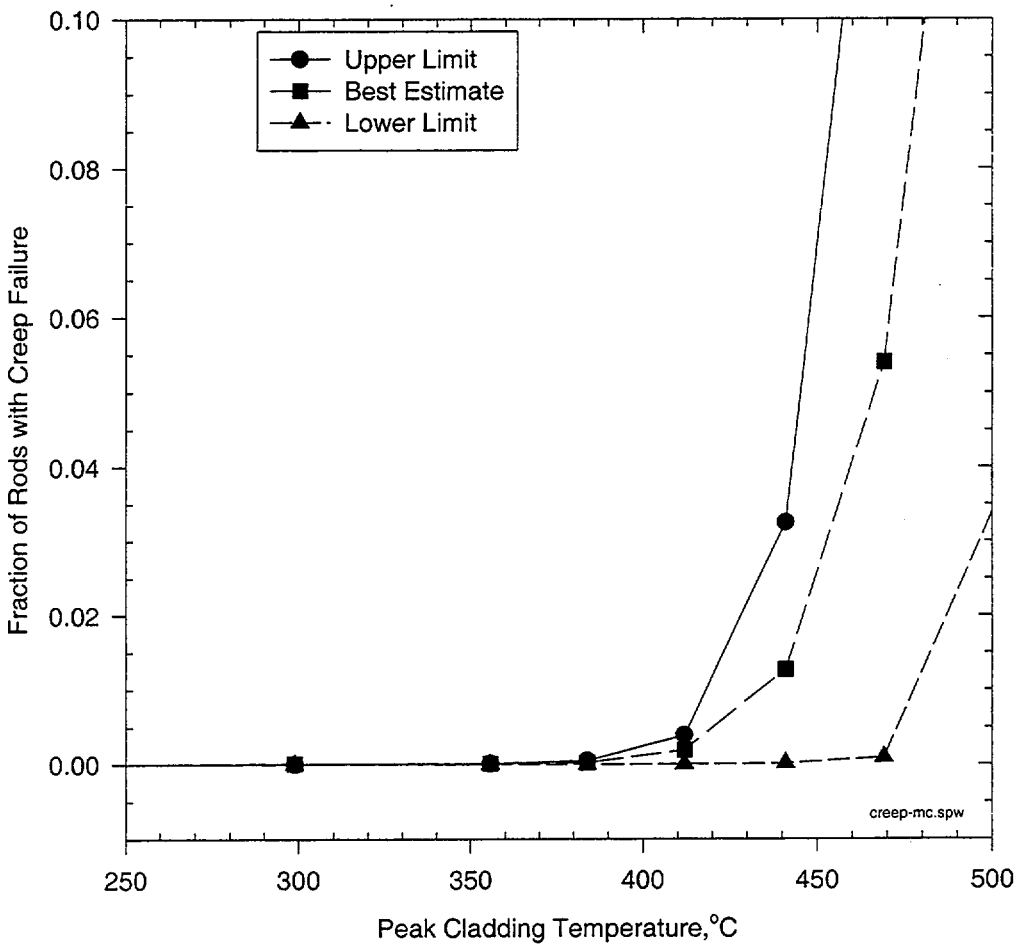

Figure 14. Creep Failure Fraction as a Function of Peak Cladding Temperature

(DTN: MO0011SPACMU07.049)

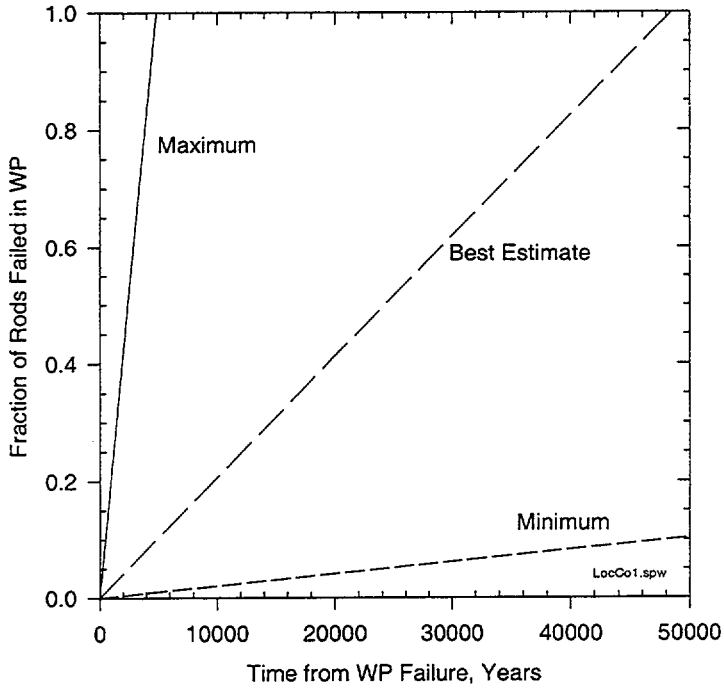

Figure 15. Example of Localized Corrosion with a Constant Water Ingression into WP

(DTN: MO0011SPACMU07.049)

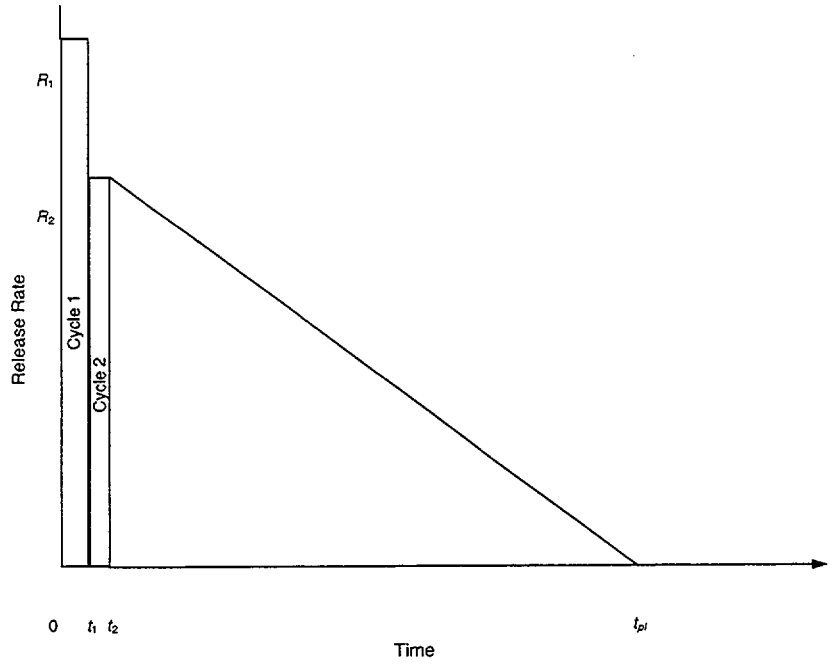

Figure 16. Radionuclide Release Rate Over Time for Fast Release

(DTN: MO0011SPACMU07.049)

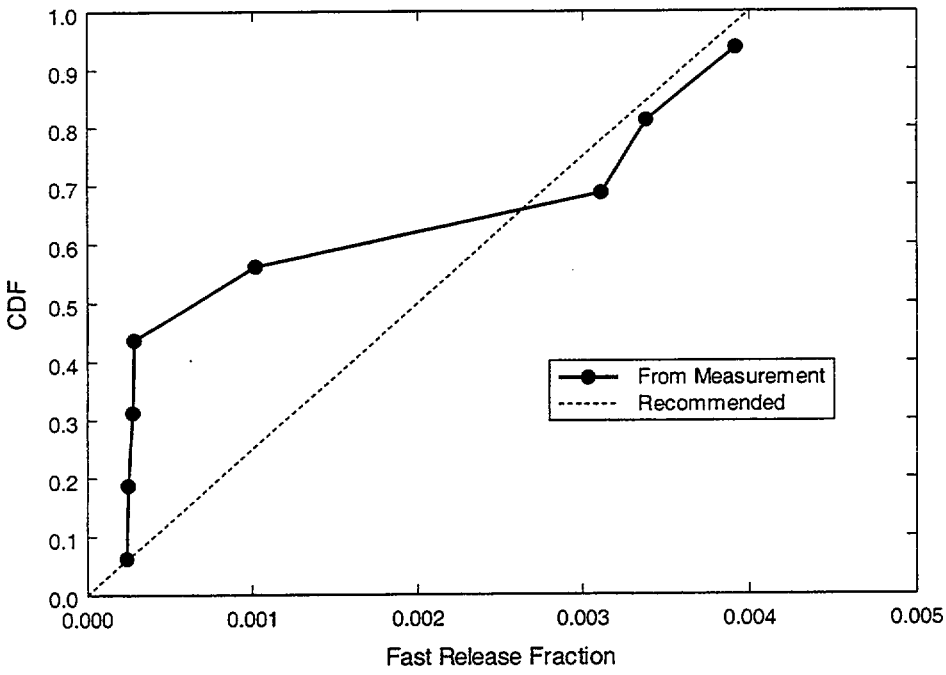

Figure 17a. CDF for Fast Radionuclide Release Fraction from Fuel Matrix

(DTN: MO0011SPACMU07.049)

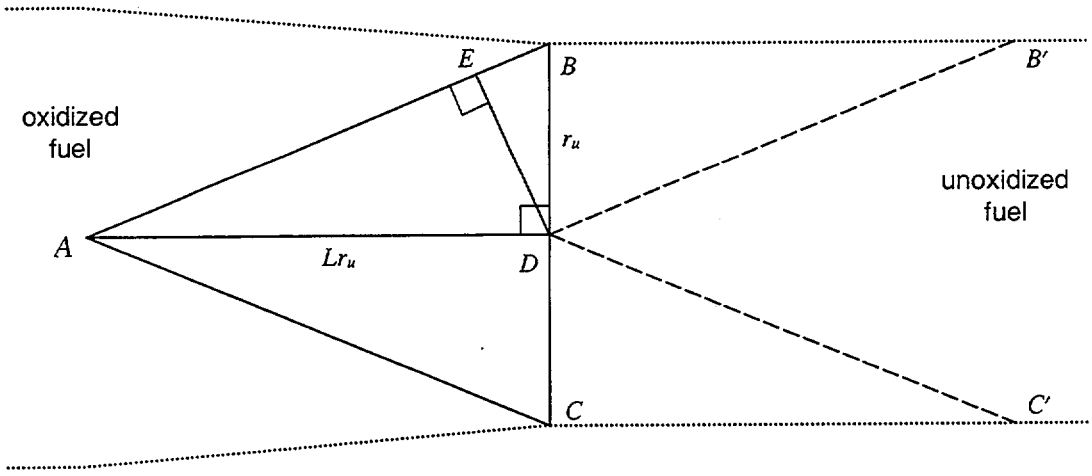

Figure 17b. Schematic Cross-section of Altering Fuel Rod in Conservative Treatment

(DTN: MO0011SPACMU07.049)

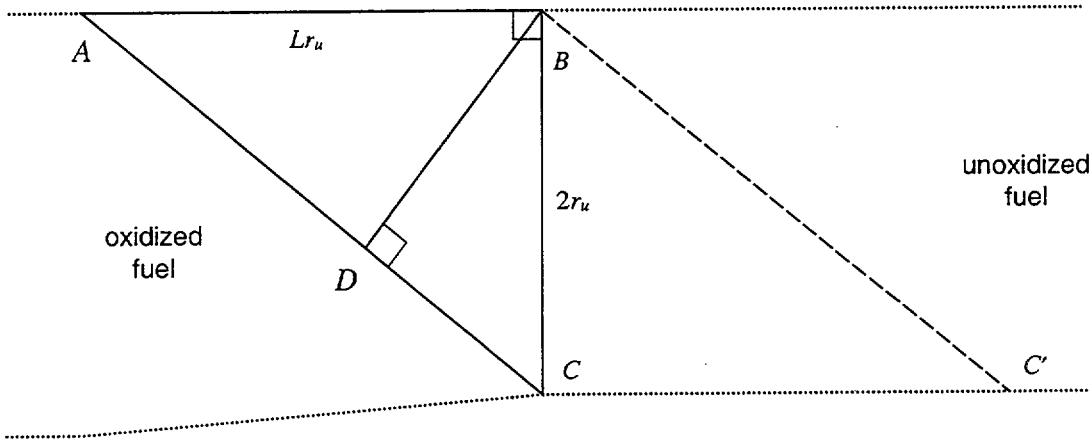

Figure 17c. Schematic Cross-section of Altering Fuel Rod in Intermediate Treatment

(DTN: MO0011SPACMU07.049)

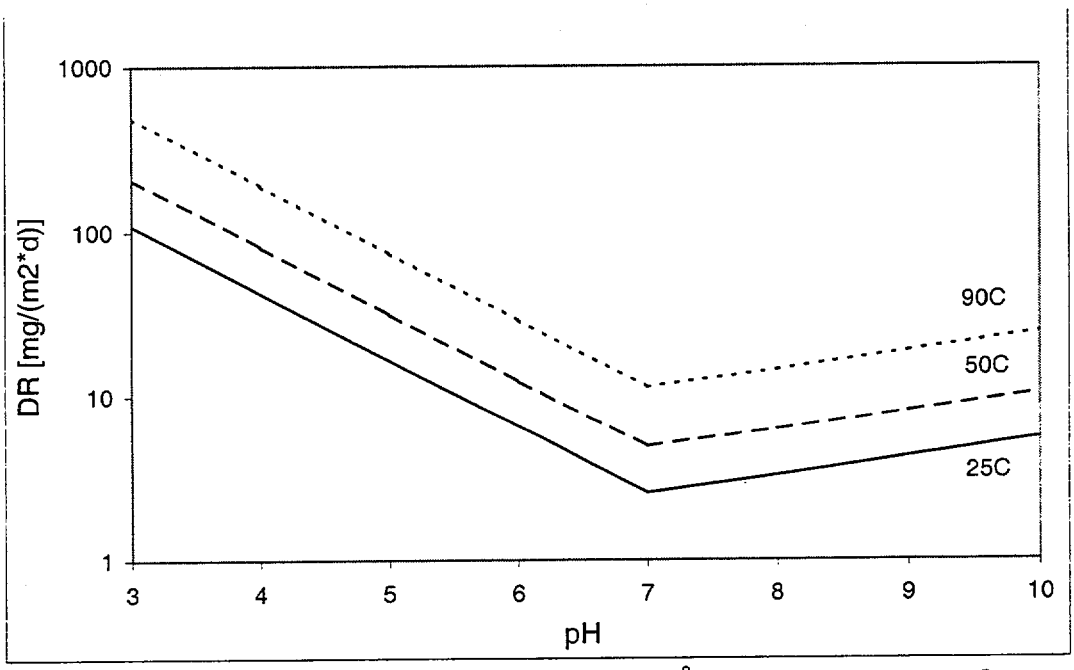

NOTE: Abstracted analysis evaluated at 10^{-3} atm. CO_2 and 0.2 atm. O_2

Figure 18. Abstracted Intrinsic Dissolution Analysis

(DTN: MOL.20000121.0161)

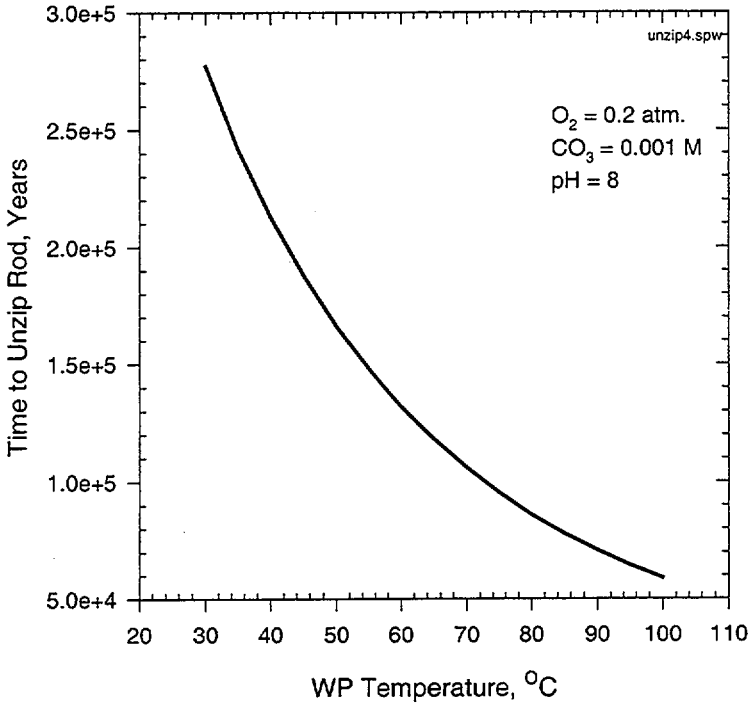

Figure 19. Unzipping Times vs. Temperature in WP

(DTN: MO0011SPACMU07.049)

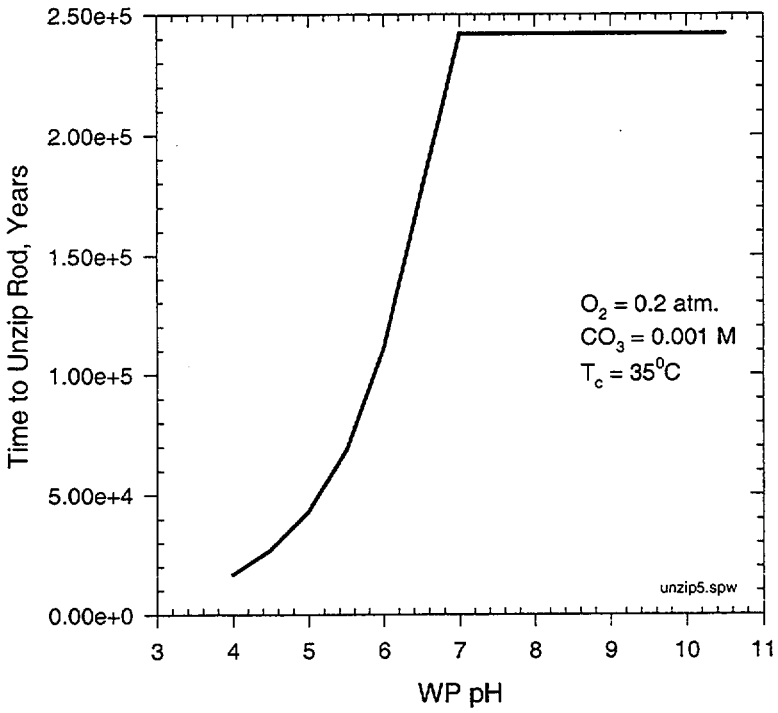

Figure 20. Unzipping Times vs. pH in Waste Package

(DTN: MO0011SPACMU07.049)

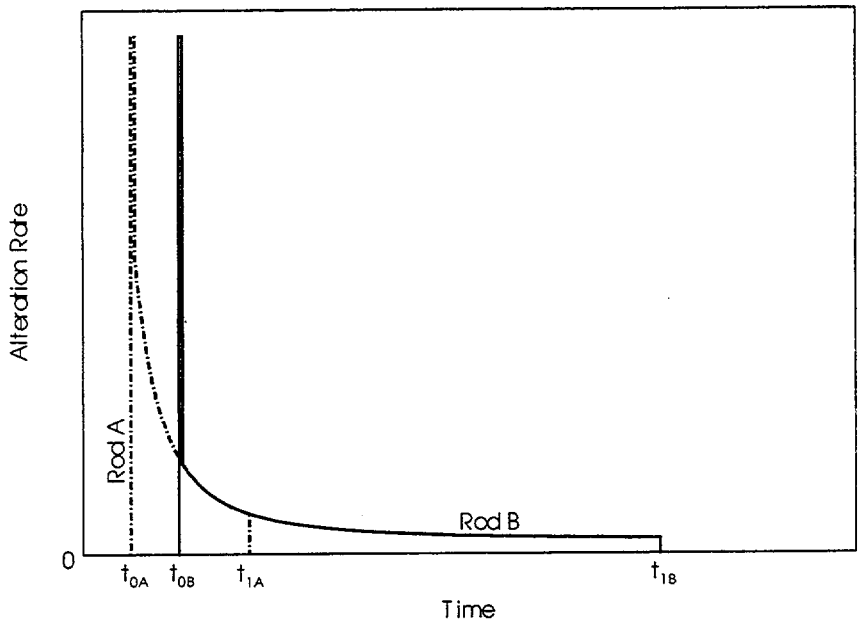

Figure 21. UO_2 Alteration Rate as a Function of Time for Two Fuel Rods (Schematic)

(DTN: MO0011SPACMU07.049)

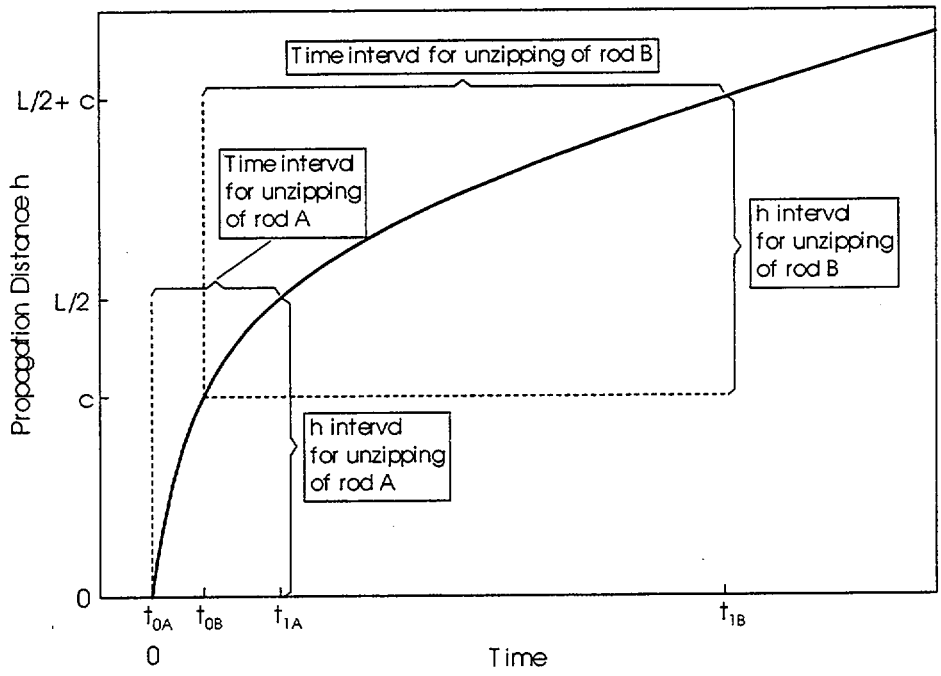

Figure 22. Propagation Distance and Unzipping of Two Fuel Rods (Schematic)

(DTN: MO0011SPACMU07.049)

9. ATTACHMENTS

The attachments are listed as follows:

Attachment	Title	Pages
I	Summary of Cladding Degradation Abstraction used in TSPA	2
II	Description of Software Routine: AMR-F0155 V2.xls	25

Attachment I

Summary of Cladding Degradation Abstraction Used in TSPA

	A	B	C	D	E	F	G	H
1	file = AMR-F0155-V2.xls							
2	**Sheet = Summary, p. 1**		**Total Cladding Abstraction**					
3								
4	**6.1) Cladding Condition as Received (to be added to creep failures)**							
5	For the 5 groups of WPs (approx. 1500 WPs / group)			Include SCC				
6	**Lower Limit=**	0.0155 %		**0.4884** %				
7	**Median=**	0.0948 %		**0.5677** %				
8	**Uppper lim=**	1.2853 %		**1.7581** %				
9	Distribution is triangular							
10	error factor =	4						
11	**CCDF**	**Lower Unc.**	**% failure, Mode**	**Upper Unc**				
12	1.0000	0.0138	0.0550	0.2200 %				
13	0.9987	0.0146	0.0585	0.2341 %				
14	**0.9849**	**0.0155**	0.0622	0.2486 %				
15	0.8561	0.0179	0.0717	0.2869 %				
16	0.6555	0.0212	0.0849	0.3397 %				
17	0.5819	0.0224	0.0895	0.3582 %				
18	0.5058	0.0237	**0.0948**	0.3793 %				
19	0.2709	0.0284	0.1136	0.4545 %				
20	0.1966	0.0361	0.1445	0.5780 %				
21	0.1084	0.0507	0.2028	0.8111 %				
22	0.0970	0.0522	0.2089	0.8357 %				
23	0.0766	0.0741	0.2965	1.1859 %				
24	0.0640	0.0746	0.2983	1.1930 %				
25	**0.0503**	0.0803	0.3213	**1.2853** %				
26	0.0373	0.1248	0.4990	1.9962 %				
27	0.0323	0.2469	0.9875	3.9499 %				
28	0.0221	0.2892	1.1568	4.6274 %				
29	0.0196	0.4496	1.7985	7.1941 %				
30	0.0190	0.5088	2.0352	8.1408 %				
31	0.0115	0.6939	2.7757	11.1029 %				
32	0.0036	0.7626	3.0505	12.2022 %				
33	0.0002	1.3214	5.2856	21.1424 %				
34	0.0000	1.3214	5.2856	21.1424 %				
35								
36								
37	**6.2) Creep&SCC Model, Fraction Perforated rods at time=0**							
38	Table gives fraction of pins considered perforated at time t=0							
39	use triangular distribution between low, best, high							
40	**WP Peak TC**	**Upper Limit**	**Mode**	**Lower limit**				
41	<=177.333	0.00000	0.00000	0.00000				
42	227	0.00010	0.00010	0.00000	Upper limit put equal to best estimate			
43	277	0.00010	0.00010	0.00000				
44	302	0.00054	0.00017	0.00000				
45	327	0.00387	0.00186	0.00000				
46	352	0.03250	0.01272	0.00010				
47	377	0.14953	0.05403	0.00090				
48	427	0.56379	0.28022	0.06171				
49	477	0.89907	0.61133	0.34176				
50	502	0.96831	0.74988	0.50675				
51	527	0.99214	0.85164	0.67265				
52	>=547.333	0.99801	0.90497	0.78409				
53								
54								
55	SCC failure fraction =		0.0047		added to rows 6,7,8			
56	**6.3) Localized Corrosion**		Uncertainty distribution log uniform between max and min					
57	**equation : fraction = M^3 water / 2.42E3M^3, max=10*fraction, min = fract/10**							
58	test case, 50 l/yr, 10,000 yrs, 1 L = 1E-3 m^3							
59	Fraction failed=	0.20661157						

	A	B	C	D	E	F	G	H
60					file = AMR-F0155-V2.xls			
61	**6.5 Fast Release Fraction, %**				**Sheet = Summary, P.2**			
62	Gap release	Iodine (I)	4.20%					
63	Gap release	Cesium (Cs)	1.40%					
64	Fast release	all radionuclides=	0 - 0.4%	uniform distribution				
65				Includes additional I, Cs				
66								
67	**6.6.1) Unzipping Velocity**							
68								
69	Perf =rods available for unzipping,sum(localized corrosion (2), creep (3), Initial failures(4))							
70	Vz = rod unzip velocity							
71	Vz = A * Vin			Active fuel length = 366 cm				
72	A = Unzip model parameter, triangle fit from lower, Mode, upper							
73		**CCDF: 100% =1, 50% =9, 10% =18, 0% = 180**						
74	Vin = Intrinsic dissolution Velocity							
75	**Vin = Dis rate (item 1) ***		**2.190E-05**	cm/yr / (mg/m2-d)				
76	Fuel exposed and disolved= Vz* Perf, check perf <=1.0							
77								
78	density, uo2			10	gm/cc	(includes 10% porosity)		
79	grain area/macro area=			6	area-micro/area-macro			
80	intrinsic, macro			0.000219	gm/cm2-yr			
81	cm/yr / (mg/m^2-d), conversion of dissolution			0.0000219	cm/yr / (mg/m2-d)			
82		to velocity						
83								
84								
85								
86								
87	**6.6.2) Abstraction of Intrinsic Dissolution Rate**							
88								
89	**log10(rate) = a0 + a1/Tk + a2* PCO3 + a3* PO2 + a4 * pH**							
90	**Term=**			**a0**	**a1**	**a2**	**a3**	**a4**
91	**pH>7**			**4.69**	**-1085**	**-0.12**	**-0.32**	**0**
92	**pH< =7**			**7.13**	**-1085**	**0**	**-0.32**	**-0.41**
93	**Example calc.**				**Tc**	**PCo3**	**PO2**	**pH**
94	**dis Rate**	**log10(dis rt)**	**Acidic solution**	**Basic solution**	**Tc**	**PCo3**	**PO2**	**pH**
95	6.066	0.783	0.6769	0.7829	50	2.7	0.7	7
96	14.224	1.153	1.0470	1.1530	90	2.7	0.7	7
97	73.624	1.867	1.8670	1.1530	90	2.7	0.7	5
98	325.638	2.513	2.5127	0.9787	70	2.7	0.7	3
99	units:	dis rate= mg/m2-d, m2 is microscopic (grains)						
100		Tc = temperature, centigrade, WP wall				Tk = Temp, Kelvin		
101		PCO3 = CO3 activity = -log10(molar CO3)						
102		PO2 = O2 activity = -log10(partial pressure O2)						
103		pH = standard,						
104	**Uncertainty in dissolution a0 +- 1.0, uniformly distributed**							
105	This equation is used in the unzipping abstraction							
106								
107	**6.7 Stainless Steel Clad Commercial Reactor Fuel**							
108								
109	**% of WPs containing SS cladding =**				**3.49**			
110	**% of fuel in these WPs with SS cladding =**				**32.89**			
111	Assumption, all SS cladding is perforated, available for unzipping							
112								
113	**6.4.1 Mechanical Failures**							
114	Fraction rods failed, rockfall = 0, PF<0.5, =2*(PF-0.5), PF > 0.5, PF = WP Patch fraction							
115	Seismic Frequency = 1.1E-6/yr							
116	Seismic event: All cladding failed (perforated)							
117	All cladding available for unzipping							
118								

Attachment II

Description of Software Routine: AMR-F0155-V2.xls

The statistical analysis of the rod creep is performed in the software routine "AMR-F0155-V2.xls" (V2 represents Version 2) which is included in the DTN: MO0011SPACMU07.049. Microsoft Excel for Windows Version 4.0 was used for the analysis and the analysis is documented in this AMR as a software routine. The analysis was performed on a Dell Pentium personal computer (CPU number 113068 located in 1526D) with a WINDOWS NT operating system. One macro is used and is listed, tested and documented in this attachment. This attachment describes the various sheets that compose this software routine, including a listing of the top rows of each sheet of the file, and correlates the various equations presented in the text of this report to the software routine.

The software routine contains 9 sheets and one macro, many of which are linked. Each sheet addresses a specific aspect of cladding condition. Table II-1 summarizes the different sheets.

Table II-1. Description of Sheets in AMR-F0155-V2.xls

Sheet Title	Subject	Supports Sheet	Uses Sheet
Creep-Lim	Creep Failure Limit Samples	Fail-Calc	Rand #
Creep-Rod	Creep strain for single rod	Creep-WP	Temp-C
Creep-WP	Calculates creep across WP	Fail-Calc	Macro: Creep1, Creep-Rod
Fail-Calc	Collects statistics on creep failure	Final Creep Results	Creep-WP, Creep-Lim
Macro: Creep1	Calls Creep-Rod from Creep-WP	Creep-WP	Creep-Rod
Rand #	Table of random numbers	All distributions	None
Summary	Summary of output passed to TSPA	Listed as Attachment I	All
Temp-C	Temperature across WP	Creep-Rod	Temp-C2
Temp-C2	Initial rod and WP temperature histories	Temp-C	None
Unzip	Time to unzip rod	Figures 19, 20	None

The Sheet "Summary" is listed as Attachment I and is not repeated in this attachment. The first 30 to 40 rows of the other sheets are included (in alphabetical order) in this attachment (Table II-5 to II-12). Many of the sheets have 2000 statistical samples and only the first few rows are included. A brief description of each sheet follows including the testing and test results.

This analysis is based on observed fuel performance for PWR fuel with Zircaloy cladding and therefore there are constraints, caveats and limitations to this analysis. This analysis is only applicable to U.S. commercial PWR and BWR fuel with Zircaloy cladding. It is also limited to fuel exposed to normal operation and anticipated operational occurrences (AOOs) and not for fuel that has been exposed to severe accidents. Fuel burnup projections have been limited to the current commercial power licensing environment

with restrictions on fuel enrichment, oxide coating thickness and rod plenum pressures. The ranges of applicability are:

1. Temperature: 27°C to 420°C. The upper temperature limit is the highest temperatures of Matsuo's experiments. This is also the approximate temperature of the inside surface of the cladding during normal operation in a PWR (340°C to 370°C, (Pescatore et al. 1990, Table 3, p. 7)). The lower limit is not important since the cladding degradation rates become negligible at these temperatures.

2. Stress: 0 to 314 MPa. The lower limit is not important because low stress does not cause damage. The upper limit is the upper limit of Murty's test data for which the creep equation was derived.

3. Burnup: 2 to 80 MWd/kgU, the approximate range of experiments reported in this AMR.

The analysis itself addresses the uncertainties of the various parameters. Uncertainty ranges are defined for each parameter based on experimental observations reported in the literature. These uncertainties are statistically combined in the sampling routine. The range for each parameter is defined and justified in the body of this AMR.

The following sections describe how the analysis is performed and the analytical sequence used.

Sheet "Fail-Calc"

The Sheet "Fail-Calc" (for failure calculation) is the main driver for the calculation of creep failures in the WP (see Table II-8 for the first 2 of 6 zones). The user inputs the shift in the WP surface temperature into Cell D22. The shift in peak vacuum drying temperature is placed into Cell K22. The shift in peak dry storage period temperature is placed into Cell L22. Usually, only one of these variables is varied for a sensitivity study. The macro: Creep1 is then started. The creep calculations are then calculated for the specific WP temperature history. The user must copy the results for this WP temperature (Cells E22 through M22) into the table of results shown in Rows 3 through Row 19. These tables are used to generate Figures 11 (Cells A3 to F13), Figure 12 (Cells G3 to J10), and Figures 13 and 14 (Cells K3 to P14). The data for Figure 13 is reproduced in the "Summary" Sheet, Rows 37 to 51. Results for SCC and hydride reorientation are given in Rows 16 to 19 and discussed in Sections 6.2.5 and 6.2.6. The SCC failure is also given in the "Summary" sheet, Row 55. The peak cladding temperature during YMP closure is calculated in Cell I22 and used for Figure 14.

The user also specifies the strain uncertainty (Cell B22, usually 0.8). Calculated strain is uniformly distributed by a multiplication factor of 0.2 to 1.8. This factor was developed in CRWMS M&O 2000m. The upper and lower creep failure criteria are also specified in Cells B23 and B24. The upper and lower creep failure criteria are used to calculate the upper and lower creep failure fractions. These are defined in Section 6.2.3.

The rod stress (room temperature) is given in Cells C29 through C2028. These are generated in Sheet "Creep-WP", Column S and have been ordered by decreasing stress (Sheet "Creep-WP", Column AA) so that trend can be observed. Column B gives the sample or case number so that specific characteristic of a sample can be determined. One rod, at the stress specified in Column C, is placed in each of the 6 zones of the WP and the creep is calculated in the Sheet "Creep-WP". Table II-2 identifies the columns used for calculating the various failure indices for the six zones. Row 26 identifies the zones. For each zone, the resulting creep strain is calculated in the Sheet: "Creep-WP" and is given in the first column of "Fail-Calc" for the specific zone. A creep strain (in percent) greater than 100 means that creep failure is expected for that rod. Creep strain of 99 means that the rod was identified as having a peak stress over 180 MPa and failure is assumed for that rod by SCC. Creep strain of 98 means that the rod was identified as having a stress at the peak temperature sufficiently high that reorientation is possible but rod failure is not expected. As the stresses decrease (i.e. at the higher row numbers in "Fail-Calc"), the strains decrease. The random sampled failure criterion is given in the second column for each zone of "Fail-Calc". This criterion is generated in the Sheet: "Creep-Lim" and will be discussed later.

The next three columns contain a rod failure index, either zero (0, i.e. the rod did not fail) or one (1, i.e. the rod failed). The creep strain uncertainty is calculated in these cells. The first column is the resulting comparison for the upper limit, using 1% creep as the failure criterion. The next column uses the full CCDF for the failure criterion and compares the creep (Column D for Zone 1) to the failure criterion (Column E for Zone 1). The third column is the resulting comparison for the lower failure limit, using 6% creep as the failure criterion.

Table II-2. Column Assignments in Sheet "Fail-Calc" for Rod Creep Failure Calculations

Zone	Creep Strain Column	Creep Failure Criteria Column	Upper Limit Failure Index	CCDF Failure Index	Lower Limit Failure Index
1	D	E	F	G	H
2	I	J	K	L	M
3	N	O	P	Q	R
4	S	T	U	V	W
5	X	Y	Z	AA	AB
6	AC	AD	AE	AF	AG

The final statistics for rod failure from creep are performed in rows 22 to 25. The fraction of the 2000 samplings failed in each zone using the three failure criteria is calculated in Row 25 and is the sum of the index column divided by 2000. Row 24 is the fraction of rods in the WP that are located in each zone. This is calculated in Table 3 and shown in Figure 3. Row 23 is the product of Rows 24 and 25 and represents the fraction of rods in the WP that are located in a zone and have failed. Row 22 (Cells F22, G22, H22) sums the zones in Row 23 for the three failure criteria and gives the fraction of rods in the WP that have failed using the three failure criteria. These results are copied into the table in Cells E3 through P14 and are used to generate Figures 11 through 14.

Tests: The stress and case number (Columns C and B, starting in Row 29) are imported from sheet "Creep-WP", Columns Z and AA and are tested by visual inspection using the case number. For Zone 1, the resultant creep values are listed in Column D. This can be tracked back to "Creep-WP". Failure criteria are given in Column E and can be tracked back to "Creep-Lim", Col. C. Col. F compares the creep, multiplied by an uncertainty, to the upper limit failure criteria (Cell B23). The creep uncertainty factor is 0.8 (Cell B22) and a uniform distribution of uncertainty is used as shown below:

$$\text{Creep} = \text{Creep(Col. D)}*[(1\text{-uncertainty}) + 2 * \text{uncertainty}* \text{rand}()] \quad \text{(Eq. II-1)}$$

$$\text{Creep} = \text{Creep(Col. D)}*[0.2 + 1.6* \text{rand}()] \quad \text{(Eq. II-2)}$$

Where rand() = a random number from Sheet "Rand #", Col. J

This calculation can be tested by hand calculations (at lower stresses where creep is near the failure criterion). Column F assigns a zero or one, depending on whether the creep exceeds the creep limit. This is tested by inspecting down the 2000 samples of decreasing stress (all 2000 samples are not actually shown in Table II-8). This calculation is repeated in Columns G, H (Zone 1), K, L, M (Zone 2), P, Q, R (Zone 3), U, V, W (Zone 4), Z, AA, AB (Zone 5), AE, AF, AG (Zone 6). The summing of the statistics is tested with visual inspection.

Sheet "Fail-Calc" used Sheets "Creep-Lim" and "Creep–WP". A description of these sheets follows.

Sheet "Creep-Lim"

This sheet contains 6000 samplings of creep failure criteria. Rows 8 through 59 give the 52 creep strains reported by 4 different experimenters and discussed in Section 6.2.3. The data from Table 6 is listed in Column C and repeated, in order of increasing strain in Column D. Column E gives the CCDF value assuming each point is equably probable. The resulting data CCDF is given in Figure 7 and has been fitted by three linear equations. The points defining the lines are given in Cells L7 to M13 and the constants to the equations are defined in Cells G5 to J6. For each CCDF probability, the equations (Section 6.2.3, Eq. 6.2-10) are evaluated in Columns H, J, and I. Column G selects whether Column H or I is more correct to use. Column F selects whether Column G or J is correct. Column F is the resulting calculated strain. Columns D, E, and F are used to generate Figure 7.

This analysis is repeated in Rows 63 through 6062 except in this region of the sheet, Column D is a random number taken from Sheet: "Rand #". Table II-3 shows the assignment of random failure criteria to WP zones. Table II-5 shows the top rows of this sheet.

Table II-3. Assignment of Creep Failure Criteria to Zones

Zone	Starting Location	Ending Location
1	C63	C2062
2	C1063	C3062
3	C2063	C4062
4	C2538	C4537
5	C3063	C5062
6	C4063	C6062

Test: The equations 6.2-10 are verified by comparing the calculated strain criteria to the experimental points at the selected CCDF points given in Cells L7 to M13. This comparison shows agreement. Figure 7 compares the calculated CCDF to the data CCDF and shows good agreement.

Sheet "Creep-WP"

In this sheet, the rod temperature coefficients are calculated for the 12,000 rods sampled across the WP (2000 stress samples, located in each of 6 zones). The temperature uncertainty (13.5%) is specified in Cell E3 and represents an uncertainty of 41.6°C from the combined WP surface temperature uncertainty (22.1°C) and the uncertainty in temperature across the WP (19.5°C). The temperature uncertainty is calculated in Sheet "TempC2" Cell N55. The 2000 stress samples are repeated in Column C. The zone numbers are given in Row 5. For each zone, the first column is the temperature shaping coefficient and the second column is the resulting creep from the Sheet "Creep-Rod". The macro "Creep1" is used to couple Sheets "Creep-WP" to "Creep-Rod" and will be described below. The temperature shaping coefficient represents the product of the uniformly distributed temperature uncertainty (Cell E3) and the WP radial temperature shaping term. The WP radial temperature shaping term is calculated in Sheet "TempC", Cells F7 to K7 and will be described in that sheet description. The radial temperature shaping term adjusts the WP center rod temperature downward for the outer zones. The rod stress (Column C) and temperature shaping coefficient (example: Column D for Zone 1) are input for the rod creep calculation (Sheet "Creep-Rod") and the resulting creep (example: Column E for Zone 1) is stored in this sheet. The macro "Creep1" couples the "Creep-WP" Sheet and the "Creep-Rod" Sheet. Table II-7 shows the top rows (Zone 1 and 2) of Sheet "Creep-WP".

The stress for each of the 2000 samples is calculated in Rows R through AJ. This was done because the original general stress presented in CRWMS M&O 2000a (Figure 18) contained the effect of localized cracks which is overly conservative and produces stresses about 4% too high (Cell AD5). The Run Number, Pressure, and crack depth and original stress (Columns R, U, AF and AC respectively) are copied from the software routine for in CRWMS M&O 2000a, Sheet = "Crack", Columns A, H, B and G. The Column Oxide Thickness (V) is copied from Sheet "Corrosion", Column C. The

cladding thickness (Column X) is calculated by subtracting the metal loss from the initial cladding thickness (Cell S3). The stress is calculated in Column S. The Free Volume (Column T) and burnup (Column W) are copied from CRWMS M&O 2000a, Sheet = "Free Vol.", Column C and B respectively. The free volume for each sample will be used later to correct the stress because of existing strain. Columns Z, AA, and AB contain the same information as Columns R, S, and T but have been ordered for decreasing stress. Columns AC and AD compare the stress with and without the crack included and show that the general stress is about 4% smaller. The ordered values of the original stress including crack do not necessary correspond to the case number because of the randomness of the crack size. The original stress is Columns AF, AG, and AH are calculations of the stress intensity factor which is used in a discussion in Section 6.2.5 of the potential of SCC. Figure 1 is generated with the results of Columns AI, and AJ.

Test: This sheet imports the stress (Column C) from "Fail-Calc" Column C. One calculation done here is the calculation of the temperature shaping coefficient (Column D for Zone 1). Using Cell D7 as a test calculation, the temperature uncertainty (Cell E3) is uniformly distributed using an equation similar to Equation II-1 and "Rand #" Cell A5 (0.232 value). The shaping coefficient for Zone 1 is in "TempC", Cell F7 and is one (1, i.e. center zone). The test calculation for Cell D7 is:

$$\begin{aligned} \text{Temp. Adj} &= \text{Shape coef} * \text{Uncertainty} \\ &= 1.0 * [\,(1.0 - 0.135) + 2 * 0.135 * 0.232] \\ &= 0.928 \text{ (Cell D7)} \end{aligned}$$

This calculation is repeated for each stress sample and each zone (Cols. D, F, H, J, L, N).

The stress calculation is tested by comparison of the earlier analysis and the newer values. This comparison (Column AD) shows the amount of stress reduction expected from removing a crack averaging 18 microns. This calculation can also be tested by verifying Row 7.

Macro: "Creep1"

A macro is used to couple the "Creep-WP" Sheet and the "Creep-Rod" Sheet. As described above, "Creep-WP" generates the temperature shaping term and contains the stress and free volume for 12,000 rods located across the WP. The Sheet "Creep-Rod" calculates the amount of creep for a single rod using these three inputs: Stress, free volume, and temperature shaping factor. "Creep-Rod" produces a single output number of creep strain for the one rod analyzed. The details of "Creep-Rod" are described below. The macro "Creep1" copies the three inputs from "Creep-WP" to "Creep-Rod" and then writes the resulting answer (creep strain) from "Creep-Rod" to "Creep-WP" for the 12,000 rods being analyzed. The actual listing of the macro is given below in numbered lines printed in italics.

First line is the Macro title:

1) *Sub Creep1()*

This next line steps down the 2000 lines of stress samples

2) For i = 0 To 1999

Zone 1

This next line copies the temperature shaping term from Sheet "Creep-WP", Row i+7, Column 4 (Column D) to Sheet "Creep-Rod", Location B3.

3) Sheets("Creep-Rod").Range("B3").Value = Sheets("Creep-WP").Cells(i + 7, 4).Value

This next line copies the free volume of each rod from Sheet "Creep-WP", Row i+7, Column 28 (Column AB) to Sheet "Creep-Rod", Location B2.

3b) Sheets("Creep-Rod").Range("B2").Value = Sheets("Creep-WP").Cells(i + 7, 28).Value

This next line copies the stress value from "Creep-WP", Row i+7 Column 3 (Column C) to Sheet "Creep-Rod", Cell B4.

4) Sheets("Creep-Rod").Range("B4").Value = Sheets("Creep-WP").Cells(i + 7, 3).Value

The next line shifts the resulting calculated strain from "Creep-Rod" Cell B5 to "Creep-WP", row i+7, Column 5 (Column E).

5) Sheets("Creep-WP").Cells(i + 7, 5).Value = Sheets("Creep-Rod").Range("B5").Value

For the next 5 WP radial zones the temperature shaping index is copied to "Creep-Rod" and the resulting creep strain is written into "Creep-WP". The same values of stress and free volume are used in all zones as was used for Zone 1 above.

Zone 2

6) Sheets("Creep-Rod").Range("B3").Value = Sheets("Creep-WP").Cells(i + 7, 6).Value

7) Sheets("Creep-WP").Cells(i + 7, 7).Value = Sheets("Creep-Rod").Range("B5").Value

Zone 3

8) Sheets("Creep-Rod").Range("B3").Value = Sheets("creep-WP").Cells(i + 7, 8).Value

9) Sheets("Creep-WP").Cells(i + 7, 9).Value = Sheets("Creep-Rod").Range("B5").Value

Zone 4

10) Sheets("Creep-Rod").Range("B3").Value = Sheets("Creep-WP").Cells(i + 7, 10).Value

11) Sheets("Creep-WP").Cells(i + 7, 11).Value = Sheets("Creep-Rod").Range("B5").Value

Zone 5

12) Sheets("Creep-Rod").Range("B3").Value = Sheets("Creep-WP").Cells(i + 7, 12).Value

13) Sheets("Creep-WP").Cells(i + 7, 13).Value = Sheets("Creep-Rod").Range("B5").Value

Zone 6

14) Sheets("Creep-Rod").Range("B3").Value = Sheets("Creep-WP").Cells(i + 7, 14).Value

15) Sheets("Creep-WP").Cells(i + 7, 15).Value = Sheets("Creep-Rod").Range("B5").Value

Bottom of the i "Do Loop".

16) Next i

Alarm to announce problem is complete

17) Beep

18) Beep

19) Beep

20) Beep

21) End Sub

Test: The macro can be tested the following ways:

A) After running the macro, "Creep-Rod" contains the last rod analyzed, 2000 stress sample, zone 6. This can be visually compared with the value stored in "Creep-WP". The cells to compare are given in Table II-4.

Table II-4. Comparison of Cells after Macro Run

Value	Creep-Rod	Creep-WP
Temperature Index	B3	N2006
Stress	B4	C2006
Strain	B5	O2006

B) The value of temperature index, free volume, and stress for any rod in "Creep-WP" can manually be copied into Cells B3 and B4 of "Creep-Rod" and the resulting strain can be compared with that in "Creep-WP".

C) While having the top of the Sheet "Creep-Rod" on the computer screen, the macro can be run. The macro may be confirmed to step down the rod sample stresses since they are ordered by decreasing stress.

D) First run the macro with very high WP temperatures ("Fail-Calc" Cell D22 = 250°C). This will fail most rods and the failure indices in "Fail-Calc" will be 1. While showing the indices for the middle of the stress samples (about Row 1000) on the computer monitor, the macro can be run again with "Fail-Calc" Cell D22 = -100°C (very cold WP). This will produce very few rod failures and the macro may be confirmed to sweep down Sheet "Fail-Calc" changing the failure indices.

Sheet "Creep–Rod"

This sheet calculates the creep strain for a single rod given the initial room temperature stress and temperature index. As described above, this sheet is used 12,000 times to calculate the creep for all the rods listed in " Creep-WP". Table II-6a and b list this sheet.

The actual calculations are performed in Rows 10 through 75. The room temperature stress is specified as input in Cell B4 and the temperature index is specified in Cell B3. The rod free volume is input and specified in Cell B2. The resulting strain is shown in Cell B5. The details of the creep analysis are as follows:

For Rows 8 through 64

Column	Description
A	Time in years, at YMP
B	Time, years, starting with vacuum drying.
C	Gives the cladding temperatures, °C, at that time. The temperature history of the rod being analyzed is of the center rod, multiplied by the scaling factor to reduce the temperature for other zones and multiplied by the uncertainty factor. The shaping factor is applied for all time, including the dry storage times. The vacuum drying and storage temperatures (Column Z) are maximum temperatures

and the mean temperature is calculated by reducing the peak temperature by the temperature uncertainty factor.

D Gives the cladding temperatures, Kelvin, at that time.

E Stress, adjusted for the gas plenum temperature at time using ideal gas law for the fission gas in the gas plenum, Mpa. The plenum temperature is the peak rod temperature (Column D) minus the time dependent temperature difference given in Column V. The rod volume (initially Cell B2) is increased by a creep produced volume for the previous time step given in Column T.

F Time in hours, from Column W for vacuum & storage, Col. A (added) for YMP

G Total running sum of creep strain (Eq. 6.2-7, below)

H Corrected total creep for temperature i and time i by using Eq. 6.2-8 on Column I

I Total (Glide +Coble) creep for temperature i and time i(Eq. 6.2-5, below)

J Glide creep for temperature and time i (Eq. 6.2-3, below)

K Coble creep for temperature i and time i (Eq. 6.2-4, below)

L Corrected total creep for temperature i but time i-1 using Eq. 6.2-8 on Column M

M Total (Glide +Coble) creep for temperature i but time i-1 (Eq. 6.2-5, below)

N Glide creep for temperature i but time i-1 (Eq. 6.2-3, below)

O Coble creep for temperature i but time i-1 (Eq. 6.2-4, below)

P Young's modulus, E (Eq. 6.2-6, below)

Q Temperature coefficient for Arrhenius term (Temperature term Eq. 6.2-1, below)

R Coble creep rate (fraction/yr) for temperature at time i (Eq. 6.2-2, below)

S Glide creep rate (fraction/yr) for temperature at time i (Eq. 6.2-1, below)

T Creep volume calculated by using Eq. 6.2-9 and strain (Column G, time = i-1.

U Not used

V Temperature difference between maximum rod temperatures and plenum region. For vacuum drying, taken from Spilker and Fleisch 1986, Fig. 14. For dry storage period, linear interpolation from vacuum to repository differences, for repository differences, from Sheet "TempC2" Column X.

W Vacuum drying time (hrs) from Spilker and Fleisch 1986, Fig. 14, dry storage time (years) from Peehs 1998, Figure 13a. Storage started 2 hours after drying.

X Maximum temperatures (Column Y) shifted by constants for vacuum drying (Sheet "Fail calc" Cell K22), and dry storage (Sheet "fail calc" Cell L22).

Y Vacuum drying temperatures from Spilker and Fleisch 1986, Fig. 14, dry storage temperatures from Peehs 1998, Figure 13a. Storage started 2 hours after drying. These temperatures are maximums and the mean values are reduced in Column C.

The creep correlation developed by Murty (Henningson, 1998, p. 57, eqs. 9b, 11, 12, and 15) was used and is repeated below from Section 6.2:

$$\dot{\varepsilon}_{Glide} = 4.97x10^{6} e^{-31200/T} \frac{E}{T} [\sinh(807 \frac{\sigma}{E})]^{3} \qquad \text{(Eq. 6.2-1)}$$

$$\dot{\varepsilon}_{Coble} = 8.83 e^{-21000/T} \frac{\sigma}{T} \qquad \text{(Eq. 6.2-2)}$$

Glide creep strain: $$\varepsilon_{glide} = \dot{\varepsilon}_{glide}t + \frac{K\varepsilon_T \dot{\varepsilon}_{glide}t}{\varepsilon_T + K\dot{\varepsilon}_{glide}t}$$ (Eq. 6.2-3)

Coble creep strain: $$\varepsilon_{Coble} = \dot{\varepsilon}_{Coble}t$$ (Eq. 6.2-4)

Total creep: $$\varepsilon = \varepsilon_{glide} + \varepsilon_{Coble}$$ (Eq. 6.2-5)

Various parameters and constants include:

$\varepsilon_T = 0.008$,

$\kappa = 10$

$E = (1.148 \times 10^5 - 59.9T) \times 10^6$, Pa (T in K) (Eq. 6.2-6)

T= temperature (K)

σ= stress (Pa)

t= time (hours)

Integration over thermal transient: $\varepsilon(t_i) = \varepsilon(T_{i-1}, t_{i-1}) + [\varepsilon(T_i, t_i) - \varepsilon(T_i, t_{i-1})]$ (Eq. 6.2-7)

The Sheet "Creep-Rod" uses a rod temperature history in Cells C10 through C64 that is developed in two different places for two different time intervals. The rod temperatures for dry storage and transportation are developed in CRWMS M&O 2000a. The temperatures in the repository are developed in Sheets "TempC" and "TempC2", which are discussed next.

This sheet can return three different results in Cell B5. To collect statistics on creep failures, B5 is put equal to Cell G76, the calculated creep strain. If the calculation is to collect statistics on SCC, then B5 is put equal to Cell B76. Cell B76 is equal to zero if the maximum stress (Cell E76) is less than 180 MPa or 99 if greater. If the calculation is to collect statistics on the potential for hydride reorientation, then B5 is put equal to Cell B77. Cell B77 is equal to zero if the maximum stress (Cell E76) is less than a predicted stress required for reorientation or 98 if greater. The stress required for reorientation is calculated using Eq. 6.2-11 which is evaluated using the maximum temperature (Cell C76). Although not used in this calculation, Cell B5 could be evaluated using logic statements to evaluate failure by a combination of creep or SCC.

Test: In Row 83 of the Sheet "Creep-Rod" is a test case. This case is presented in CRWMS M&O 2000m and is an analysis of three experiments reported by Matsuo. The test conditions are: time duration = 960 hours, temperature = 360C, stress = 118 MPa (at 360°C). The measured strains (three tests) were 0.33, 0.40, and 0.44%. The reference, CRWMS M&O 2000m, reports a calculated creep of 0.517%, the same result as shown in Cell G83. This demonstrated that the equations were programmed correctly. Visual inspection and hand calculations were also performed. The summing of the creep strains (Column G) is tested with a hand calculation of the first few points.

Sheet "TempC2"

Cells A5 through B39 (Table II-11a) contain the WP surface temperature history from CRWMS M&O 2000h. Cells D5 through T44 give the WP internal temperatures from CRWMS M&O 2000f, Table 6-2, p. 29. Cells U5 to U44 give the temperature difference between the WP surface and center rod. Rows 46 through 91 interpolate in time the WP surface temperatures and internal temperature difference so that temperatures are available at the same times and can be added. The results of the interpolation are listed in Cells G46 through I90. These are copied to Sheet "TempC", Cells A8 through F51.

The temperature uncertainty is also calculated in Cells L46 through N55. The difference between the WP surface maximum temperature and average temperature (at the time of maximum temperature) for the WP is 22.1°C (CRWMS M&O 2000h). The uncertainty in temperature across the WP is the difference in peak center rod temperatures for a WP with helium fill (325.8°C, CRWMS M&O 2000f, Table 6-2, page 29) and the peak temperature with air and water in the WP (345.3°C, CRWMS M&O 2000g, Table 6-2, p.29) or 19.5°C. These two uncertainties are added and the total uncertainty is calculated to be 13.5% in Cell N55.

The gas plenum temperature history is calculated in Cells V5 through X44. Column V contains the reported temperatures for the upper region of the rod in CRWMS M&O 2000f, Table 6-4, Node #1. Column W is the time, repeated from Column D. Column X is the difference in temperature between the plenum and the center rod temperature as a function of time. When there are temperatures in Column V, it is a simple subtraction. Where no temperatures exist in Column V, a linear interpolation is used to complete Column X. In Cells J46 through K91 the plenum temperature differences are interpolated to be at the correct time intervals that is used for the rod creep calculations. Cells K48 through K90 are copied to Sheet "Creep-Rod", Cells V33 through V75.

Tests: Rows 7 through 44 are a repeat of input temperatures and times and are tested by inspection. Column U (not shown in Table II-11a) is the difference between Columns F and T and is verified by hand calculation. The interpolation of WP temperatures is in Cells C46 through C91 and the interpolation of temperature difference across the WP is in Cells F7 through F90. Both are tested by visual inspection and hand calculations. Column X is tested by hand calculations and inspection.

Sheet "TempC"

Sheet "TempC2" calculated the WP surface temperature history and the WP internal temperature difference history. These are imported into Cells A8 through F51 of Sheet "TempC". Sheet "TempC" (see Table II-10a, b) develops the temperature history for the rods that are located in the five non-center zones. The ratio of the temperature in any zone divided by the center rod temperature is the temperature shaping factor.

The temperature in the various zones is calculated in Cells A57 through F72. Column A gives the location for the temperatures as shown in Figure 3 and supplied by CRWMS M&O 2000f, Table 6-2, p. 29). Column B gives the temperature at the time that the temperatures peak for the 15 locations across the WP (Row 19 of Sheet "TempC2"). The

time for the peak temperature is used because the greatest cladding creep occurs at the peak temperature. Column C gives the points that are averaged to give the rod temperatures in the various zones (see Table 3 and Figure 3). The results are in Column D and temperature differences between locations 1-6 and the surface (i.e. location 15) are in Column E. The reduction factor (temperature difference in each zone/temperature difference for center zone) is given in Column F and copied to Cells F6 to K6.

The temperature distribution, both in time and radial location, is given in Cells F8 through K51. These are calculated by adding the product of the zone temperature index (Cells F6 through K6) and center rod temperature difference (Column E) to the WP surface temperature (Column B + Cell B55 for WP temperature shift). The gross temperature index is then calculated and given in Cells F7 through K7. This is used in "Fail-Calc" to calculate the temperature for each rod. Cells F5 through K5 give the fraction of rods from the WP in each zone. This is the fraction that is given in Table 3 and also used in "Fail-Calc".

Test: This sheet averages the temperatures for the 6 zones. Testing is by visual inspection and hand calculations.

Sheet "Rand #" (Random Number Sheet)

This sheet contains 2000 rows of random numbers that were fixed after they were generated (see Table II-9). This has the same effect as using a fixed seed in a random number generator and is needed if the user is to get the same answer each time he accesses the spreadsheet. Row 4 identifies which calculation uses each column. Column P contains the sample number, which is available for tracking the results for any specific sample.

Test: This sheet is tested by inspection. As a test, the calculated mean and median for Cells A5 through O2004 are:

Test mean = 0.4992
Test median = 0.4989

These values are very close to the theoretical value of 0.5.

Sheet "Unzip"

This sheet calculated the time to unzip the cladding as a function of temperature (Rows 9 to 25) used for Figure 19 and pH (Rows 27 to 40) used for Figure 20. The intrinsic dissolution equation is given in Rows 4 to 7. For the temperature and chemical conditions given in Columns E through J, the dissolution rate is calculated in Column A. The unzipping velocity is calculated in Column K and the time to unzip a rod is calculated in Column L.

Test: This is tested by hand calculations. In addition, the calculations can be compared with the dissolution test calculation in Sheet "Summary," by applying the same chemical and temperature conditions.

Table II-5. Listing of Top Rows of Sheet: "Creep-Lim"

	A	B	C	D	E	F	G	H	I	J	K	L	M
1	creep limit								file = AMR-F0155-V2.xls				
2													
3				Fig. 7	Fig. 7	Fig. 7							
4	ccdf	strain %	test of data						Sheet = Creep-Lim				
5	CCDF Shift		Mean=	3.5358			a=	4.93	7.807	135			
6	0.019231		Median=	2.8650			b=	5.33	6.7685	14.4		points for calc a,b	
7	Count		Data points,%	Ordered data, %	CCDF	Final Calc fail strain	Z1 vs Z2	Z1	Z2	Z3		F.Strain = b-a*CCDF	
8	1	3.62	1.1	0.4	1.000	0.400	0.400	0.400	-1.039	-120.600		Data to be fit	
9	2	Chung avg	0.8	0.58	0.981	0.495	0.495	0.495	-0.888	-118.004		CCDF	F. Strain
10	3		0.4	0.8	0.962	0.590	0.590	0.590	-0.738	-115.408		1	0.4
11	4		1	1	0.942	0.684	0.684	0.684	-0.588	-112.812		0.5	2.865
12	5		11.7	1.07	0.923	0.779	0.779	0.779	-0.438	-110.215		0.06	6.3
13	6		2.5	1.1	0.904	0.874	0.874	0.874	-0.288	-107.619		0.02	11.7
14	7		1.4	1.24	0.885	0.969	0.969	0.969	-0.138	-105.023			
15	8		2.4	1.4	0.865	1.064	1.064	1.064	0.012	-102.427			
16	9		3.3	1.47	0.846	1.158	1.158	1.158	0.163	-99.831			
17	10		4.7	1.53	0.827	1.253	1.253	1.253	0.313	-97.235			
18	11		6	1.64	0.808	1.348	1.348	1.348	0.463	-94.638			
19	12		4.7	1.73	0.788	1.443	1.443	1.443	0.613	-92.042			
20	13		6	2.06	0.769	1.538	1.538	1.538	0.763	-89.446			
21	14		3.6	2.08	0.750	1.633	1.633	1.633	0.913	-86.850			
22	15		4.7	2.15	0.731	1.727	1.727	1.727	1.063	-84.254			
23	16	4.222857	2.73	2.22	0.712	1.822	1.822	1.822	1.214	-81.658			
24	17	Garde 86 a	1.24	2.28	0.692	1.917	1.917	1.917	1.364	-79.062			
25	18		4.19	2.28	0.673	2.012	2.012	2.012	1.514	-76.465			
26	19		1.53	2.4	0.654	2.107	2.107	2.107	1.664	-73.869			
27	20		2.15	2.41	0.635	2.201	2.201	2.201	1.814	-71.273			
28	21		4.03	2.45	0.615	2.296	2.296	2.296	1.964	-68.677			
29	22		6.9	2.5	0.596	2.391	2.391	2.391	2.114	-66.081			
30	23		5.6	2.5	0.577	2.486	2.486	2.486	2.264	-63.485			
31	24		4.5	2.58	0.558	2.581	2.581	2.581	2.415	-60.888			
32	25		4.7	2.69	0.538	2.675	2.675	2.675	2.565	-58.292			
33	26		1.07	2.73	0.519	2.770	2.770	2.770	2.715	-55.696			
34	27		5.23	3	0.500	2.865	2.865	2.865	2.865	-53.100			
35	28		9.06	3.16	0.481	3.015	3.015	2.960	3.015	-50.504			
36	29		6.19	3.3	0.462	3.165	3.165	3.055	3.165	-47.908			
37	30	2.614118	2.69	3.3	0.442	3.315	3.315	3.149	3.315	-45.312			
38	31	Garde 96 a	6.47	3.6	0.423	3.466	3.466	3.244	3.466	-42.715			
39	32		3.3	4.03	0.404	3.616	3.616	3.339	3.616	-40.119			
40	33		5.04	4.19	0.385	3.766	3.766	3.434	3.766	-37.523			
41	34		2.41	4.5	0.365	3.916	3.916	3.529	3.916	-34.927			
42	35		2.22	4.5	0.346	4.066	4.066	3.623	4.066	-32.331			
43	36		3.16	4.7	0.327	4.216	4.216	3.718	4.216	-29.735			
44	37		0.58	4.7	0.308	4.366	4.366	3.813	4.366	-27.138			
45	38		2.28	4.7	0.288	4.516	4.516	3.908	4.516	-24.542			
46	39		2.08	4.7	0.269	4.667	4.667	4.003	4.667	-21.946			
47	40		2.28	5	0.250	4.817	4.817	4.098	4.817	-19.350			
48	41		1.64	5	0.231	4.967	4.967	4.192	4.967	-16.754			
49	42		2.58	5.04	0.212	5.117	5.117	4.287	5.117	-14.158			
50	43		2.06	5.23	0.192	5.267	5.267	4.382	5.267	-11.562			
51	44		1.73	5.6	0.173	5.417	5.417	4.477	5.417	-8.965			
52	45		1.47	6	0.154	5.567	5.567	4.572	5.567	-6.369			
53	46		2.45	6	0.135	5.718	5.718	4.666	5.718	-3.773			
54	47	4.333333	2.5	6	0.115	5.868	5.868	4.761	5.868	-1.177			
55	48	Goll avg.	3	6.19	0.096	6.018	6.018	4.856	6.018	1.419			
56	49		4.5	6.47	0.077	6.168	6.168	4.951	6.168	4.015			
57	50		5	6.9	0.058	6.612	6.318	5.046	6.318	6.612			
58	51		5	9.06	0.038	9.208	6.468	5.140	6.468	9.208			
59	52		6	11.7	0.019	11.804	6.618	5.235	6.618	11.804			
60	test line			rand.=		0.950	0.647	0.647	0.647	-0.648	-113.850		
61				Fig. 7	Fig. 7	Fig. 7							
62			Fail Strain	rand, f.Strain		Final Calc fail strain	Z1 vs Z2	Z1	Z2	Z3		test of sampling	
63			0.90	0.898514		0.900	0.900	0.900	-0.246	-106.899		mean=	3.40
64			5.19	0.202301		5.189	5.189	4.333	5.189	-12.911		median=	2.80
65			2.36	0.60249		2.360	2.360	2.360	2.065	-66.936			

Table II-6a. Listing of Top Rows of Sheet: "Creep-Rod" (Col. A-L)

	A	B	C	D	E	F	G	H	I	J	K	L
1	Calculation of creep for a given stress and temperature profile							file = AMR-F0155-V2.xls				
2	free volume	23.551314	Input					Sheet = Creep-Rod				
3	TC Unc	0.8845441	Input									
4	Room TC stress	15.08801	Input									
5	Resultant strain	8.11E-04	Output		resulting strain (B5) = G76 for creep, B76 for SCC, B77 for reorientation, can change B5 to count what failures wanted							
6												
7		Columns B,C (with WP temperature shift = 0) used for Figure 6						Corrected				Corrected
8	YMP time	total Time	T,C	Temperature	Stress	Time, hrs	Total strain,%	%	%	%	%	Creep tot,t(i-1
9		Yrs	C	K	Mpa	hrs	run sum	e(Ti,ti)	e(Ti,ti)	e-glide	e-coble	e(Ti,ti-1)
10		0	61			0						
11		2.28E-04	54	330.5	16.62	2	6.04E-11	6.04E-11	2.27E-20	9.06E-26	2.27E-20	
12		4.57E-04	122	395.6	19.89	4	4.04E-09	1.39E-08	1.56E-15	1.56E-18	1.56E-15	9.89E-09
13		6.85E-04	207	479.7	24.13	6	3.10E-07	1.71E-06	3.00E-11	3.98E-12	2.60E-11	1.40E-06
14		9.13E-04	237	510.3	25.22	8	1.40E-06	8.29E-06	7.65E-10	2.95E-10	4.70E-10	7.20E-06
15		1.14E-03	268	540.9	26.32	10	5.51E-06	3.99E-05	1.91E-08	1.32E-08	5.93E-09	3.57E-05
16		1.37E-03	291	563.9	26.80	12	1.64E-05	1.28E-04	2.08E-07	1.74E-07	3.38E-08	1.17E-04
17		1.60E-03	314	586.9	27.29	14	4.45E-05	3.88E-04	2.02E-06	1.86E-06	1.65E-07	3.60E-04
18		1.83E-03	329	602.2	27.17	16	9.39E-05	7.83E-04	8.53E-06	8.07E-06	4.56E-07	7.33E-04
19		2.05E-03	306	579.2	26.91	18	1.11E-04	3.09E-04	1.27E-06	1.13E-06	1.32E-07	2.91E-04
20		2.28E-03	291	563.9	26.14	20	1.19E-04	1.58E-04	3.23E-07	2.68E-07	5.49E-08	1.50E-04
21		2.51E-03	283	556.2	25.75	22	1.24E-04	1.15E-04	1.68E-07	1.32E-07	3.61E-08	1.10E-04
22		2.74E-03	275	548.6	25.59	24	1.28E-04	8.41E-05	8.81E-08	6.47E-08	2.35E-08	8.06E-05
23		2.97E-03	268	540.9	25.20	26	1.30E-04	6.04E-05	4.48E-08	3.00E-08	1.48E-08	5.81E-05
24		0.5	252	525.6	24.46	4.41E+03	4.55E-04	3.54E-04	1.68E-06	8.71E-07	8.08E-07	2.89E-05
25		1.0	246	519.5	24.18	8.79E+03	5.61E-04	3.70E-04	1.84E-06	8.35E-07	1.01E-06	2.65E-04
26		2.0	237	510.3	23.78	1.75E+04	6.58E-04	3.37E-04	1.51E-06	5.40E-07	9.72E-07	2.40E-04
27		3.0	226	498.9	23.26	2.63E+04	7.01E-04	2.39E-04	7.53E-07	1.87E-07	5.66E-07	1.96E-04
28		4.0	218	491.2	22.94	3.51E+04	7.26E-04	1.93E-04	4.82E-07	9.04E-08	3.92E-07	1.67E-04
29		6.0	207	479.7	22.48	5.26E+04	7.50E-04	1.37E-04	2.40E-07	2.81E-08	2.12E-07	1.13E-04
30		8.0	199	472.1	22.21	7.01E+04	7.65E-04	1.10E-04	1.52E-07	1.27E-08	1.40E-07	9.54E-05
31		10.0	193	466.0	22.02	8.76E+04	7.74E-04	9.13E-05	1.04E-07	6.50E-09	9.78E-08	8.18E-05
32		20.0	184	456.8	22.15	1.75E+05	7.98E-04	8.24E-05	8.46E-08	3.47E-09	8.11E-08	5.87E-05
33	0	20.00	-33	240.3	11.26	1.75E+05	7.98E-04	1.31E-13	7.94E-26	1.19E-36	7.94E-26	1.31E-13
34	50	70.00	18	291.2	13.83	6.13E+05	7.98E-04	4.27E-10	1.25E-18	5.08E-26	1.25E-18	2.32E-10
35	50.2	70.20	98	370.8	17.83	6.15E+05	7.98E-04	8.19E-07	6.65E-12	9.21E-16	6.65E-12	8.17E-07
36	50.4	70.40	112	384.8	18.52	6.17E+05	7.98E-04	2.24E-06	5.24E-11	2.17E-14	5.24E-11	2.24E-06
37	50.6	70.60	126	399.3	19.25	6.18E+05	7.98E-04	5.89E-06	3.79E-10	4.51E-13	3.79E-10	5.88E-06
38	50.8	70.80	141	413.7	19.97	6.20E+05	7.98E-04	1.45E-05	2.39E-09	7.61E-12	2.38E-09	1.44E-05
39	51	71.00	155	428.2	20.69	6.22E+05	7.98E-04	3.35E-05	1.34E-08	1.07E-10	1.33E-08	3.34E-05
40	52	72.00	175	448.2	21.70	6.31E+05	7.99E-04	9.91E-05	1.24E-07	3.18E-09	1.20E-07	9.85E-05
41	53	73.00	184	457.3	22.17	6.39E+05	8.00E-04	1.59E-04	3.24E-07	1.36E-08	3.10E-07	1.58E-04
42	55	75.00	182	454.8	22.05	6.57E+05	8.01E-04	1.42E-04	2.57E-07	9.47E-09	2.48E-07	1.40E-04
43	57	77.00	179	452.5	22.01	6.75E+05	8.03E-04	1.28E-04	2.10E-07	6.90E-09	2.03E-07	1.27E-04
44	59	79.00	177	450.4	21.92	6.92E+05	8.05E-04	1.17E-04	1.72E-07	5.04E-09	1.67E-07	1.15E-04
45	60	80.00	176	449.3	21.86	7.01E+05	8.05E-04	1.11E-04	1.56E-07	4.33E-09	1.52E-07	1.11E-04
46	70	90.00	166	439.2	21.44	7.88E+05	8.09E-04	6.93E-05	5.94E-08	9.35E-10	5.85E-08	6.55E-05
47	80	100.00	143	416.1	20.32	8.76E+05	8.10E-04	1.99E-05	4.60E-09	1.75E-11	4.58E-09	1.89E-05
48	90	110.00	127	400.4	19.58	9.64E+05	8.10E-04	7.91E-06	6.95E-10	9.21E-13	6.94E-10	7.55E-06
49	100	120.00	112	384.8	18.84	1.05E+06	8.11E-04	2.92E-06	9.00E-11	3.84E-14	8.99E-11	2.80E-06
50	110	130.00	99	372.3	18.21	1.14E+06	8.11E-04	1.24E-06	1.57E-11	2.53E-15	1.57E-11	1.20E-06
51	120	140.00	88	361.5	17.68	1.23E+06	8.11E-04	5.67E-07	3.14E-12	2.08E-16	3.14E-12	5.47E-07
52	130	150.00	79	352.0	17.20	1.31E+06	8.11E-04	2.73E-07	7.00E-13	2.02E-17	7.00E-13	2.64E-07

	A	B	C	D	E	F	G	H	I	J	K	L	M	N
73	900	920.00	5	277.8	13.80	8.06E+06	8.11E-04	2.81E-10	5.30E-19	3.91E-27	5.30E-19	2.73E-10	5.01E-19	3.70E-29
74	950	970.00	3	276.6	13.76	8.50E+06	8.11E-04	2.45E-10	3.99E-19	2.48E-27	3.99E-19	2.38E-10	3.78E-19	2.35E-29
75	1000	1020.00	2	275.4	13.72	8.94E+06	8.11E-04	2.12E-10	2.99E-19	1.56E-27	2.99E-19	2.07E-10	2.84E-19	1.48E-29
76	SCC flag	0	329		27.29	Limited Strain	8.11E-04							
77	Reorie.Flag	0			137.59781									
78														
79														
80	Test Problem									eq. 11	eq.12			
81	YMP time	total Time	T,C	Temperature	Stress	Time, hrs	Total strain		%	%	%		t(i-1)	t(i-1)
82		Yrs	C	K	Mpa	hrs	run sum		e(Ti,ti)	e-glide	e-coble		e(Ti,ti-1)	e-glide
83		0.11	360	633.2	118.00	9.60E+02	0.517		5.17E-01	5.16E-01	6.23E-04		na	na
84					Test problem answer =		0.517							
85				room temp stress=		38.4								
86		0.01	510	783.2	100.24	4.80E+01	35.242		3.52E+01	3.52E+01	1.23E-02		na	na
87														

Table II-6b. Listing of Top Rows of Sheet: "Creep-Rod" (Col. M-Y)

	M	N	O	P	Q	R	S	T	U	V	W	X	Y
1					file = AMR-F0155-V2.xls								
2					Sheet = Creep-Rod								
3													
4										delt T center-rod end			Input assumption
5					free vol constant	4.227							
6												peak shifted Dry	Peak Dry Temp
7													
8	Creep tot,t(i-1)	t(i-1)	t(i-1)			fraction	fraction	creep volume			total Time	T,C	
9	e(Ti,ti-1)	e-glide	e-coble	E	Tp Coe	Ec	Es-gl				hrs/Yrs	C	c
10										0	0	80	80
11	na	na	na	9.50E+10	1.01E-41	1.14E-22	4.12E-29	0.00E+00		0.0	2.00	70	140
12	7.82E-16	7.79E-21	7.81E-18	9.11E+10	5.57E-35	3.91E-18	3.54E-22	2.55E-10		0.0	4.0	160	230
13	2.00E-11	2.65E-14	1.73E-13	8.61E+10	5.69E-29	4.33E-14	6.03E-16	1.71E-08		0.0	6.0	270	340
14	5.74E-10	2.21E-12	3.53E-12	8.42E+10	2.81E-27	5.88E-13	3.35E-14	1.31E-06		10.0	8.0	310	380
15	1.53E-08	1.05E-10	4.75E-11	8.24E+10	8.94E-26	5.93E-12	1.20E-12	5.90E-06		20.0	10.0	350	420
16	1.73E-07	1.45E-09	2.81E-10	8.10E+10	9.35E-25	2.81E-11	1.32E-11	2.33E-05		35.0	12.0	380	450
17	1.73E-06	1.59E-08	1.42E-09	7.96E+10	8.14E-24	1.18E-10	1.21E-10	6.92E-05		50.0	14.0	410	480
18	7.46E-06	7.06E-08	3.99E-09	7.87E+10	3.14E-23	2.85E-10	4.59E-10	1.88E-04		70.0	16.0	430	500
19	1.13E-06	1.01E-08	1.18E-09	8.01E+10	4.03E-24	7.36E-11	5.73E-11	3.97E-04		50.0	18.0	400	470
20	2.91E-07	2.41E-09	4.94E-10	8.10E+10	9.35E-25	2.74E-11	1.22E-11	4.70E-04		50.0	20.0	380	450
21	1.53E-07	1.20E-09	3.29E-10	8.15E+10	4.37E-25	1.64E-11	5.45E-12	5.03E-04		50.0	22.0	370	440
22	8.08E-08	5.93E-10	2.15E-10	8.19E+10	2.00E-25	9.78E-12	2.45E-12	5.25E-04		45.0	24	360	430
23	4.13E-08	2.77E-10	1.36E-10	8.24E+10	8.94E-26	5.68E-12	1.05E-12	5.40E-04		45.0	26.0	350	350
24	9.91E-09	5.14E-11	4.77E-11	8.33E+10	1.67E-26	1.83E-12	1.80E-13	5.50E-04		44.3	0.5	330	330
25	9.24E-07	4.19E-09	5.05E-09	8.37E+10	8.28E-27	1.15E-12	8.64E-14	1.92E-03		43.7	1.0	322	322
26	7.57E-07	2.71E-09	4.87E-09	8.42E+10	2.81E-27	5.54E-13	2.80E-14	2.37E-03		42.3	2.0	310	310
27	5.02E-07	1.25E-09	3.77E-09	8.49E+10	6.89E-28	2.15E-13	6.45E-15	2.78E-03		41.0	3.0	295	295
28	3.62E-07	6.78E-10	2.94E-09	8.54E+10	2.60E-28	1.12E-13	2.34E-15	2.96E-03		39.7	4.0	285	285
29	1.60E-07	1.87E-10	1.41E-09	8.61E+10	5.69E-29	4.03E-14	4.86E-16	3.07E-03		37.0	6.0	270	270
30	1.14E-07	9.49E-11	1.05E-09	8.65E+10	1.98E-29	1.99E-14	1.64E-16	3.17E-03		34.4	8.0	260	260
31	8.34E-08	5.20E-11	7.82E-10	8.69E+10	8.32E-30	1.12E-14	6.74E-17	3.23E-03		31.7	10.0	252	252
32	4.23E-08	1.73E-11	4.06E-10	8.74E+10	2.17E-30	4.63E-15	1.80E-17	3.27E-03		18.4	20.000	240	240
33	7.94E-26	1.19E-38	7.94E-28	1.00E+11	3.99E-57	4.53E-33	6.17E-45	3.37E-03		18.4			
34	3.56E-19	1.45E-28	3.56E-21	9.74E+10	2.99E-47	2.03E-26	7.53E-35	3.37E-03		18.4			
35	6.64E-12	9.18E-18	6.63E-14	9.26E+10	2.89E-37	1.08E-19	1.36E-24	3.37E-03		18.5			
36	5.23E-11	2.17E-16	5.23E-13	9.17E+10	6.17E-36	8.50E-19	3.20E-23	3.37E-03		18.6			
37	3.78E-10	4.50E-15	3.78E-12	9.09E+10	1.16E-34	6.12E-18	6.63E-22	3.37E-03		18.7			
38	2.39E-09	7.59E-14	2.38E-11	9.00E+10	1.77E-33	3.84E-17	1.12E-20	3.37E-03		18.8			
39	1.33E-08	1.06E-12	1.32E-10	8.92E+10	2.25E-32	2.13E-16	1.56E-19	3.37E-03		18.9			
40	1.22E-07	3.13E-11	1.19E-09	8.80E+10	5.83E-31	1.91E-15	4.58E-18	3.37E-03		18.8			
41	3.19E-07	1.34E-10	3.06E-09	8.74E+10	2.33E-30	4.85E-15	1.93E-17	3.38E-03		18.6			
42	2.50E-07	9.22E-11	2.41E-09	8.76E+10	1.60E-30	3.77E-15	1.31E-17	3.38E-03		18.3			
43	2.05E-07	6.72E-11	1.98E-09	8.77E+10	1.14E-30	3.01E-15	9.30E-18	3.39E-03		16.7			
44	1.68E-07	4.92E-11	1.63E-09	8.78E+10	8.20E-31	2.41E-15	6.63E-18	3.39E-03		16.3			
45	1.54E-07	4.27E-11	1.50E-09	8.79E+10	6.99E-31	2.17E-15	5.61E-18	3.40E-03		16.5			
46	5.28E-08	8.31E-12	5.20E-10	8.85E+10	1.41E-31	7.42E-16	1.08E-18	3.40E-03		14.6			
47	4.14E-09	1.58E-13	4.12E-11	8.99E+10	2.74E-33	5.23E-17	1.82E-20	3.42E-03		13.6			
48	6.32E-10	8.38E-15	6.31E-12	9.08E+10	1.44E-34	7.21E-18	8.69E-22	3.42E-03		12.5			
49	8.25E-11	3.52E-16	8.24E-13	9.18E+10	6.07E-36	8.55E-19	3.32E-23	3.43E-03		11.5			
50	1.45E-11	2.33E-17	1.45E-13	9.25E+10	4.02E-37	1.38E-19	2.02E-24	3.43E-03		11.4			
51	2.92E-12	1.93E-18	2.92E-14	9.31E+10	3.31E-38	2.56E-20	1.54E-25	3.43E-03		11.3			
52	6.53E-13	1.89E-19	6.53E-15	9.37E+10	3.21E-39	5.32E-21	1.40E-26	3.43E-03		11.2			

Table II-7a. Listing of Top Rows of Sheet: "Creep-WP" (Col. A-O)

	A	B	C	D	E	F	G	H	I	J	K	L	M	N	O
1	file = AMR-F0155-V2.xls														
2	**Sheet = creep-WP**														
3				**Temp range**	0.135006637	cell is TempC2ln55									
4	figure 1 from ccdf&stress														
5				Zone1	Zone1	Zone2	Zone2	Zone 3	Zone 3	Zone 4	Zone 4	Zone 5	Zone 5	Zone 6	Zone 6
6	**CCDF**	**Case Number**	**Stress, Mpa**	**Temperature adj.**	**Creep**	**Temperature adj.**	**Creep**	**Temperature adj.**	**Creep**	**Temperature adj.**	**Creep**	**Temperature adj.**	**Creep**	**Temperature adj.**	**Creep**
7	100.00	278	143.79	0.928	0.585	0.995	1.370	0.987	1.235	0.995	1.378	0.917	0.520	0.986	1.229
8	99.95	1814	135.84	0.935	0.552	0.860	0.307	0.872	0.333	1.100	3.622	0.946	0.620	0.999	1.209
9	99.90	1653	125.45	1.030	1.409	0.926	0.433	0.992	0.883	1.027	1.358	1.031	1.415	1.041	1.613
10	99.85	1282	121.76	1.112	3.359	1.108	3.230	0.962	0.583	1.098	2.915	1.054	1.785	0.957	0.556
11	99.80	837	108.26	0.947	0.412	1.026	0.919	0.916	0.339	0.955	0.438	1.053	1.273	0.970	0.495
12	99.75	1368	104.66	1.029	0.864	1.105	2.040	1.052	1.127	0.913	0.320	0.849	0.165	0.829	0.123
13	99.70	730	102.70	1.007	0.654	1.029	0.843	0.956	0.412	0.898	0.282	1.055	1.150	0.975	0.476
14	99.65	51	97.97	1.085	1.466	1.091	1.578	0.879	0.218	1.093	1.612	1.005	0.588	1.038	0.852
15	99.60	1660	95.31	0.907	0.277	1.085	1.438	0.911	0.287	1.091	1.546	1.046	0.899	0.925	0.317
16	99.55	484	94.24	1.010	0.582	1.043	0.838	1.094	1.536	1.071	1.167	1.009	0.575	0.945	0.353
17	99.50	346	91.94	0.868	0.169	0.917	0.286	0.933	0.322	0.952	0.358	0.914	0.280	1.012	0.563
18	99.45	881	89.36	0.939	0.322	0.958	0.361	1.082	1.157	0.848	0.115	1.032	0.656	0.960	0.364
19	99.40	1675	87.98	0.912	0.256	0.932	0.302	0.930	0.298	1.012	0.511	1.039	0.671	0.853	0.122
20	99.35	994	87.91	0.988	0.426	1.087	1.155	1.021	0.565	1.055	0.803	0.858	0.130	0.908	0.249
21	99.30	1000	86.42	0.936	0.308	1.117	1.659	0.953	0.341	1.025	0.582	1.059	0.841	0.810	0.056
22	99.25	1270	86.18	0.893	0.206	0.968	0.370	0.892	0.202	0.942	0.320	1.012	0.509	0.870	0.150
23	99.20	1274	84.13	1.006	0.472	1.062	0.841	0.938	0.305	0.943	0.314	0.895	0.202	1.024	0.556
24	99.15	756	83.68	0.874	0.149	1.074	0.918	0.870	0.141	0.951	0.328	0.989	0.406	1.008	0.469
25	99.10	860	82.39	1.103	1.218	0.896	0.197	1.063	0.772	1.066	0.798	0.924	0.264	0.796	0.039
26	99.05	1051	81.82	1.104	1.209	0.894	0.189	1.076	0.883	1.003	0.437	1.064	0.774	0.888	0.175
27	99.00	769	81.77	0.879	0.155	1.018	0.497	1.104	1.257	1.047	0.656	0.836	0.079	0.949	0.316
28	98.95	1289	81.36	0.919	0.248	1.063	0.751	0.872	0.138	0.860	0.115	0.842	0.085	0.819	0.058
29	98.90	1696	80.68	0.926	0.264	0.894	0.186	1.092	1.064	1.086	0.995	0.917	0.242	0.976	0.365
30	98.85	1848	80.51	1.032	0.552	0.983	0.381	0.950	0.315	0.979	0.373	0.953	0.320	0.875	0.142
31	98.80	1851	80.05	0.972	0.356	0.924	0.257	0.905	0.211	1.080	0.937	1.028	0.533	0.865	0.121
32	98.75	242	79.79	0.994	0.401	1.023	0.499	1.097	1.088	1.100	1.134	1.011	0.451	0.957	0.325
33	98.70	1129	77.65	1.078	0.828	1.039	0.554	0.918	0.230	1.000	0.405	0.855	0.096	0.917	0.228

Table II-7b. Listing of Top Rows of Sheet: "Creep-WP" (Col. R-AJ)

	R	S	T	U	V	W	X	Y	Z	AA	AB	AC	AD	AE	AF	AG	AH	AI
1															file = AMR-F0155-V2.xls			
2	Revised stress, no crack depth														**Sheet = creep-WP**			
3	Init clad thick,um	571.5	Rod ID,cm	0.83566												median KI=	0.2189425	
4	source = CRWMS M&O 2000a, Table 2															average	0.2488412	Figure 1
5												average re	0.964859	avc	1.86E+01	min	0.0009083	
6	Run Number	Stress, Mpa	Free Volume, cm^3	Pressure, Mpa	Oxide thick,um	burnup, MWd/kgU	Clad thick, um		Run Number	Stress, Mpa	Free Volume	Old Stress, Mpa	new/old		Crack depth um	stress intensity, KI	ordered stress intensity factor, KI	CCDF
7	1	44.59123	16.83867	5.603587	81.25439	53.70135	525.0689		278	143.7911	15.23529	146.3432	0.982561		1.22E+01	2.76E-01	1.2762005	100.00
8	2	57.26634	17.05513	7.047896	100.2177	52.51857	514.2327		1814	135.8418	14.04772	137.1501	0.99046		4.59E+01	6.88E-01	1.104459	99.95
9	3	37.07603	16.89311	4.796443	54.18466	41.5617	540.5373		1653	125.4528	13.58287	131.4007	0.954735		1.14E+01	2.22E-01	1.0817672	99.90
10	4	32.42635	20.04486	4.226396	47.08804	25.27753	544.5925		1282	121.7598	15.60985	122.572	0.993374		1.59E+01	2.29E-01	1.0559368	99.85
11	5	34.04718	17.28306	4.351306	65.6316	51.14611	533.9962		837	108.2634	13.5694	108.3693	0.999022		2.55E+01	3.05E-01	0.9757994	99.80
12	6	37.23014	17.11583	4.939122	30.07806	41.66811	554.3125		1368	104.6597	11.8616	105.69	0.990251		5.04E+00	1.48E-01	0.9697506	99.75
13	7	34.10704	17.29901	4.506149	34.07579	44.2231	552.0281		730	102.7006	13.28473	105.1156	0.977025		1.67E+01	2.47E-01	0.9476987	99.70
14	8	33.46315	20.0406	4.334942	52.89786	33.76025	541.2727		51	97.9655	13.91428	98.1148	0.998478		4.04E+01	3.77E-01	0.8895748	99.65
15	9	33.91591	16.89443	4.125382	110.7224	56.90564	508.23		1660	95.30679	16.65611	96.78587	0.984718		2.69E+01	3.12E-01	0.8772347	99.60
16	10	39.69846	17.63917	5.050171	69.93842	43.85713	531.5352		484	94.23832	15.5213	94.99411	0.992044		1.55E+00	8.77E-02	0.8674957	99.55
17	11	70.50608	13.96719	8.58283	110.0192	67.32736	508.6319		346	91.94112	15.30847	94.75012	0.970354		2.12E+01	5.76E-01	0.8523651	99.50
18	12	41.08055	17.91485	5.363549	45.45406	52.14267	545.5263		881	89.35731	13.77788	93.7453	0.953192		2.48E+00	1.15E-01	0.8451236	99.45
19	13	44.71429	15.63941	5.555889	91.58309	56.13609	519.1668		1675	87.97635	11.25101	92.03635	0.955887		2.19E+01	3.71E-01	0.8398349	99.40
20	14	28.38946	18.06925	3.598381	73.32151	46.32247	529.602		994	87.91307	12.72292	91.45178	0.961305		8.02E+00	1.43E-01	0.8374381	99.35
21	15	33.30635	16.94835	4.172024	84.20543	52.47268	523.3826		1000	86.42267	16.48333	89.97976	0.960468		1.74E+01	2.46E-01	0.8350688	99.30
22	16	57.8419	13.83666	7.22446	86.85217	59.74539	521.8702		1270	86.17822	15.94901	89.80696	0.959594		3.40E+01	5.98E-01	0.8254535	99.25
23	17	35.70475	17.77004	4.669601	43.83081	44.2841	546.4538		1274	84.12955	18.03868	87.95838	0.95647		2.02E+01	2.84E-01	0.8146719	99.20
24	18	55.83917	12.45005	6.838463	104.6422	65.41946	511.7045		756	83.67796	13.77461	87.696	0.954182		4.81E+01	6.86E-01	0.7942219	99.15
25	19	28.61562	19.47052	3.744469	43.3171	29.19671	546.7474		860	82.38567	12.73797	87.1707	0.945107		4.11E+00	1.03E-01	0.7708889	99.10
26	20	22.24686	20.33374	2.951746	29.95469	29.03157	554.383		1051	81.81711	12.77551	87.08287	0.939532		3.00E+00	6.83E-02	0.7644065	99.05
27	21	49.25359	14.43801	5.933835	119.2075	63.36707	503.3814		769	81.77139	15.55988	87.07072	0.939138		8.51E-01	8.05E-02	0.7604519	99.00
28	22	42.6772	16.67565	5.510405	56.00909	54.9621	539.4948		1289	81.35812	11.85039	85.20141	0.954892		4.57E+01	5.11E-01	0.7371226	98.95
29	23	42.54401	14.99163	5.230103	101.229	53.9356	513.6549		1696	80.67915	16.03886	84.02641	0.960164		1.77E+00	1.00E-01	0.7362501	98.90
30	24	25.59575	19.42822	3.348748	43.47684	41.37019	546.6561		1848	80.50599	16.88934	83.58869	0.963121		1.79E+01	1.92E-01	0.7320046	98.85
31	25	32.93473	17.09022	4.126522	83.97263	48.17238	523.5156		1851	80.05491	18.44872	83.38844	0.960024		2.88E+01	3.13E-01	0.7311479	98.80
32	26	38.80983	17.26596	4.876848	81.2949	45.6953	525.0458		242	79.78764	14.94674	83.13646	0.959719		1.40E+00	8.14E-02	0.7245512	98.75
33	27	25.10873	18.79855	3.317783	33.93856	34.95485	552.1065		1129	77.65119	14.13877	82.21657	0.944471		2.50E+01	2.22E-01	0.7242008	98.70
34	28	32.24036	19.19215	4.28428	28.4622	43.39678	555.2359		258	77.57283	12.2074	82.14834	0.944302		2.02E+01	2.57E-01	0.7148991	98.65
35	29	28.0517	17.46193	3.657369	46.7863	39.87069	544.765		1502	77.1061	14.05996	80.41535	0.958848		7.63E+00	1.37E-01	0.7037955	98.60
36	30	36.04739	17.2921	4.649386	57.0212	56.30822	538.9165		1723	77.02389	13.19753	78.04799	0.986879		4.94E+00	1.42E-01	0.7013293	98.55
37	31	38.99448	17.45982	4.915316	78.43269	45.29677	526.6813		1040	76.15913	14.98834	77.79606	0.978959		7.76E+01	6.09E-01	0.7006071	98.50

Table II-8. Listing of top Rows of Sheet: "Fail-Calc"

	A	B	C	D	E	F	G	H	I	J	K	L	M	N	O	P
1	file = AMR-F0155-V2.xls															
2	sheet = fail calc															
3	Upper Limit	Mode fail fra.	Lower limit	Peak Clad T,YMP	Peak Vacu C	Vacuum Shift	Upper Limit	Mode fail fra.	Dry S Shift	Peak Dry St. T	WP Shift	WP Peak TC	Upper Limit	Mode fail fra.	Lower limit	Peak Clad T,YMP
4	0.00000	0.00000	0.00000	242	425	-75	0	0	0	350	-100	177	0.00000	0.00000	0.00000	242
5	0.00000	0.00000	0.00000	242	430	-70	0.00010	0.00010	25	375	-50	227	0.00000	0.00010	0.00000	299
6	0.00000	0.00010	0.00000	242	450	-50	0.00039	0.00039	50	400	0	277	0.00010	0.00010	0.00000	356
7	0.00010	0.00010	0.00000	242	475	-25	0.00248	0.00239	75	425	25	302	0.00054	0.00017	0.00000	384
8	0.00029	0.00010	0.00000	242	500	0	0.00400	0.00275	80	430	50	327	0.00387	0.00186	0.00000	412
9	0.00062	0.00019	0.00000	242	525	25	0.00780	0.00520	90	440	75	352	0.03250	0.01272	0.00010	441
10	0.00201	0.00073	0.00000	242	550	50	0.01671	0.00967	100	450	100	377	0.14953	0.05403	0.00090	469
11	0.00544	0.00274	0.00010	242	575	75	0.03660	0.01781	110	460	150	427	0.56379	0.28022	0.06171	526
12	0.01654	0.00721	0.00010	242	600	100	Above table used for dry storage study, Figure 12				200	477	0.89907	0.61133	0.34176	583
13	0.05147	0.01910	0.00029	242	625	125					225	502	0.96831	0.74988	0.50675	611
14	Above table used for vacuum dry study, Figure 11										250	527	0.99214	0.85164	0.67265	639
15											270	547	0.99801	0.90497	0.78409	662
16		WP shift	WP Peak T,	Fraction			WP shift	WP Peak T,C	Fraction		Above table used for repository temperature study, Figures 13, 14					
17	SCC only	-100	177	0.00458		reor only	-100	177	0.04665							
18	SCC only	0	277	0.00473		reor only	0	277	0.05754							
19	SCC only	50	327	0.00525		reor only	50	327	0.07655							
20	SCC and reorientation calculations for Section 6.2.5 and 6.2.6															
21				WP Shift	WP Peak TC	Upper Limit	Mode fail fra.	Lower limit	Peak Clad T,YMP	Peak Vacu C	Vacuum Shift	Dry Storage Shift	Peak Dry St. T			
22	Strain Uncertanty	0.8		50	327	0.07655	0.07655	0.07655	412	430	-70	0	350			
23	Upper fail index	1		Product		0.0020	0.0020	0.0020			0.0028	0.0028	0.0028			0.0107
24	lower fail index	6		Weight		0.0191	0.0191	0.0191			0.0286	0.0286	0.0286			0.1143
25				Fail Fract.		0.1055	0.1055	0.1055			0.0990	0.0990	0.0990			0.0935
26				Zone1	Zone1	Zone1	Zone1	Zone1	Zone2	Zone2	Zone2	Zone2	Zone2	Zone 3	Zone 3	Zone 3
27		Case Number	Stress	Creep	Fail criteria	Upper Fail index	Mean fail index	lower fail index	Creep	Fail criteria	Upper Fail index	Mean fail index	lower fail index	Creep	Fail criteria	Upper Fail index
28	CCDF	Case Number	Mpa													
29	100.00	278	143.79	98.00	0.90	1	1	1	98.00	10.59	1	1	1	98.00	4.10	1
30	99.95	1814	135.84	98.00	5.19	1	1	1	98.00	4.76	1	1	1	98.00	4.22	1
31	99.90	1653	125.45	98.00	2.36	1	1	1	98.00	4.96	1	1	1	98.00	0.59	1

Table II-9. Listing of Top Rows of Sheet: "Rand #"

	A	B	C	D	E	F	G	H	I	J	K	L	M	N	O	P
1	This sheet contains columns of random numbers used for the Fuel Rod Characteristics analysis.										file = AMR-F0155-V2.xls					
2	Each column is used for the calculation noted at the column title.										**Sheet = Rand #**			Test mean=		0.499266
3														Test median=		0.498918
4	**Temp C Zone 1**	**Temp C Zone 2**	**C Fail 1**	**C fail 2**	**C fail3**	**Temp C Zone 3**	**Temp C Zone 4**	**Temp C Zone 5**	**Temp C Zone 6**	**Creep Zone 1**	**Creep Zone 2**	**Creep Zone 3**	**Creep Zone 4**	**Creep Zone 5**	**Creep Zone 6**	**sample Numb.**
5	0.232125157	0.516956	0.898514	0.341278	0.252533	0.511765	0.5829651	0.372403	0.774887	0.907806	0.565085	0.78631	0.291068	0.008969	0.304836	278
6	0.260801258	0.013344	0.202301	0.325831	0.527147	0.080065	0.9805385	0.483736	0.827744	0.082132	0.156488	0.477543	0.877331	0.632386	0.522495	1814
7	0.611550437	0.260707	0.60249	0.961042	0.184783	0.532937	0.7045435	0.814733	0.997821	0.538518	0.795879	0.497769	0.025485	0.024826	0.676389	1653
8	0.916302715	0.942135	0.962604	0.856405	0.362758	0.417997	0.9748709	0.904772	0.658456	0.001064	0.642174	0.045457	0.446272	0.929563	0.921059	1282
9	0.303152686	0.633244	0.464965	0.313843	0.050209	0.245376	0.4313241	0.902375	0.707738	0.37262	0.800444	0.416413	0.337563	0.113341	0.489146	837
10	0.608346534	0.928968	0.860576	0.868715	0.571496	0.758004	0.2687656	0.10529	0.141523	0.801439	0.531167	0.694463	0.556408	0.709841	0.083036	1368
11	0.525643003	0.645791	0.562003	0.642536	0.809432	0.398187	0.2128283	0.911822	0.729427	0.674119	0.837233	0.223768	0.974851	0.740532	0.542972	730
12	0.814069086	0.878078	0.942233	0.120734	0.667336	0.108182	0.9557985	0.715991	0.985694	0.714568	0.147389	0.527129	0.468213	0.583775	0.009915	51
13	0.154437886	0.855915	0.204424	0.209041	0.862437	0.228251	0.9494977	0.875037	0.527814	0.589483	0.100436	0.041125	0.281319	0.57724	0.142589	1660
14	0.537888612	0.697416	0.931116	0.541668	0.418117	0.918156	0.87147	0.731154	0.609767	0.678485	0.347365	0.242657	0.302111	0.639761	0.817272	484
15	0.012881751	0.224804	0.523471	0.558834	0.174458	0.311268	0.4175848	0.359659	0.877115	0.840512	0.939072	0.99203	0.449321	0.419228	0.568701	346
16	0.272310328	0.380314	0.877117	0.088857	0.152823	0.872308	0.0213482	0.821689	0.667509	0.167748	0.327253	0.377774	0.527356	0.827036	0.011365	881
17	0.173095511	0.282452	0.385406	0.57389	0.332895	0.299575	0.6460735	0.849652	0.239043	0.217598	0.393851	0.968861	0.46561	0.171292	0.892369	1675
18	0.455396338	0.860426	0.220105	0.270136	0.729667	0.643266	0.8090247	0.141085	0.461249	0.173429	0.471333	0.048189	0.146099	0.960079	0.823007	994
19	0.262097141	0.974244	0.411747	0.358742	0.282369	0.384184	0.6968916	0.923988	0.064526	0.499425	0.370053	0.268013	0.293764	0.908877	0.852225	1000
20	0.104180317	0.415629	0.817962	0.885715	0.273157	0.154268	0.3817272	0.741897	0.304504	0.662366	0.1651	0.38071	0.782422	0.280987	0.363107	1270
21	0.523601867	0.770218	0.7902	0.472109	0.191046	0.330107	0.3839852	0.285223	0.928834	0.207384	0.519091	0.060718	0.954674	0.223067	0.586194	1274
22	0.03158437	0.814461	0.486774	0.96999	0.683511	0.071018	0.4166439	0.650973	0.863908	0.266536	0.415849	0.027207	0.887569	0.091811	0.03196	756
23	0.882318223	0.148933	0.428463	0.786398	0.801301	0.79784	0.8507878	0.400024	0.005518	0.866388	0.354817	0.844226	0.268876	0.111094	0.183474	860
24	0.884378554	0.140584	0.059966	0.288652	0.727938	0.848031	0.6145644	0.944955	0.379771	0.264858	0.288673	0.696882	0.932439	0.348612	0.036161	1051
25	0.051703482	0.605217	0.459057	0.59192	0.056347	0.954266	0.7790187	0.058199	0.623037	0.076714	0.431409	0.285329	0.597299	0.555278	0.952178	769
26	0.201558558	0.772629	0.859033	0.338219	0.679984	0.080997	0.0693279	0.078083	0.102318	0.861205	0.600412	0.254087	0.481931	0.413529	0.658711	1289
27	0.226445835	0.141331	0.059152	0.853156	0.680851	0.907389	0.9279805	0.372846	0.731816	0.9021	0.847846	0.523331	0.754028	0.690311	0.415791	1696
28	0.617316359	0.474331	0.226888	0.000613	0.242927	0.373387	0.5228757	0.510876	0.326576	0.405368	0.553833	0.134339	0.720795	0.381479	0.501697	1848
29	0.39518612	0.25315	0.135734	0.505745	0.398258	0.205293	0.9070353	0.806201	0.285979	0.700445	0.742133	0.162156	0.067707	0.198539	0.138376	1851
30	0.476381941	0.622672	0.753326	0.573011	0.439503	0.925896	0.9826611	0.737173	0.657319	0.276697	0.57785	0.746092	0.642148	0.838553	0.891215	242
31	0.788442292	0.684409	0.262751	0.63772	0.094331	0.253119	0.5999432	0.129762	0.496581	0.377893	0.674795	0.605688	0.578291	0.742935	0.903628	1129
32	0.553292172	0.835082	0.720968	0.003514	0.768129	0.329453	0.1537642	0.098457	0.251898	0.404138	0.031788	0.852339	0.692154	0.854748	0.815359	258
33	0.662464615	0.56007	0.257341	0.857962	0.114005	0.657153	0.6566995	0.09525	0.954779	0.318068	0.343866	0.524909	0.427381	0.192976	0.212502	1502
34	0.168922185	0.294365	0.197952	0.122797	0.274607	0.762047	0.0203188	0.931454	0.3647	0.390098	0.178208	0.207206	0.779757	0.029485	0.826781	1723
35	0.489717156	0.302747	0.641695	0.527485	0.612699	0.013991	0.9514105	0.889598	0.130097	0.767429	0.665162	0.865437	0.014424	0.376113	0.721532	1040
36	0.970456976	0.746844	0.990076	0.555013	0.714524	0.854649	0.9344917	0.215021	0.912331	0.032349	0.871176	0.931439	0.914746	0.963721	0.077258	1418

Table II-10a. Listing of Top Rows of Sheet: "TempC"

	A	B	C	D	E	F	G	H	I	J	K	L
1	file = AMR-E0155-V2.xls											
2	**Sheet = TempC (Temperature, C)**											
3	Temperature Calculations				Components of below table shown on Fig. 5, Table 3							
4					radal zone	1	2	3	4	5	6	sum
5					Fraction	1.91E-02	2.86E-02	0.11429	2.10E-01	0.33333	0.29524	1.0000
6		average			TC Adj (inWP)	1	9.334E-01	0.887987	0.819805	0.660714	0.446429	
7					**TC adj (gross)**	1	0.99015053	0.983424	0.973334	0.949792	0.918081	
8	YMP-Time	WP Wall TC			inside WC Delta TC	Zone1 Center rod TC	Z 2	Z 3	Z 4	Z 5	Z 6	
9	0	24.61			38.20	-37.19	-39.73	-41.47	-44.07	-50.15	-58.34	
10	50	82.26			38.20	20.46	17.92	16.18	13.58	7.50	-0.69	
11	50.2	176.54			33.90	110.44	108.18	106.64	104.33	98.93	91.67	
12	50.4	193.16			33.10	126.26	124.06	122.55	120.30	115.03	107.94	
13	50.6	209.79			32.80	142.59	140.40	138.91	136.67	131.46	124.43	
14	50.8	226.41			32.50	158.91	156.75	155.27	153.05	147.88	140.92	
15	51	243.03			32.20	175.23	173.09	171.63	169.43	164.31	157.41	
16	52	266.46			31.40	197.86	195.77	194.34	192.20	187.20	180.47	
17	53	277.33			30.80	208.13	206.08	204.68	202.58	197.68	191.08	
18	55	275.61			29.70	205.31	203.33	201.98	199.95	195.23	188.86	
19	57	273.88			28.90	202.78	200.85	199.54	197.57	192.97	186.78	
20	59	272.15			28.20	200.35	198.47	197.19	195.27	190.78	184.74	
21	60	271.29			27.90	199.19	197.33	196.06	194.16	189.72	183.74	
22	70	262.65			25.10	187.75	186.08	184.94	183.23	179.23	173.86	
23	80	238.65			23.00	161.65	160.12	159.07	157.50	153.84	148.92	
24	90	222.46			21.40	143.86	142.44	141.47	140.01	136.60	132.02	
25	100	206.28			19.90	126.18	124.85	123.95	122.59	119.43	115.16	
26	110	193.19			18.90	112.09	110.83	109.97	108.68	105.68	101.63	
27	120	181.91			18.00	99.91	98.71	97.89	96.67	93.80	89.95	
28	130	172.06			17.10	89.16	88.02	87.24	86.07	83.35	79.69	
29	140	164.01			16.30	80.31	79.23	78.48	77.37	74.78	71.29	
30	150	159.43			15.40	74.83	73.81	73.11	72.06	69.61	66.31	
31	160	154.86			15.03	69.89	68.89	68.20	67.18	64.79	61.57	
32	180	146.41			14.29	60.70	59.75	59.10	58.13	55.86	52.79	
33	205	141.57			13.37	54.94	54.05	53.44	52.53	50.40	47.54	
34	232	137.27			12.37	49.63	48.81	48.25	47.41	45.44	42.79	
35	250	134.99			11.70	46.69	45.91	45.38	44.58	42.72	40.22	
36	265	133.10			11.43	44.53	43.77	43.25	42.47	40.65	38.20	
37	310	128.79			10.62	39.41	38.70	38.22	37.49	35.80	33.53	
38	350	125.73			9.90	35.63	34.97	34.52	33.84	32.27	30.15	
39	365	124.58			9.71	34.29	33.64	33.20	32.54	30.99	28.91	
40	450	119.04			8.60	27.64	27.07	26.68	26.09	24.72	22.88	
41	480	117.09			8.30	25.39	24.84	24.46	23.89	22.57	20.79	
42	550	113.40			7.60	21.00	20.49	20.15	19.63	18.42	16.79	
43	615	109.97			7.15	17.12	16.64	16.32	15.83	14.69	13.16	
44	650	108.49			6.90	15.39	14.93	14.62	14.15	13.05	11.57	
45	695	106.59			6.59	13.17	12.73	12.43	11.98	10.94	9.53	
46	750	104.68			6.20	10.88	10.46	10.18	9.76	8.77	7.44	
47	790	103.29			5.96	9.25	8.85	8.58	8.17	7.22	5.95	
48	850	101.45			5.60	7.05	6.67	6.42	6.04	5.15	3.95	
49	900	99.91			5.40	5.31	4.95	4.71	4.34	3.48	2.32	
50	950	98.71			5.20	3.91	3.57	3.33	2.98	2.15	1.04	
51	1000	97.52			5.00	2.52	2.18	1.96	1.61	0.82	-0.25	
52	Columns A,B,E,F used in Fig. 5											

Table II-10b. Listing of Rows 53 to 72 of Sheet: "TempC"

	A	B	C	D	E	F	G	H	I
53	file = AMR-F0155-V2.xls								
54	**Sheet = TmpC (Temperature, C)**								
55	WP wall shift TC	5.00E+01	(defined fail calc sheet)						
56		**Calculation of shaping factors for temperatures across WP**							
57	Location	Temperature	points averaged	Zone TC	delta TC from surface	reduction factor			
58	1	313.4	1	313.4	30.8	1			
59	2	309.3	1&2	311.35	28.75	0.9334416			
60	3	308.8	5&6	309.95	27.35	0.887987			
61	4	308.8	6&7	307.85	25.25	0.8198052			
62	5	309	9&10	302.95	20.35	0.6607143			
63	6	310.9	10&11	296.35	13.75	0.4464286			
64	7	304.8							
65	8	304.3							
66	9	304.1							
67	10	301.8							
68	11	290.9							
69	12	289.8							
70	13	283.4							
71	14	282.9							
72	15	282.6							

Table II-11a. Listing of Top Rows of Sheet: "TempC2", Columns A to P

	A	B	C	D	E	F	G	H	I	J	K	L	M	N	O	P
1	file = AMR-F0155-V2.xls		sheet = TempC2													
2	Takes input temperatures for WP and Interior and aligns them up to the same time steps															
3	Average Waste Package Surface Temp (C)															
4	RIP_Tavg_csnf_dsps_bc_bin20-60_mean			*Radial Temperature Distribution for EDA II (Axial Peaking Factor of 1.102)*											file = anderson11-11	
5	Time(yr)	Bin Weight= 0.528528		Time (years)	WP Heat (W)	Node										
6	Time, Yr	T,C				1	2	3	4	5	6	7	8	9	10	11
7	0.0	24.6		50	4374.9	147.5	139.8	139.1	139.1	139.5	145.0	135.3	134.8	134.5	135.1	119.8
8	1.0	78.7		50.1	4369.5	236.9	231.5	230.9	231.0	231.2	234.4	226.9	226.5	226.2	224.9	212.5
9	2.0	87.2		50.2	4364.2	263.0	258.0	257.4	257.4	257.7	260.4	253.2	252.8	252.5	250.7	238.4
10	5.0	95.0		50.3	4359.0	273.0	268.1	267.5	267.6	267.8	270.4	263.4	262.9	262.6	260.8	248.8
11	30.0	90.6		50.4	4353.5	278.8	274.0	273.5	273.5	273.7	276.2	269.3	268.9	268.6	266.7	254.7
12	40.0	85.7		50.5	4348.3	282.9	278.1	277.6	277.6	277.9	280.3	273.4	273.0	272.7	270.7	258.9
13	50.0	82.3		50.6	4342.8	286.0	281.3	280.8	280.8	281.0	283.4	276.6	276.2	275.9	273.9	262.1
14	50.2	176.5		50.7	4337.6	288.7	284.0	283.5	283.5	283.8	286.1	279.4	278.9	278.6	276.5	264.9
15	51.0	243.0		50.8	4332.3	291.0	286.4	285.9	285.9	286.1	288.4	281.8	281.3	281.0	278.9	267.3
16	52.0	266.5		50.9	4327.1	293.0	288.5	288.0	288.0	288.2	290.4	283.8	283.4	283.1	281.0	269.4
17	53.0	277.3		51	4321.6	294.8	290.3	289.8	289.8	290.0	292.2	285.7	285.2	284.9	282.8	271.3
18	70.0	262.7		52	4269.1	306.3	302.0	301.5	301.5	301.7	303.7	297.4	297.0	296.7	294.4	283.3
19	80.0	238.6		53	4217.0	313.4	309.3	308.8	308.8	309.0	310.9	304.8	304.3	304.1	301.8	290.9
20	100.0	206.3		54	4165.8	317.9	313.9	313.4	313.4	313.6	315.4	309.4	309.0	308.7	306.4	295.7
21	110.0	193.2		55	4115.0	321.2	317.3	316.8	316.8	317.0	318.8	312.9	312.5	312.2	309.9	299.4
22	120.0	181.9		56	4064.8	323.4	319.6	319.1	319.1	319.3	321.0	315.2	314.8	314.5	312.2	301.9
23	130.0	172.1		57	4015.4	324.8	321.0	320.5	320.5	320.7	322.4	316.7	316.3	316.0	313.7	303.5
24	140.0	164.0		58	3966.5	325.7	322.0	321.5	321.5	321.7	323.4	317.7	317.3	317.1	314.8	304.8
25	160.0	154.9		59	3918.2	325.8	322.1	321.6	321.7	321.9	323.5	317.9	317.5	317.3	315.0	305.1
26	180.0	146.4		60	3881.0	325.4	321.7	321.3	321.3	321.5	323.1	317.6	317.2	316.9	314.7	304.9
27	205.0	141.6		70	3670.6	320.5	317.2	316.7	316.8	316.9	318.4	313.4	313.1	312.8	310.9	302.0
28	232.0	137.3		80	3481.2	309.7	306.6	306.2	306.2	306.4	307.8	303.2	302.9	302.6	300.9	292.8
29	265.0	133.1		90	3308.6	298.4	295.4	295.1	295.1	295.2	296.7	292.3	292.0	291.8	290.3	282.7
30	310.0	128.8		100	3152.7	287.9	285.1	284.7	284.7	284.9	286.3	282.2	281.9	281.7	280.4	273.3
31	365.0	124.6		110	2511.0	281.8	279.1	278.8	278.8	278.9	280.3	276.4	276.1	275.9	274.7	268.0
32	420.0	120.8		120	2369.0	275.9	273.3	273.0	273.0	273.1	274.5	270.7	270.5	270.3	269.2	262.8
33	480.0	117.1		130	2235.0	269.4	266.9	266.6	266.6	266.7	268.0	264.4	264.2	264.0	263.0	256.9
34	545.0	113.4		140	2108.6	262.3	259.8	259.5	259.5	259.7	261.0	257.5	257.3	257.2	256.3	250.4
35	615.0	110.0		150	1989.3	254.7	252.4	252.1	252.1	252.2	253.5	250.2	250.0	249.9	249.0	243.4
36	695.0	106.6		250	1448.6	222.7	220.8	220.6	220.6	220.7	221.8	219.2	219.0	218.9	218.5	214.2
37	790.0	103.3		350	1306.2	206.3	204.6	204.5	204.5	204.5	205.6	203.3	203.2	203.1	202.8	199.1
38	900.0	99.9		450	1193.2	194.9	193.4	193.3	193.3	193.4	194.3	192.3	192.2	192.1	191.9	188.7
39	1030.0	96.8		550	1101.5	185.5	184.1	184.0	184.0	184.1	184.9	183.1	183.0	183.0	182.8	180.0
40				650	1025.9	178.1	176.8	176.7	176.7	176.8	177.6	175.9	175.9	175.8	175.7	173.1
41				750	957.6	171.5	170.4	170.2	170.3	170.3	171.0	169.6	169.5	169.4	169.3	167.0
42				850	895.4	165.9	164.8	164.8	164.8	164.8	165.5	164.1	164.0	164.0	163.9	161.8
43				950	586.1	161.2	160.2	160.2	160.2	160.2	160.8	159.6	159.5	159.5	159.4	157.5
44				1050	539.9	157.5	156.6	156.5	156.5	156.6	157.2	156.0	155.9	155.9	155.9	154.0

Table II-11b. Listing of Top Rows of Sheet: "TempC2", Columns P to X

	P	Q	R	S	T	U	V	W	X
1									
2				file = AMR-F0155-V2.x		sheet = TempC2			
3									
4	nderson11-11-99.xls								
5							temp, fuel end	time	delt-T, center-rod end
6	11	12	13	14	15	del-T,cl-sur			18.4
7	119.8	118.6	109.8	109.5	109.3	38.2	129.1	50	18.4
8	212.5	211.4	203.9	203.4	203.2	33.7		50.1	18.45
9	238.4	237.3	229.8	229.4	229.1	33.9		50.2	18.5
10	248.8	247.6	240.4	240.0	239.7	33.3		50.3	18.55
11	254.7	253.6	246.4	246.0	245.7	33.1		50.4	18.6
12	258.9	257.8	250.7	250.2	249.9	33.0		50.5	18.65
13	262.1	261.0	254.0	253.5	253.2	32.8		50.6	18.7
14	264.9	263.8	256.8	256.3	256.0	32.7		50.7	18.75
15	267.3	266.2	259.3	258.8	258.5	32.5		50.8	18.8
16	269.4	268.3	261.4	260.9	260.7	32.3		50.9	18.85
17	271.3	270.2	263.3	262.8	262.6	32.2	275.9	51	18.9
18	283.3	282.2	275.6	275.1	274.9	31.4		52	18.75
19	290.9	289.8	283.4	282.9	282.6	30.8		53	18.6
20	295.7	294.7	288.4	287.9	287.7	30.2		54	18.45
21	299.4	298.3	292.2	291.7	291.5	29.7	302.9	55	18.3
22	301.9	300.9	294.8	294.3	294.1	29.3	306.5	56	16.9
23	303.5	302.5	296.6	296.1	295.9	28.9	308.1	57	16.7
24	304.8	303.8	297.9	297.4	297.2	28.5	309.2	58	16.5
25	305.1	304.1	298.3	297.9	297.6	28.2	309.5	59	16.3
26	304.9	303.9	298.2	297.7	297.5	27.9	308.9	60	16.5
27	302.0	301.1	296.0	295.6	295.4	25.1	305.9	70	14.6
28	292.8	292.0	287.2	286.9	286.7	23.0		80	13.56667
29	282.7	282.0	277.6	277.2	277.0	21.4		90	12.53333
30	273.3	272.6	268.4	268.1	268.0	19.9	276.4	100	11.5
31	268.0	267.3	263.3	263.0	262.9	18.9		110	11.40421
32	262.6	262.2	258.4	258.1	257.9	18.0		120	11.30842
33	256.9	256.3	252.7	252.4	252.3	17.1		130	11.21263
34	250.4	249.8	246.4	246.1	246.0	16.3		140	11.11684
35	243.4	242.9	239.6	239.4	239.3	15.4		150	11.02105
36	214.2	213.8	211.2	211.0	211.0	11.7		250	10.06316
37	199.1	198.8	196.6	196.5	196.4	9.9		350	9.105263
38	188.7	188.4	186.5	186.4	186.3	8.6		450	8.147368
39	180.0	179.7	178.0	177.9	177.9	7.6		550	7.189474
40	173.1	172.9	171.4	171.3	171.2	6.9		650	6.231579
41	167.0	166.8	165.4	165.4	165.3	6.2		750	5.273684
42	161.8	161.6	160.4	160.3	160.3	5.6		850	4.315789
43	157.5	157.3	156.1	156.1	156.0	5.2		950	3.357895
44	154.0	153.9	152.8	152.7	152.7	4.8	155.1	1050	2.4

Table II-11c. Listing of Rows 45 to 92 of Sheet: "TempC2"

	A	B	C	D	E	F	G	H	I	J	K	L	M	N	O
45	file = AMR-F0155-V2.xls		sheet = TempC2												
46	Time(yr)	Bin Weight= 0.528528	Tc, Interpolate	Time, WP internals	Internal del TC	Internal Delta Tc, Interpolated	WP Temp	Delit Tc internal	Center Rod Temperature	delt-T, center-rod end	delt-T, center-rod end	Uncertainties			
47	Time, Yr	T.C. WP	T.C.WP	time, yr	Tc	Tc	Tc	Tc	Tc	Tc	Tc				
48	0.0	24.6		0	38.2		24.6	38.2	62.8	18.4	18.4	WP surface			
49	50.0	82.3		50	38.2		82.3	38.2	120.5	18.4	18.4	Max -avg		22.1	deg C
50	50.2	176.5		50.2	33.9		176.5	33.9	210.4	18.5	18.5				
51	50.4		193.1605	50.4	33.1		193.2	33.1	226.3	18.6	18.6	unceert interior		19.5	
52	50.6		209.785	50.6	32.8		209.8	32.8	242.6	18.7	18.7	air vs He			
53	50.8		226.4095	50.8	32.5		226.4	32.5	258.9	18.8	18.8		Sum	41.6	
54	51.0	243.0		51	32.2		243.0	32.2	275.2	18.9	18.9				
55	52.0	266.5		52	31.4		266.5	31.4	297.9	18.75	18.8	fraction uncert		0.135007	
56	53.0	277.3		53	30.8		277.3	30.8	308.1	18.6	18.6				
57	55		275.605706	55	29.7		275.6	29.7	305.3	18.3	18.3				
58	57		273.878412	57	28.9		273.9	28.9	302.8	16.7	16.7				
59	59		272.151118	59	28.2		272.2	28.2	300.4	16.3	16.3				
60	60		271.287471	60	27.9		271.3	27.9	299.2	16.5	16.5				
61	70.0	262.7		70	25.1		262.7	25.1	287.8	14.6	14.6				
62	80.0	238.6		80	23		238.6	23	261.6	13.56667	13.6				
63	90		222.463	90	21.4		222.5	21.4	243.9	12.53333	12.5				
64	100.0	206.3		100	19.9		206.3	19.9	226.2	11.5	11.5				
65	110.0	193.2		110	18.9		193.2	18.9	212.1	11.40421	11.4				
66	120.0	181.9		120	18		181.9	18	199.9	11.30842	11.3				
67	130.0	172.1		130	17.1		172.1	17.1	189.2	11.21263	11.2				
68	140.0	164.0		140	16.3		164.0	16.3	180.3	11.11684	11.1				
69	150		159.4335	150	15.4		159.4	15.4	174.8	11.02105	11.0				
70	160.0	154.9		160.0		15.03	154.9	15.03	169.9		10.92526				
71	180.0	146.4		180.0		14.29	146.4	14.29	160.7		10.73368				
72	205.0	141.6		205.0		13.365	141.6	13.365	154.9		10.49421				
73	232.0	137.3		232.0		12.366	137.3	12.366	149.6		10.23558				
74	250		134.992364	250	11.7		135.0	11.7	146.7	10.06316	10.1				
75	265.0	133.1		265.0		11.43	133.1	11.43	144.5		9.919474				
76	310.0	128.8		310.0		10.62	128.8	10.62	139.4		9.488421				
77	350		125.728091	350	9.9		125.7	9.9	135.6	9.105263	9.1				
78	365.0	124.6		365.0		9.705	124.6	9.705	134.3		8.961579				
79	450.0		119.042696	450	8.6		119.0	8.6	127.6	8.147368	8.1				
80	480.0	117.1		480.0		8.3	117.1	8.3	125.4		7.86				
81	550.0		113.397704	550	7.6		113.4	7.6	121.0	7.189474	7.2				
82	615.0	110.0		615.0		7.145	110.0	7.145	117.1		6.566842				
83	650.0		108.490063	650	6.9		108.5	6.9	115.4	6.231579	6.2				
84	695.0	106.6		695.0		6.585	106.6	6.585	113.2		5.800526				
85	750.0		104.675474	750	6.2		104.7	6.2	110.9	5.273684	5.3				
86	790.0	103.3		790.0		5.96	103.3	5.96	109.2		4.890526				
87	850.0		101.446073	850	5.6		101.4	5.6	107.0	4.315789	4.3				
88	900.0	99.9		900.0		5.4	99.9	5.4	105.3		3.836842				
89	950.0		98.7139538	950	5.2		98.7	5.2	103.9	3.357895	3.4				
90	1000.0		97.5151077	1000		5	97.5	5	102.5		2.878947				
91	1030.0	96.8		1050	4.8					2.4	2.4				
92															

Table II-12. Listing of Top Rows of Sheet: "Unzip"

	A	B	C	D	E	F	G	H	I	J	K	L
1	file = AMR-F0155-V2.xls											
2	Sheet = Unzip											
3	velocity conversion =		0.0000219	cm/yr /(mg/m2-d)			Fuel length	366	cm (CRWMS M&O 2000a, Table 2)			
4	**log10(rate) = a0 + a1/Tk + a2* PCO3 + a3* PO2 + a4 * pH**											
5			**Term=**	**a0**	**a1**	**a2**	**a3**	**a4**				
6	**Basic**	**pH>7**		**4.69**	**-1085**	**-0.12**	**-0.32**	**0**		E10 to E25 and L10 to L25		
7	**Acidic**	**pH< =7**		**7.13**	**-1085**	**0**	**-0.32**	**-0.41**		used in Figure 19		
8	**Example calculation**				**Tc**	**PCo3**	**PO2**	**pH**				
9	**dis Rate**	**log10(dis rt)**	**Acidic solution**	**Basic solution**	**Tc**	**PCo3**	**PO2**	**pH**	**M-CO3**	**Atm. O2**	**Velocity, cm/yr**	**yrs to unzip**
10	15.757	1.197	0.7175	1.1975	100	3	0.69897	8	0.001	0.2	3.11E-03	5.89E+04
11	14.387	1.158	0.6780	1.1580	95	3	0.69897	8	0.001	0.2	2.84E-03	6.45E+04
12	13.102	1.117	0.6373	1.1173	90	3	0.69897	8	0.001	0.2	2.58E-03	7.09E+04
13	11.902	1.076	0.5956	1.0756	85	3	0.69897	8	0.001	0.2	2.35E-03	7.80E+04
14	10.781	1.033	0.5527	1.0327	80	3	0.69897	8	0.001	0.2	2.13E-03	8.61E+04
15	9.739	0.989	0.5085	0.9885	75	3	0.69897	8	0.001	0.2	1.92E-03	9.53E+04
16	8.771	0.943	0.4631	0.9431	70	3	0.69897	8	0.001	0.2	1.73E-03	1.06E+05
17	7.875	0.896	0.4163	0.8963	65	3	0.69897	8	0.001	0.2	1.55E-03	1.18E+05
18	7.048	0.848	0.3681	0.8481	60	3	0.69897	8	0.001	0.2	1.39E-03	1.32E+05
19	6.286	0.798	0.3184	0.7984	55	3	0.69897	8	0.001	0.2	1.24E-03	1.48E+05
20	5.587	0.747	0.2672	0.7472	50	3	0.69897	8	0.001	0.2	1.10E-03	1.66E+05
21	4.947	0.694	0.2144	0.6944	45	3	0.69897	8	0.001	0.2	9.75E-04	1.88E+05
22	4.364	0.640	0.1599	0.6399	40	3	0.69897	8	0.001	0.2	8.60E-04	2.13E+05
23	3.834	0.584	0.1036	0.5836	35	3	0.69897	8	0.001	0.2	7.56E-04	2.42E+05
24	3.353	0.525	0.0455	0.5255	30	3	0.69897	8	0.001	0.2	6.61E-04	2.77E+05
25	2.920	0.465	-0.0146	0.4654	25	3	0.69897	8	0.001	0.2	5.76E-04	3.18E+05
26	Variation in pH			H27 to H40 and L27 to L40 used for Figure 20								
27	55.412	1.744	1.7436	0.5836	35	3	0.69897	4	0.001	0.2	1.09E-02	1.68E+04
28	34.562	1.539	1.5386	0.5836	35	3	0.69897	4.5	0.001	0.2	6.81E-03	2.69E+04
29	21.558	1.334	1.3336	0.5836	35	3	0.69897	5	0.001	0.2	4.25E-03	4.31E+04
30	13.446	1.129	1.1286	0.5836	35	3	0.69897	5.5	0.001	0.2	2.65E-03	6.90E+04
31	8.387	0.924	0.9236	0.5836	35	3	0.69897	6	0.001	0.2	1.65E-03	1.11E+05
32	5.231	0.719	0.7186	0.5836	35	3	0.69897	6.5	0.001	0.2	1.03E-03	1.77E+05
33	3.834	0.584	0.5136	0.5836	35	3	0.69897	7	0.001	0.2	7.56E-04	2.42E+05
34	3.834	0.584	0.3086	0.5836	35	3	0.69897	7.5	0.001	0.2	7.56E-04	2.42E+05
35	3.834	0.584	0.1036	0.5836	35	3	0.69897	8	0.001	0.2	7.56E-04	2.42E+05
36	3.834	0.584	-0.1014	0.5836	35	3	0.69897	8.5	0.001	0.2	7.56E-04	2.42E+05
37	3.834	0.584	-0.3064	0.5836	35	3	0.69897	9	0.001	0.2	7.56E-04	2.42E+05
38	3.834	0.584	-0.5114	0.5836	35	3	0.69897	9.5	0.001	0.2	7.56E-04	2.42E+05
39	3.834	0.584	-0.7164	0.5836	35	3	0.69897	10	0.001	0.2	7.56E-04	2.42E+05
40	3.834	0.584	-0.9214	0.5836	35	3	0.69897	10.5	0.001	0.2	7.56E-04	2.42E+05